THESIS

FACIES RECONSTRUCTION AND DETRITAL ZIRCON GEOCHRONOLOGY OF THE INGLESIDE/CASPER FORMATION

Submitted by

Kajal Nair

Department of Geosciences

In partial fulfillment of the requirements

For the Degree of Master of Science

Colorado State University

Fort Collins, Colorado

Spring 2018

Master's Committee:

Advisor: Sven Egenhoff
Co-Advisor: John Singleton

Monique Rocca

ABSTRACT

FACIES RECONSTRUCTION AND DETRITAL ZIRCON GEOCHRONOLOGY OF THE INGLESIDE/CASPER FORMATION

Mixed siliciclastic-carbonate deposits of the Ingleside/Casper Formation in northern Colorado and southeastern Wyoming developed along the flanks of the Ancestral Front Range during the Late Paleozoic. This study establishes a sedimentological model for the Ingleside/Casper Formation along with using detrital zircon data to identify siliciclastic sediment sources for Late Paleozoic deposits in two Ancestral Rocky Mountain basins along the Ancestral Front Range and Uncompahgre Highlands.

The stratigraphic successions of the Ingleside/Casper Formation display a diverse suite of carbonate and siliciclastic lithofacies in close lateral and vertical association with each other. The six different siliciclastic facies and their subfacies identified in this study include: (1) cross-bedded sandstone (tabular cross-bedded sandstone and trough cross-bedded sandstone), (2) horizontally-bedded sandstone, (3) massive sandstone, (4) conglomeratic sandstone, (5) ripple-laminated sandstone (asymmetric current ripples, moderately-steeply climbing ripples, and gently climbing ripples), and (6) silt-rich siliciclastic mudstone. The three different carbonate facies and their subfacies identified in this study include: (1) carbonate mudstone-wackestone, (2) carbonate packstone (packstone with non-skeletal grains and packstone with bioclasts), and (3) carbonate grainstone (grainstone with non-skeletal grains and grainstone with bioclasts). Thinning and/or pinching out of carbonate facies accompanied with a gradual increase in siliciclastic sedimentation is observed laterally across the study area from north to south. Eight stratigraphic intervals are recognized from correlations across a north-south transect of 120 km and each interval displays a lithofacies assemblage dominated either by carbonates or siliciclastics. Both carbonate and siliciclastic successions display small-scale fining-upward trends, with coarsening-upwards being partially or wholly absent across the study area. One of the eight intervals (termed Interval 6) is of significant interest in this study because

it displays a unique lithofacies assemblage, with it being the only interval where trough cross-beds of facies 1B occur. Overall, carbonate units vary in the extent to which they onlap onto siliciclastic strata throughout the succession: Intervals 1 to 4 record a successive advance of onlap towards the south, whereas intervals 5 to 8 record a retreat of onlap and a successive northwards migration of carbonate strata.

The nine different lithofacies and their subfacies identified in this study represent an array of shallow-marine paleoenvironments that include foreshore, shoreface, offshore transition, and offshore, and terrestrial settings comprising coastal eolian dunes and fluvial systems. Stratigraphic distribution of facies suggests that deposition in a shallow-marine environment alternated between dominantly siliciclastic and dominantly carbonate, mainly as a result of fluctuations in the input of siliciclastic sediment and its effect on carbonate deposition. In a distal direction, both siliciclastic and carbonate facies graded into carbonate mudstone that is identified as the most distal setting across all stratigraphic successions studied here. The Ingleside/Casper succession is interpreted to consist of two superimposed scales of sea-level fluctuations with the small-scale cycles represented by deepening-upwards successions across the study area, and a superimposed large-scale sea level curve recorded in the varying onlap of carbonates. The superimposed curve shows an overall transgression in the lower part of the succession succeeded by a regression in the upper part. Independent of this type of sea-level curve, dry eolian dunes dominated the stratigraphic record during Interval 6 and reflect a sharp change in climate to more arid conditions that accompanied the exclusive formation of dunes during this time.

The sedimentological study suggests that deposition of the Casper/Ingleside Formation was governed by the two orders of sea-level oscillations and also climate change, both operating on two separate scales. The general fall in sea level and increase in aridity in the upper Ingleside/Casper Formation is attributed to the onset of a major Gondwanan glaciation phase that culminated during the Pennsylvanian-Permian transition which is likely to be located at the very top of this unit. Based on exclusively sedimentological considerations, this study therefore suggests that the Ingleside Formation, which is typically assigned a Permian age, was most likely deposited during the Late Pennsylvanian. This interpretation is also based on

the correlation of the Coloradoan Ingleside Formation to the Casper Formation in Wyoming that contains a known Late Pennsylvanian fussuline assemblage.

This study also presents new detrital zircon U-Pb geochronology data from the type section of the Ingleside Formation at Owl Canyon, and the Molas and Hermosa Formations near Molas Lake to understand Late Paleozoic sediment provenance and dispersal patterns across Colorado. U-Pb ages on 120-150 zircons were determined from each sample using LA-ICPMS, and ages with excessive discordance (>20% discordant or <5% reverse discordant) were rejected. All samples contain between 5% and 10% concordant Paleozoic aged zircons ranging from 330-490 Ma. Other significant age distribution peaks identified range between 990-1200 Ma, 1340-1500 Ma, 1600-1800 Ma, and 2500-3500 Ma.

The wide spread of zircon age populations record a mixed Laurentian derivation comprising local and distal sediment sources. Paleozoic-age zircons are interpreted to coincide with high magmatic flux during the Taconic and Acadian orogenies in the Appalachian orogen. The diverse components in the U-Pb age data suggest that a widespread sand-dispersal system that transported local and distant sediment sources along the Ancestral Rockies was operational during the Late Paleozoic. Areas of eolian recycling observed in the Ingleside and Molas Formations points towards eolian systems playing an important role in transportation of distally-sourced zircons during Late Paleozoic time. Additionally, the U-Pb detrital zircon data indicate that a shift from non-marine to marine deposition across the Fountain-Ingleside transition was accompanied by a decrease in locally-sourced detrital zircons, most likely marking the cessation of Ancestral Front Range uplift. Conversely, the shift from non-marine to marine deposition across the Molas-Hermosa contact was accompanied by an increase in locally-sourced detrital zircons, most likely marking the initiation of the Uncompahgre uplift.

ACKNOWLEDGEMENTS

I am thankful to Sven Egenhoff and John Singleton for encouraging me to constantly push boundaries throughout the research and writing of this thesis. Tireless discussions with and edits from both of them have made this thesis a work that I am proud of.

I would like to acknowledge the Central Minerals Resources team and the Core Research Center at USGS, Denver for their part in assisting me with data that makes up a substantial part of this thesis and for answering my endless questions. A special mention also goes out to CSU alumnus, Scott Larson, for providing me with his maps of the Front Range, making the fieldwork process significantly easier.

I have learned over the course of two years that it takes a village to research and write a thesis and I would like to thank friends and peers at CSU for being mine. A very warm thank you to Andy Auer, Evan Strickland, and Kathryn Schuller for being supremely enthusiastic field assistants and to Nikki Seymour for all her help while I was still learning the particulars of zircon geochronology.

Finally, a very special thank you to my family for their patience and humor through it all.

TABLE OF CONTENTS

PART 1: FACIES RECONSTRUCTION OF THE INGLESIDE/CASPER FORMATION

INTRODUCTION

Mixed carbonate-siliciclastic systems are known to be sensitive to allocyclic changes, such as variations in sea-level, climate, and tectonics (Wilson, 2008; Schwarz et al., 2016). In most cases, these governing parameters are strongly interlinked, and it is difficult to differentiate the effects of each of these variables (Blakey and Middleton 1983; Chan and Kocurek 1988). Although mixed carbonate-siliciclastic systems are only rarely described in literature (Schwartz et al. 2016; Jordan and Mountney 2012), the few studies that center on those sedimentary systems conclude that at least two of these allocyclic controls often go hand in hand: sea-level and climate. Previous approaches to understanding these controls in time-equivalent successions to the here studied Ingleside Formation suggested that regressions and lowstands are often accompanied by arid climate conditions, whereas transgressions and highstands correspond to humid climates (Loope, 1984; Heckel, 1994, Blakey, 2004). Jordan and Mountney (2012) use detailed facies analyses to reach the same conclusion for the basal Permian Cutler Formation in Utah.

The present study introduces the sedimentology of the Ingleside and Casper Formations, a mixed carbonate-siliciclastic succession deposited along the eastern flank of the Front Range of Colorado and Wyoming (Figure 7). The Ingleside and Casper successions are characterized by a distinct cyclic architecture of alternating carbonate and siliciclastic units several meters to tens of meter-thick (Fig. 8). The age of this unit is believed to be lower Permian based on a single finding of one benthic foraminifera (Hoyt and Chronic, 1961). The well-developed cyclicity likely resulted from the waxing and waning ice sheets in Gondwana (Heckel, 2008; Birgenheier et al., 2009). The sedimentological response to these sea-level changes, though, seems to vary significantly across the Laurentian continent depending on the specific climate of the region: Utah and Colorado experienced a rather arid climate during the Late Paleozoic, whereas humid conditions prevailed in Illinois and Kansas. (Joeckel, 1999; Cecil, 2003; Blanchard et al., 2016). Consequently, mid-continent cyclothems contain coals and black shales (Heckel 1986), whereas sediments from the western interior of Laurentia are devoid of organic-rich deposits but contain eolianites and dune deposits (Jordan and Mountney, 2012).

The Ingleside Formation along the Front Range of Colorado shows that two of the three variables that governed this sedimentary system – sea-level and climate, can be clearly separated, and seem to act on different time scales. This mixed carbonate-siliciclastic system is therefore unique in the sense that it does not directly link climate to distinct positions of sea-level. Rather, this study demonstrates that several mixed carbonate-siliciclastic cycles developed prior to a major change in climate that was independent of cyclic short-term sea-level changes. Detailed facies analyses and architecture in this study is based on a total of 13 lithological sections and 75 petrographic thin sections across a 120 km northeast-southwest transect and a 38 km east-west transect. The conclusions drawn enable a better understanding of the sedimentary evolution and preservation of this mixed siliciclastic and carbonate shoreline and nearshore system deposited along the eastern flank of the Ancestral Rocky Mountains.

GEOLOGICAL BACKGROUND

The intracontinental deformation that resulted in the Ancestral Rocky Mountain (ARM) system of western Laurentia is primarily centered on the Pennsylvanian Period. This deformation remains poorly understood and has been recognized as part of a large region of intraplate tectonics. Various models invoke stresses along the Ouachita-Marathon belt, transpressional regimes along the Sonora margin, and reactivation of pre-existing basement faults to explain ARM deformation (Kluth and Coney, 1981; Marshak et al, 2000; Dickson and Lawton, 2003; Leary et al., 2017).

Synchronous with the tectonism, the Late Paleozoic was a time of southern hemisphere glaciation in Gondwanaland. The resultant global icehouse conditions and eustatic sea level changes led to deposition of cyclic stratal sequences throughout the western United States (Crowell, 1978). Sea level lows at this time were primarily characterized by eolian dune deposits over most of the western United States, while sea level highs were characterized by cyclic alterations of limestone and shale formations (Heckel, 1986; Blakey, 2008).

In present-day Colorado ARM tectonic uplifts developed during this time include the Apishapa highland, Uncompahre highland, and Ancestral Front Range highland (Mallory, 1960; Curtis, 1958). Of these, the Ancestral Front Range highland extended from the present-day Sangre de Cristo Mountains in southern Colorado to the present-day Sierra Madre in south-central Wyoming (Tweto, 1980; Maughan, 1993).

Adjacent to the Ancestral Front Range Highland lay a shallow-marine basin wherein the Pennsylvanian seas transgressed from the north and east (Blakey, 2008; Curtis, 1958; Williams, 1962; Tenney, 1963). Vigorous uplift of the Ancestral Front Range Highland around the Middle Pennsylvanian time resulted in extensive erosion of previously deposited Pennsylvanian and Mississippian sediments (Eardley, 1951; De Voto, 1980). Great quantities of arkose were deposited in alluvial fans and braided stream systems adjacent to the uplift. These deposits, collectively identified as the Fountain Formation, were deposited directly upon Precambrian crystalline rocks and thin abruptly towards the northeast (Knight, 1929). The advancing sea during the Late Pennsylvanian resulted in partial marine erosion of the Fountain Formation and subsequent deposition of sandstone and interfingering carbonate units of the Casper and Ingleside Formations. The entire extent of the Ingleside Formation in Colorado overlies the Fountain Formation. The Casper Formation in Wyoming, on the other hand, interfingers with the Fountain Formation up to a point where the Fountain Formation thins out. Further north, limestone deposits of the Madison Formation directly underlie the Casper Formation (Tenney, 1963).

Lee (1927) traced the Fountain Formation and overlying Ingleside Formation from Colorado to central Wyoming and concluded that the greater part of the Casper Formation is continuous with the Ingleside Formation. Agatston (1954), Knight (1929), and Miller and Thomas (1936) suggested that the Fountain Formation represented a river system that was deposited in an advancing Pennsylvanian sea and that the Fountain and Casper Formations are, in part at least, contemporaneous. Knight also concluded that the Ingleside Formation is equivalent to the upper part of the Casper Formation. These studies were initially based on sparse fossil data and long distance correlations (Maughan et al., 1961). This relationship was later also established based on Wolfcampian fusulinids in the Ingleside Formation (Hoyt et al., 1961) and equivalent strata of the Upper Casper Formation, while fusulinids from the Fountain Formation and Lower and Middle Casper Formation were found to be older and ranged in age from Virgilian to Missourian (Chronic, 1958; Burns and Nestell, 2009). Beveling of the Casper and Ingleside Formations along the flanks of the Ancestral Front Range was a result of the uplift and subsequent vigorous erosion at the time (Maughan, 1980).

In Late Pennsylvanian and Early Permian times, the Ancestral Rocky Mountain uplift stabilized and slowly declined. Chronic (1958) suggested that this decline was accompanied by a fall in relative sea level and a gradual change in climate from humid with alternating semi-arid intervals to more arid conditions. Climate at this time resulted in deposition of cross-bedded, eolian sandstones that make up the upper parts of the Ingleside and Casper Formations (Maughan et al., 1960).

A sharp contact separates the eolian sandstones of the Ingleside and Casper Formations from overlying Early Permian age mudstone and very fine-grained sandstone of the Owl Canyon Formation. This contact marks a gradual rise in sea level, and the overlying siliciclastic mudstone-dominated deposits are representative of a tidal flat complex reflecting renewed sea-level rise (Howe, 1970; Maughan, 1980).

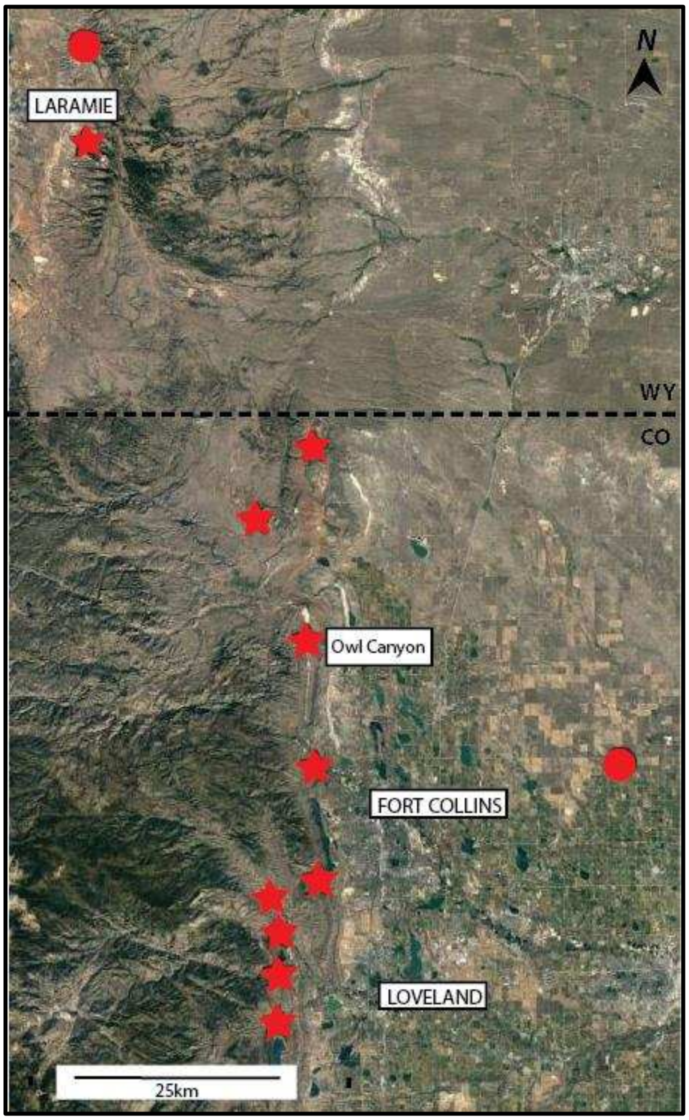

Figure 1: Location of measured outcrop sections and drill cores. Stars mark outcrop sections and circles mark drill core sections.

FACIES IDENTIFICATION

Facies 1: Cross-bedded Sandstone

Description

The cross-bedded sandstone facies is composed of calcite-cemented, fine-grained, quartz-rich sandstones that are typically normally graded. Open intergranular porosity can be as high as 10%. Thirty-three paleocurrent analyses data from the type section at Owl Canyon reveal that the cross-beds dip at shallow angles that range between 10^{o} and 30^{o}, and the mean dip azimuth is 131° (Figure 2C). This facies typically overlies or underlies horizontally-bedded sandstones with gradational or sharp contacts.

Based on the geometry of the crossbeds, two subfacies have been identified.

1A. Tabular Cross-bedded Sandstones

Sets of cross-laminated sands are separated by bounding surfaces and form lenticular or wedge-shaped units that are commonly a few centimeters thick. Fine to very fine, well-sorted, and rounded to sub-angular sand grains make up the cross-laminated strata. The bounding surfaces are composed of fine to very coarse, moderately rounded to angular, poorly-sorted sand grains (Figure 2A). The sandstones are commonly quartz arenites, usually comprising less than 1% feldspar and mica particles. In some places, however, this subfacies can contain up to 5% muscovite flakes. Rarely, skeletal fragments and carbonate aggregate grains occur.

1B. Trough Cross-bedded Sandstones

Sets of centimeter- and meter-scale concave upward cross strata occur locally and make up discontinuous units of the trough cross-bedded sandstone facies. Typically, this subfacies is composed of well-sorted, rounded to sub-angular grains that range in size from coarse silt to fine sand (Figure 2B). In places, the sand and silt grains are visibly segregated into fine laminations that are usually between 1mm and 5mm thick. Compositionally, the sandstones are quartz-rich with up to 5% feldspar and mica particles. When observed in core, the cross laminae within these trough units are thickest along the deepest points of the troughs and continuously thin towards the edges. The fine-grained population is also noted to form darker colored laminae than the over- and underlying coarse grained sediments.

Interpretation:

The cross-bedded sandstones of Facies 1 indicate deposition in a lower flow regime environment as shown by the presence of cross beds in both sub-facies. Internal laminations reflect short fluctuations in energy conditions, with the dominance of fining-upward laminae suggesting settling of progressively finer particles in decelerating flow conditions. This facies commonly overlies horizontally-bedded sandstones of Facies 2, further indicating a decrease of flow velocity from upper to lower flow regime conditions. The inclination of the cross beds shows that sediment transport was preferably from the north and west during deposition.

1A. Tabular Cross-bedded Sandstone.

The tabular cross-beds of Subfacies 1A are here interpreted to represent dunes formed in a marine environment. This environment contained two clearly separate grain populations: the fine, rounded to subangular, well-sorted sand reflects a greater transport path and abrasion in comparison to the coarse, moderately-rounded to angular, poorly-sorted sand. It seems most likely that the coarse-grained sand making up the lower portion of the sandstone laminae represents particles introduced only a short time before deposition whereas the fine-grained sand reflects intense reworking and abrasion, either within or outside of this sedimentary system. The arrangements of these two populations of grains into single laminae, however, also indicates that deposition occurred in pulses of varying energy: relatively high-energy moved and laid down the coarse grains, whereas slightly lower energy resulted in deposition of the fine grains. It seems reasonable to assume that at least one of the sources of the sediment, likely the coarse-grained sand fraction, originated from crystalline basement; this origin is still reflected in the muscovite flakes that locally blanket individual bedding planes in Facies 1A.

1B. Trough cross-bedded Sandstone

The trough cross-bedded sandstones of subfacies 1B are most likely a result of local dunes formed in an eolian environment. Two separate grain size populations are recognized in this subfacies and they were likely deposited by two different processes. Fine sand particles were possibly carried up the stoss side of the dune by saltation and creep, while very fine to coarse silt particles were transported by suspension. As wind velocity gradually decreased, fine sand particles accumulate in the troughs, followed by silt and very fine sand grains settling out of suspension. It is likely that the fine grains fell between the interstices of stationary coarse sediments, preventing them being picked up by further airflow (Fryberger and Schenk, 1988). Sediments thus sheltered from further migration result in the two separate grain populations observed in this subfacies. This sequestering of small population of very fine sediments and bimodal grain size distribution is characteristic of most eolian depositional systems (Brookfield, 1977; Hunter, 1977; Fryberger and Schenk, 1988). The darker color associated with the finer grained sediments in this subfacies is most likely due to the presence of clay.

Facies 2: Horizontally-bedded Sandstone

Description

The horizontally bedded sandstone facies (Facies 2) is characterized by millimeter- to centimeter-scale internal laminations and displays sharp to gradational contacts to over- and underlying beds. Beds of this facies generally display a tabular geometry in outcrop and range in thickness from 1-20 cm (Figure 3A). Individual laminae of this facies are usually horizontally continuous, composed of moderately sorted fine- to very fine-grained, mostly quartz sand, along with quartz and calcite clasts between a few millimeters and 2 cm in diameter. Laminations are typically only a few grain diameters thick. Most of the laminae display a well-defined fining upwards trend. Coarsening upwards are rare and composed of coarse sand to granule-sized particles of quartz, calcite, and feldspar at the base of each lamina, grading into fine- and very fine-grained sandstone at the top. Texturally, these sandstones are well sorted. Sets of these sandstones typically underlie, and in some places overlie cross-bedded sandstone packages of Facies 1. In places, carbonate skeletal fragments and/or aggregate grains occur. Diagenetic carbonate concretions between 1-12 centimeters thick are also present as prominent features within this facies.

Interpretation:

The laterally persistent plane beds that are characteristic of Facies 2 appear to mark deposition of sand sheets under upper flow regime conditions as indicated by the planar laminations. The regularity of the flat bedding surfaces and lack of bed irregularities point towards an environment with only gentle topography. The flows were depositing sediment in pulses showing varying flow velocities which is reflected in the stacking of laminae in this facies; similarly, most of these pulses likely represents decelerating flows which resulted in the dominance of fining-upward laminae in Facies 2. Nevertheless, some of the flows must have accelerated, too, thereby depositing the rarely occurring coarsening-upwards laminae. Alternatively, shifts in boundary shear stress conditions may have resulted in the observed planar laminations (Allen, 1984), whereby coarsening upward laminae reflect an increase in shear stress associated with large eddies in the flow (Cheel and Middleton, 1986). It is assumed that the lithic and skeletal fragments represent oversize clasts that are likely exotic to the environment. The skeletal fragments may have been eroded from laterally exposed carbonate deposits, and re-deposited in Facies 2. The lithic fragments, however, most likely originated from the Ancestral Rocky Mountains (cf. Dickinson and Lawton, 2003) and were transported as bed load in these relatively high-energy flows.

Facies 3: Massive Sandstone

Description:

Massive, fine-grained, quartz-rich, well sorted, calcite-cemented sandstones form laterally continuous packages of regular thickness, ranging between 1m and 2.5m. They commonly over- or underlie cross-bedded sandstones (Facies 1) or horizontally bedded sandstones (Facies 2) and are separated from them by gradational contacts. In some places, massive sandstone beds are found underlying siliciclastic mudstone (Facies 6) units with a sharp or erosional contact in-between. This facies displays fluid escape structures in some places and is moderately to heavily bioturbated (Figure 3B).

Interpretation:

Regular geometry and lateral continuity of the massive sandstone indicates that deposition took places on regular surfaces under essentially constant physical conditions. The presence of fluid escape structures and bioturbation in this facies makes it plausible that sedimentary structures, if originally present, have been destroyed by reworking of the sediment by organisms and/or liquefaction. The structureless character of this facies therefore is interpreted to be a result of secondary processes. The presence of abundant burrows also points to a well oxygenated depositional environment for this facies.

Facies 4: Conglomeratic Sandstone

Description:

The conglomeratic sandstones of Facies 4 are typically dark red or purple in color and appear as discontinuous lenses with sharp bounding surfaces. This facies typically displays thickness less than 2m meters and width less than 3 meters. A concave-up to irregular, erosive base and a convex-up to planar top are distinctive characteristics of this facies (Figure 3C). Laterally, these lenses are no more than 3 meters wide and taper out into fine-grained sandstones of Facies 1B or 2. Planar laminations are weakly developed or absent, and weak normal grading is observed in some places. Compositionally, this facies consists of medium-grained sand, granules, and pebbles less than 0.5 cm in diameter, embedded in a fine-grained sand matrix. Sediments are typically poorly sorted, subrounded to angular and include quartz clasts and lithic fragments. Subrounded chert nodules, a few millimeters to 2cms in diameter, are observed in some places.

Interpretation:

Laterally discontinuous conglomeratic sandstone lenses of Facies 4 reflect irregular pulses of high energy conditions during deposition. Poorly sorted, coarse, and dominantly angular grains point to short sediment transport paths. It is reasonable to conclude that the Ancestral Rocky Mountains are the primary sediment source for this facies. Sediments were likely transported as bed load, eroding and incising into underlying fine sand dominated bed (Miall, 1985). This bed load transport developed the concave up to irregular, erosive base characteristic of Facies 4. As gravel and sand deposits aggraded over time, it resulted in the convex upward top (c.f. McGowen and Groat, 1971). Additionally, planar lamination points to deposition in an upper flow regime condition, and weak normal grading is indicative of a gradually decelerating flow.

Facies 5: Ripple-Laminated Sandstone

Description:

Ripple laminated, fine-grained sandstones occur locally and are observed in association with cross-bedded (Facies 1) and horizontally bedded sandstone (Facies 2) or siliciclastic mudstone (Facies 6) units. Based on the type and geometry of ripples, three subfacies have been identified:

5A. Asymmetric Current Ripples:

Centimeter-scale beds displaying moderately asymmetrical current ripples are found overlying horizontally laminated sandstones. Ripple crests are generally broad and rounded and the troughs are narrow. The stoss and lee sides display a straight to convex-up profile (Figure 3D). These structures occur as sinuous crests or lingoids, and ripple height ranges between 1cm and 3cms.

5B. Moderately-Steeply Climbing Ripples:

Moderately-steeply climbing ripples occur in centimeter-scale beds and are observed interbedded with or overlying silt-rich siliciclastic mudstones (Facies 6) and separated from them by erosional contacts. Composed of fine-grained sand sediment, the climbing ripples display heights ranging between 1cm and 3cms, and angles of climb between 10^{o} and 30^{o}. Distinct lee side laminae are observed in this subfacies, while stoss side laminae are wholly or partially absent (Figure 3E).

5C. Gently Climbing Ripples:

Gently climbing ripples make up beds that range from a few centimeters to 3m in thickness and are composed of medium-grained sand to silt- sized sediments. This subfacies commonly under- or overlies trough cross-bedded (Facies 1B) or horizontally bedded (Facies 2) sandstones. Typically, these ripples display low angles of climb that range between 0^{o} and 5^{o} and ripple heights less than 2mm. In outcrop, these ripples are best described as laterally continuous, with long, parallel to subparallel crests. Internal cross laminations are lacking within the ripples that make up this subfacies. In some places, fine-grained laminae stand out at greater relief than adjacent coarse-grained laminae (Figure 3F).

Interpretation:

5A. Asymmetric Current Ripples:

A low energy depositional condition is suggested for this facies based on the fine-sand grain size and small ripple heights. The general asymmetric profile, rounded crests, narrow troughs, and biconvex flanks of these ripples are characteristic of a unidirectional-dominant flow (Dumas et al., 2005). Ripples of this form are indicative of a general lower flow regime (Simons et al., 1965), with increasing energy conditions evidenced in the tendency of ripple crests to become discontinuous and transition from sinuous to lingoid ripples.

5B. Moderately-Steeply Climbing Ripples:

The formation and preservation of climbing ripples is an indicator of rapid rates of sedimentation under the action of unidirectional currents. Ripples in this subfacies do not display the steep angles of climb commonly found in climbing ripples sequences that originate by fall-out from suspension (Ashley, 1982). It is likely that these ripples were dominantly developed when bedload transport rates over migrating ripples decreased downstream. Bedload transport processes are further evidenced by the lack of grain size segregation that is typical of this subfacies and the erosional contacts that separate these ripples from underlying beds. Based on depositional energy conditions and the general association of this subfacies with siliciclastic mudstones of Facies 6 these ripples are interpreted to have been deposited in shallow marine conditions.

5C. Gently Climbing Ripples:

Low angles of climb documented in this subfacies indicate deposition on gently-sloping surfaces. Great crest lengths are typical of wind ripples and is attributed to the tendency of individual wind ripples to persist during long distances of migration (Hunter, 1977). Further, fine-grained individual laminae standing out at greater relief to adjacent coarse-grained laminae are a distinctive feature of eolian sediments known as pinstripe laminations. They are presumed to be a result of coarse-grained laminae losing moisture more rapidly and weathering more readily, leaving the fine-grained laminae in relief (Fryberger and Schenk, 1988).

Facies 6: Silt-rich Siliciclastic Mudstone

Description:

The siliciclastic mudstone facies (Facies 6) occurs in thin beds, typically as thin as 5-15 centimeters, and in some places reaching a thickness of 60 centimeters to a meter. The mudstone beds are distinctively dark red in color and, based on correlation, laterally continuous for several kilometers (Figure 4C). Generally, structureless mudstones are intercalated with submillimeter thick, subparallel to wavy laminae of fine-grained sand and silt. The laminae are commonly not well-defined and tend to display irregular lateral thicknesses. Locally, millimeter-scale siltstone ripples with mud- and siltstone foresets are observed (Figure 4B). Minor amounts of bioturbation in the form of vertical or horizontal burrows occurs in this facies locally (Figure 4A). Generally, horizontal burrows are submillimeter-scale to 2mm in diameter, unbranched, and lenticular shaped. Vertical burrows are indistinct, submillimeter-scale, and cut across the laminations. Admixtures of silt and very fine-grained sand comprise anywhere between 20% and 50% of this facies. Beds of Facies 6 are commonly found overlying horizontally bedded (Facies 2) or climbing ripple-laminated sandstones (Facies 5C), and in some places overlie carbonate mudstones of Facies 7. Sharp or erosional contacts separate this facies from overlying and underlying units.

Interpretation:

Based on the accumulation of two grain size populations and observed sedimentary structures, the deposition of this facies was likely the product of two different processes and energy conditions. Suspension settling could be the process by which some, though not all of the mudstones were deposited. Even though no unequivocal evidence for this depositional process exists the massive nature of the mudstones may be a result of relatively rapid settling of mudstone floccules from the water column. Nevertheless, bed load transport also played a role in depositing this facies: the irregular lateral thickness of mud and silt laminae, and the local presence of mud- and siltstone ripples suggest influence of advective flow during deposition (cf. Schieber et al., 2007; Egenhoff and Fishman, 2013). Bioturbation further points to an oxygenated environment of deposition which is also suggested by its red color. Nevertheless, its intercalation with sand- and silt-bearing facies throughout the measured sections, and the presence of sand- and siltstone laminae in these mudstones point towards a setting relatively close to the shoreface. The depositional environment suggested for this facies was likely below fair weather wave base but within the reach of currents that were responsible for the offshore transport and deposition of the sandy and silty laminae.

Facies 7: Carbonate Mudstone

Description:

The carbonate mudstone to wackestone facies (Facies7) occurs as meter-thick beds forming units of between 2m and 45m in thickness. In some places, randomly oriented skeletal fragments and sand- and silt-sized quartz carbonate grains comprise between 5% and 30% of this facies. Horizontal burrows of submillimeter-scale diameter~~s~~ occur locally, are infilled with carbonate mud, and comprise 2-5% of this facies (Figure 5B). In some places, patches of light and dark micrite are observed. Spherical to subspherical, millimeter to centimeter sized, isolated vugs, are irregularly dispersed throughout this facies. These are either partially or completely filled with quartz cement or evaporite minerals, or comprise open porosity. This facies typically overlies coarse-grained carbonates of facies 8 and 9, horizontally-bedded sandstones (Facies 2), and tabular cross-bedded sandstones (Facies 1A). Sandstone units belonging to Facies 1A and 2 typically overlie this facies. However, in some places, carbonate packstones of Subfacies 8A and 9A are also observed as overlying units. Sharp contacts characteristically separate this facies from overlying and underlying units (Figure 5A).

Interpretation:

This facies represents a low energy environment which is reflected in the dominance of carbonate mud. It was most likely deposited below storm wave base as no clear tempestites are preserved. Nevertheless, some of the skeletal fragments may have been broken, partly abraded and concentrated through currents forming the wackestones, and these may represent thin storm beds. However, the diffuse bioturbation in these rocks has obliterated all original sedimentary fabric, and therefore no clear interpretation of the origin of these shell concentrations is possible. It seems plausible that this facies was deposited at a distinct distance from the shoreline as only small amounts of siliciclastic debris in the form of quartz grains is present. The quartz grains, nevertheless, are significantly larger than the carbonate mud, and are therefore also interpreted as originating from the nearshore environment. They were most likely brought into the system by offshore-directed, storm-induced currents (Wilson et al., 2013).

This facies is likely highly bioturbated even though clear individual burrows are rarely preserved. The bioturbation is reflected in the random orientation of lithoclasts and skeletal fragments (cf. Egenhoff et al., 2010). Coarse sand-sized quartz grains are embedded in carbonate mud and must have brought into the system by high-energy. It is suggested that the quartz grains originally formed laminae before they were randomly dispersed in the mud by organisms. The apparent lack of distinct burrow traces is most likely a function of a low contrast in color and sediment texture between the burrows and surrounding matrix (Berger et al., 1979). However, the light color as well as the likely high bioturbation index inferred from grain distribution and orientation of skeletal fragments indicates an overall well-oxygenated depositional environment for this facies. The vugs that are characteristic for this facies most likely originated from a dissolution event during diagenesis (cf. Clark, 1986).

Facies 8: Carbonate Packstone

Description:

Highly variable in bioclast and non-skeletal components, Facies 8 occurs as beds that range in thickness from 0.5m to 5m. Based on the predominant components, two subfacies have been identified:

8A: Carbonate Packstones with Non-Skeletal Grains:

Carbonate packstones observed across the study area dominantly belong to this subfacies. Spherical to subspherical, submillimeter-scale ooids comprise up to 25% of this subfacies. They are commonly heavily recrystallized and only partly display internal structures. Broken shells, commonly showing a micritic rim, occur in varying abundances that range from 5% to 20%. Less prominent grains include oncoids (5-10%), and fine-sand sized, angular to subrounded quartz and calcite (1-5%). Heavily micritized, ellipsoidal, millimeter-scale aggregate grains composed of lithoclasts and/or bioclast fragments occur locally. All skeletal and non-skeletal grains are randomly oriented and show even distributions throughout beds of this subfacies. All grains in this subfacies are moderately sorted. As much as 50% of the carbonate packstones with non-skeletal grains is composed of carbonate mud (Figure 6A). Typically, this subfacies is overlain and underlain by beds of carbonate mud- to wackestones (Facies 7), tabular cross-bedded sandstones (Facies 1A), or massive sandstones (Facies 3), and is separated from them by sharp contacts.

8B: Carbonate Packstones with Bioclasts:

A diverse assemblage of poorly sorted and randomly oriented skeletal fragments, ranging in size from submillimeter-scale to 4mm, and generally occurring in abundances of 30%-40% define subfacies 8B (Figure 6B). Bioclasts include brachiopods, gastropods, bryozoans, trilobites, echinoderms, fusulinids, and other foraminifera. Rounded to sub-angular, fine sand-sized grains that are predominantly quartz occur in small abundances of up to 3%. Carbonate mud makes up 60-70% of this subfacies. Beds of carbonate packstones with bioclasts occurs only locally in the study area and display an upward fining into carbonate wackestones of Facies 7. This subfacies is generally underlain by massive sandstones (Facies 3) and separated from them by a sharp contact.

Interpretation:

8A: Carbonate Packstones with Non-Skeletal Grains:

The diverse assemblage of non-skeletal and skeletal components occurring in this facies is interpreted to originate from various depositional environments, most likely reflecting varying energy conditions.

Especially the mixing of the dominant carbonate grains with the quartz sand suggests varying origins for the grain types in this setting, a siliciclastic environment for the quartz, and a variety of carbonate settings for the non-skeletal and skeletal grains. Even more striking, the strongly bimodal distribution of this facies with the grains on the coarse end, and the carbonate mud on the fine end, reflect strongly fluctuating energy conditions during deposition of this facies. The coarse-grained carbonates and the quartz sand reflect high-energy deposition with transport mechanisms that most likely involved bedload processes in order to transport particles that size. The carbonate mud, in contrast, represents intervals when low energy deposition prevailed. It is unclear, though, whether this carbonate mud was transported by suspension settling as often suggested for packstones (Lehrmann et al., 2001; Boggs, 2005), or by bedload transport as proposed by Schieber et al. (2013). The micritic rim observed around many of the particles is likely a result of degradation by microbes destroying the outer laminae of individual particles (Reid et al., 1992).

8B: Carbonate Packstones with Bioclasts:

The presence of fragmented skeletal material and subrounded quartz grains indicate that the grain portion of these packstones were most likely deposited in a high-energy regime responsible for both breaking the shells and rounding the quartz grains. Nevertheless, the poor sorting of the carbonate grains being the dominant components of Facies 8B indicates that different energy levels most likely contributed to the observed size distribution. The lack of micritic rims around all carbonate grains also suggests that abrasion during deposition likely eroded them off if they had been developed around some grains, and that these carbonates must have been deposited in an agitated environment. The quartz grains, in contrast, must have originated from a nearby siliciclastic environment, and being swept into the packstone depositional setting. All of the carbonate and quartz grains are envisioned to have been transported predominantly by bedload processes as suggested by their sizes. Nevertheless, the carbonate mud that makes up a significant portion of this facies indicates overall low-energy sedimentation which is in stark contrast to the high-energy deposition of the grains. It is likely that this mud was either deposited from suspension (cf. Lehrmann et al., 2001) or bedload (Schieber et al. 2013), but in case of the latter nevertheless from a much lower-energy current than the ones depositing the grains. The transition from the packstones of Facies 8B to overlying wackestones is interpreted to represent an overall decrease in energy and, when occurring in centimeter- to decimeter-scale beds, likely shows deposition by waning currents that originated during storms.

Facies 9: Carbonate Grainstone

Description

Carbonate grainstones in the study area typically occur in laterally discontinuous packages up to 4m thick. Based on the dominance of either non-skeletal carbonate grains or bioclasts, sorting, and grain size, three subfacies are identified:

9A. Oolitic Carbonate Grainstone:

Oolitic carbonate grainstones make up laterally discontinuous units across the stratigraphic succession and range in thickness between 0.5 and 3m. Up to 60% ooids with small admixtures of skeletal fragments and sand-sized lithoclasts comprise this subfacies. Ooids are generally spherical to sub-spherical in shape and display good to moderate sorting (Figure 6C). The thickness of the cortex varies from greater to less than half the diameter of the ooids, and in places superficial ooids (Carozzi 1964) are dominant. Partial or complete recrystallization and oomoldic porosity are common and may obliterate the internal texture of this facies. Admixtures of skeletal fragments generally make up between 1 and 2% of the facies. Ooids and skeletal fragments both tend to display micritic rims around them. Fine sand-sized quartz and carbonate grains can comprise up to 5% of this facies. Both inter- and intraparticle pore space is entirely occluded by granular and drusy clear calcite cements. Typically, this subfacies is underlain by massive sandstones (Facies 3). Overlying units commonly belong to carbonate mudstones-wackestones facies (Facies 7), horizontally-bedded sandstones (Facies 2) or massive sandstone (Facies 3). Contacts are gradational to sharp.

9B. Well- to Moderately-Sorted Fossiliferous Carbonate Grainstone:

Beds of well- to moderately-sorted fossiliferous carbonate grainstone generally display thicknesses between 0.5 and 4 m and are laterally discontinuous. A diverse population of well to moderately sorted, submillimeter to millimeter sized, randomly oriented, whole fossils and skeletal fragments (Figure 6D) including gastropods, fusulinids, brachiopods, bivalves, bryozoans, algae, and trilobite fragments, make up the grains of this facies. Bioclasts typically display heavy micritic rims and comprise between 40% and 60% of the subfacies. Well to moderately sorted, fine sand-sized grains that are dominantly quartz typically comprise as much as 15% of the sediment. This subfacies is commonly underlain by massive sandstones (Facies 3) and separated from them by gradational contacts. Overlying units include carbonate mudstones-wackestones facies (Facies 7), horizontally-bedded sandstones (Facies 2) or massive sandstone (Facies 3) and upper contacts are gradational or sharp.

9C. Poorly-Sorted Fossiliferous Carbonate Grainstone:

This subfacies shows poor sorting of the fossil and lithoclast components (Figure 6E). A diverse assemblage of heavily recrystallized skeletal fragments and whole fossils make up around 50% of the sediment. Fossil components range in size from submillimeter-scale to 2cms and include fusulinids, gastropods, echinoderms, trilobites, and bivalves. Lithoclasts are dominantly comprised of quartz, along with some calcite and feldspar. They display subrounded to angular grains that range from sand- to granule-size and comprise up to 25% of the subfacies. Shelter porosity infilled with cement or submillimeter-scale broken shells and quartz grains is common. This subfacies is observed at only one stratigraphic section located in Laramie (Figure 7A), where it forms a 1.5m thick unit overlying a massive sandstone and separated from it by a sharp contact.

Interpretation:

9A. Oolitic Carbonate Grainstone:

The grainstones have most likely been deposited by constant movement as reflected in the regular thickness of the ooid laminae, and the fact that the skeletal grains occur exclusively as broken shell fragments. The well to moderate sorting of the grains suggest overall constant energy conditions during deposition. The environment must have consisted mostly of ooids with only minor amounts of hard parts form skeletal organisms that were incorporated in this grainstone. The ooids and skeletal grains were most likely moved exclusively by bed load processes in a constantly agitated environment prior to deposition. However, the micritic rims in this subfacies suggest that this ooid environment did experience some quiescence post deposition, where borers could alter the outermost rims of all grains, ooids, and skeletal fragments (Wilkinson et al., 1985; Margolis and Rex, 1971).

Nevertheless, the quartz sand grains in this facies argue for some amount of detrital input during deposition, likely from a nearby source. Rounded carbonate clasts, in contrast, reflect erosion and reworking, likely of previously deposited micritic carbonate sediments. Whether these sediments were eroded within the realm of deposition of the ooid grainstone or from a nearby setting remains unclear.

9B. Well- to Moderately-Sorted Fossiliferous Carbonate Grainstone:

The wide range of bioclasts and biogens that comprise this subfacies argues for a well oxygenated environment of deposition where a variety of organisms could thrive. Nevertheless, the locally moderate sorting of the components indicates varying energy conditions during deposition. The thick micritic rims around many of the grains also argue for episodic quiet-water conditions that alternated with a high-energy environment that is recorded in the lack of micrite in this subfacies. The thinning and swelling of beds containing Subfacies 9A deposits reflect deposition in bioclastic and biogenic grainstone shoals of laterally varying thickness. These shoals were likely deposited above normal wave base in constantly agitated water as indicated by the absence of micrite. Nevertheless, these grainstone shoals must have been in the vicinity of a siliciclastic source which accounted for the abundance of quartz grains in this subfacies. The well- to moderately-sorted fossiliferous carbonate grainstones did preserve their original mound-like morphology, especially when overlain by fine-grained, low-energy deposits such as the carbonate mudstones and wackestones, but also when overlain by high-energy, horizontally-bedded upper flow regime sandstones.

9C. Poorly-Sorted Fossiliferous Carbonate Grainstone:

The mixture of biogenic grains and siliciclastic detritus reflects deposition of this subfacies at the interface of a carbonate and a siliciclastic environment, nevertheless still in a carbonate-dominated realm. This subfacies did, however, receive abundant input from a nearby siliciclastic setting, as reflected in the abundance of detrital grains. Nevertheless, the large diversity of fossil-derived grain types in this subfacies suggests living conditions were good. The variety of grain sizes present in these grainstones reflects strongly fluctuating energy conditions during deposition. A high-energy environment is likely represented by the granule-size detrital extra-clasts (and to a lesser extent by the quartz sand) that were brought in from an adjacent facies, as well as by the broken nature of several of the grains, and by the lack of micrite. An alternating low(er) energy environment is indicated by micritic rims around many of the grains, and by the presence of up to sub-millimeter grains throughout this facies. Similar to Subfacies 9B it is suggested that the thinning and swelling of beds of this subfacies represents their original shoal-like morphology during deposition.

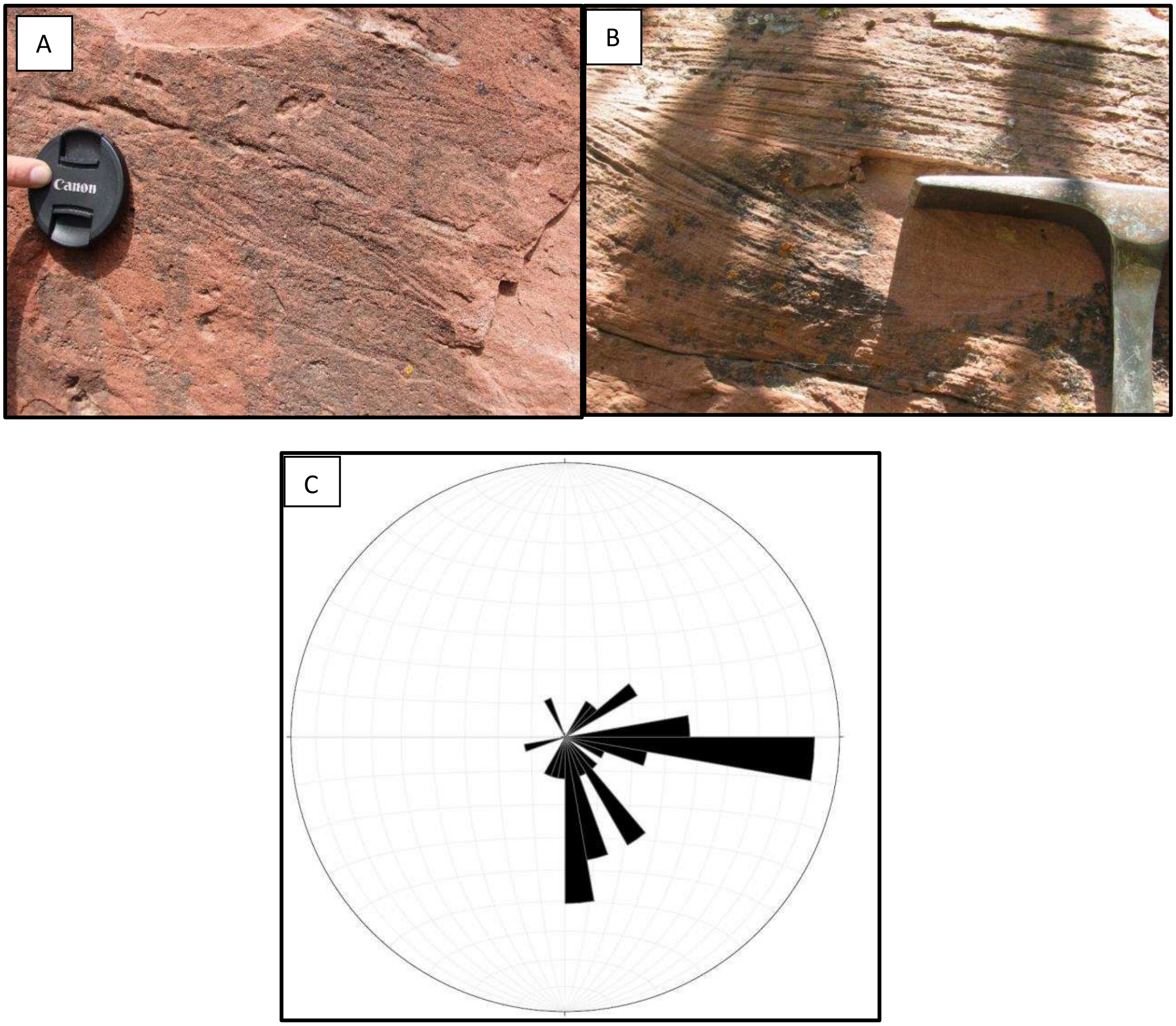

Figure 2: (A) Tabular cross-bedded sandstone (Facies 1A) display sets of cross-laminated sands separated by bounding surfaces. (B) Trough cross-bedded sandstone (Facies 1B) display fine laminations comprised of fine sand and silt grains. (C) Thirty-three paleocurrent analyses from the Ingleside Formation outcrop at Owl Canyon show a dominantly S- and E- sediment transportation direction

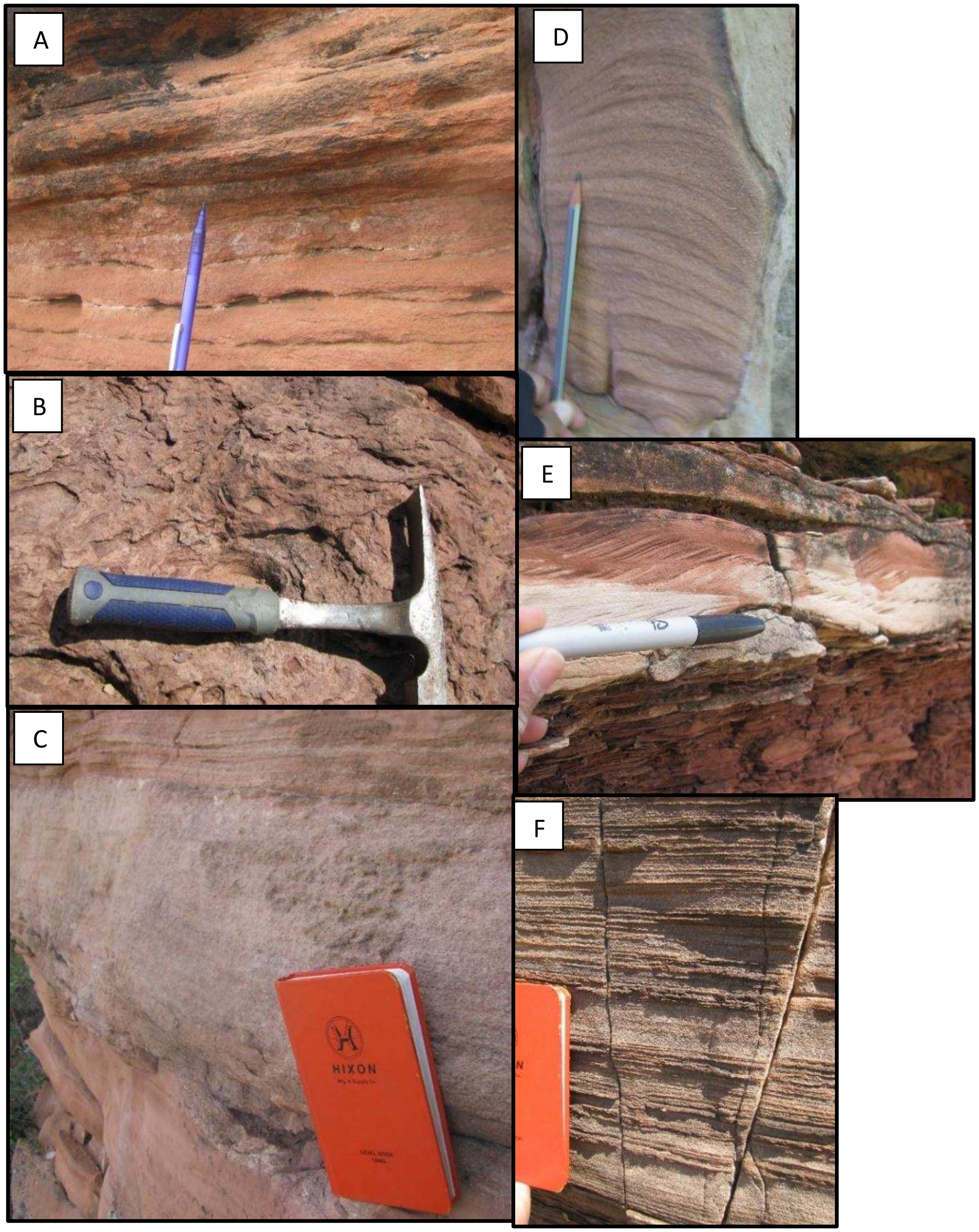

Figure 3: (A) Horizontally-bedded sandstone (Facies 2) comprises thin, cm-scale beds (B) Heavy bioturbation in massive sandstone (Facies 3) beds. (C) Conglomeratic sandstone (Facies 4) typically display irregular, erosive base and planar top (D). Asymmetric ripple-laminated sandstone (Facies 5A) displaying straight to convex-up profiles. (E) Moderately-steeply climbing ripples overlying a siliciclastic mudstone unit (Facies 6) with stoss side laminae partially preserved. (F) Gently climbing ripples with fine-grain laminae in greater relief than coarse grained laminae.

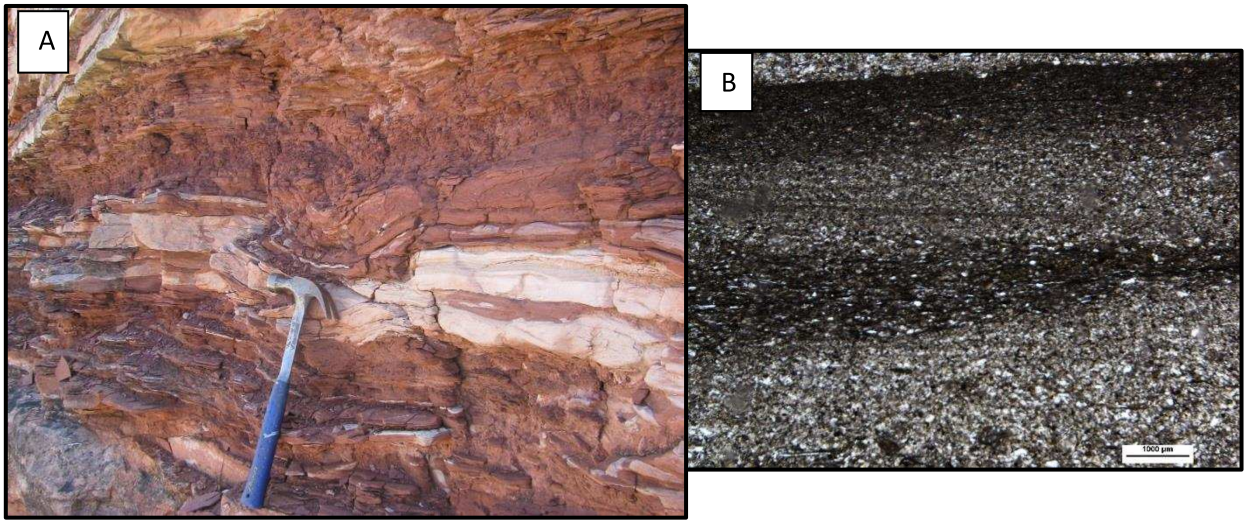

Figure 4: (A) Dark red, laterally continuous units of silt-rich siliciclastic mudstone. (B) Facies 6 is composed of admixtures of silt and very fine sand that make up irregular laminae. Locally display siltstone ripples with mud foresets observed.

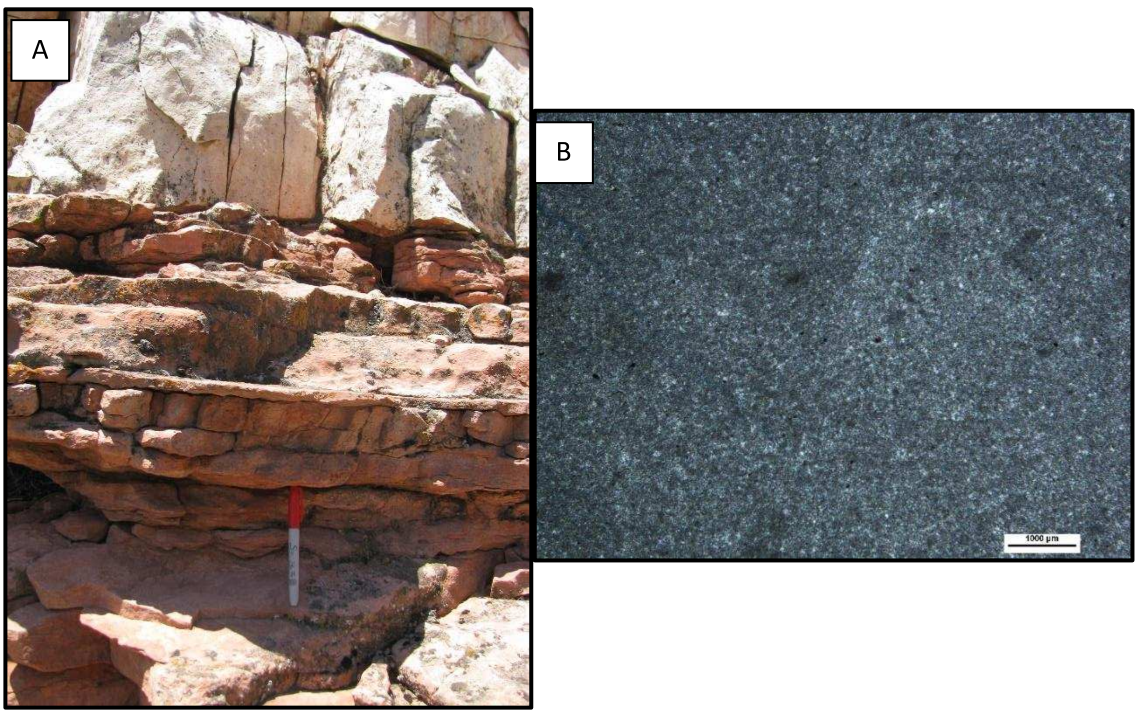

Figure 5 (A) Carbonate mudstone (Facies 7) beds are generally separated by a sharp contact from overlying and underlying sandstone units. (B) Thin section photomicrographs of carbonate mudstone typically show horizontal burrows and light and dark patches of micrite.

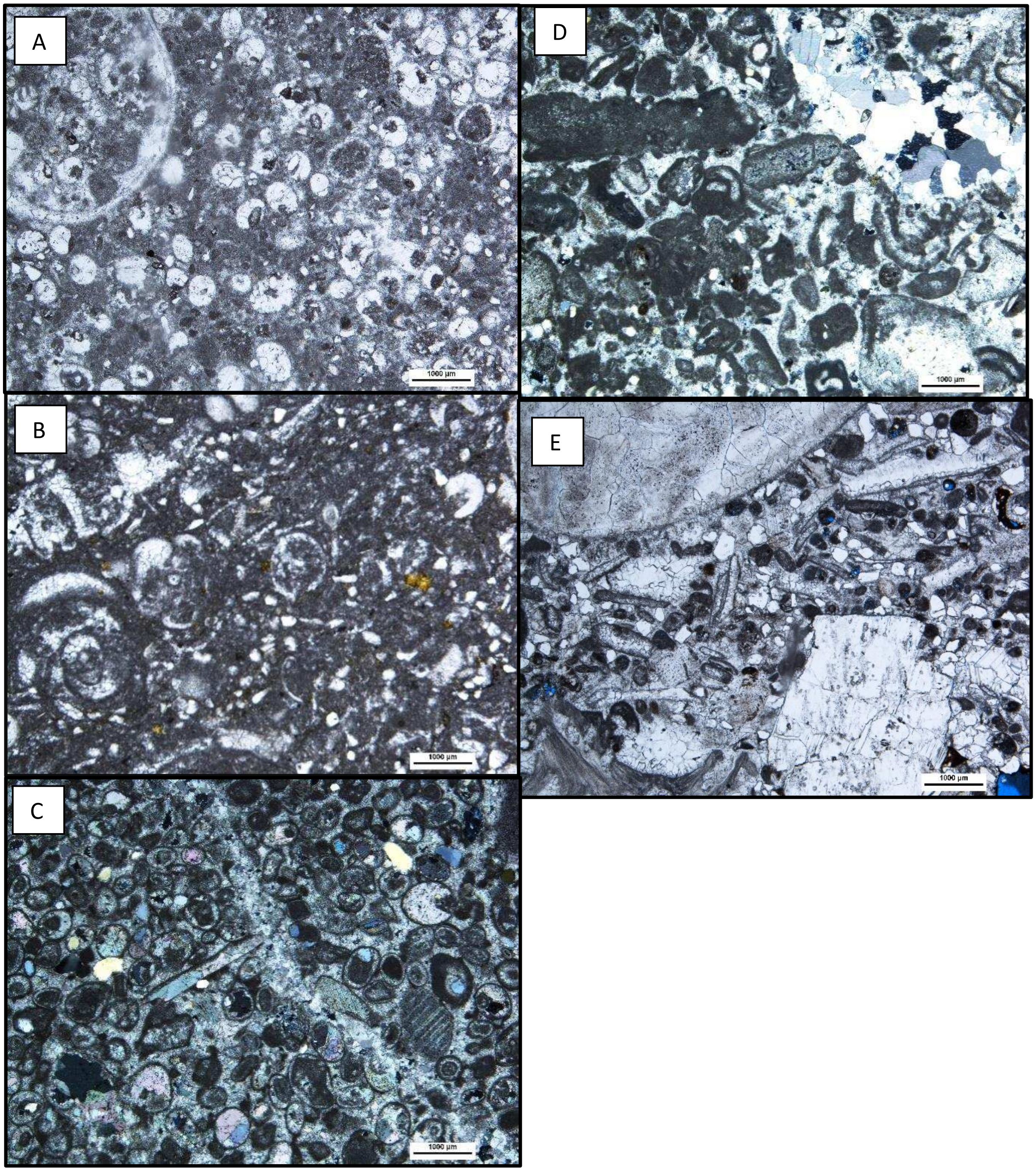

Figure 6: (A) Facies 8A is moderately sorted and dominantly composed of ooids with some bioclast admixtures. (B) Facies 8B shows a diverse bioclast composition, with some lithoclast components. (C) Facies 9A is dominantly composed of moderately sorted ooids, components show thin micritic rims. Photomicrograph depicts recrystallization of oomoldic porosity. (D) Facies 9B shows a diverse component of skeletal fragments that typically display thick micritic rims. (E) Lithoclast and bioclast component of Facies 9C are clearly poorly sorted.

FACIES ARCHITECTURE

The Ingleside (Colorado) and equivalent Casper (Wyoming) Formations are characterized by an intercalation of carbonate and siliciclastic units. Thickness of the stratigraphic sections in our study area generally increase from 5 to 105 meters in the southwest-northeast direction and from 60 to 90 meters in the west to east direction. In this study, the succession is subdivided into eight stratigraphic intervals with each interval displaying a unique lithological assemblage that is either dominated by carbonate facies, dominated by siliciclastic facies, or purely carbonate or siliciclastic. Not all intervals are present in each of the thirteen measured sections. Twelve of the sections form a north-south transect, covering a distance of approximately 120 km (Figure 1). One measured section (Core 1-Upper Ferch) is located 30 km east of this transect, allowing a glimpse into a more carbonate-dominated succession. The eight intervals are generally characterized by a sharp basal contact from carbonates to siliciclastic, or vice versa. Over the lateral distance of 120 km, the north-south transect also reflects a transition from a mixed carbonate-siliciclastic to a purely siliciclastic succession with carbonate units thinning and pinching out towards the south. In this study, the carbonates are subdivided into dominantly fine-grained (Facies 7) versus dominantly coarse-grained (Facies 8 and 9) units. In general, fine-grained carbonates transition laterally into coarse-grained carbonates southwards. Fossiliferous carbonate beds grade into coarse-grained carbonate beds composed of non-skeletal grains in the same direction. The southernmost occurrence of carbonates is in the Bellvue Dome section (Figure 7A).

The basal contact of this unit is often defined by a transition from dark red and purple siliciclastics of the underlying Fountain Formation, to the pink- or orange-colored sandstones of the Ingleside/Casper Formation. The contact of the Ingleside and the underlying Fountain Formation varies southward from gradational to sharp, and is found to occur at stratigraphically higher parts of the Ingleside Formation further south.

The eight stratigraphic intervals that can only be recognized in the northern portion of the northeast-southwest transect are described below. The interval numbers increase upsection, with Interval 1 being the oldest, and Interval 8 the youngest.

Interval 1: At the northernmost section of the study area (Core R114), Interval 1 is composed only of fossiliferous carbonates (Facies 8B and F9B) and mud-supported carbonates (Facies 7). Further south, tabular cross-bedded sandstones (Facies 1A) define the base of the Ingleside Formation. These are overlain by a succession of intercalating units of oolitic carbonates (Facies 8A and F9A) and thin beds of massive sandstones (Facies 3). Stratigraphic sections of this interval display a general fining-upwards trend that in some places is overlain by a coarsening-upwards trend. Interval 1 pinches out between Owl Canyon and Bellvue Dome and cannot be traced further south.

Interval 2: Interval 2 is dominantly composed of tabular cross-bedded (Facies 1A), horizontally bedded (Facies 2), and massive (Facies 3) sandstone beds. Laterally discontinuous, thin units of siliciclastic mudstones (Facies 6) are observed in some places. This interval displays a general fining-upwards trend. The furthest southward occurrence of Interval 2 is at Owl Canyon.

Interval 3: Interval 3 displays a carbonate succession that shows a general fining-upwards trend. The base of Interval 3 is composed of fossiliferous grainstone beds (Facies 9B and 9C) at the northernmost sections (Core R114 and Laramie outcrop), and fossiliferous packstone beds (Facies 8B) further south at Owl Canyon. The coarse-grained basal carbonates are in some place overlain by carbonate mudstones (Facies 7). Similar to underlying intervals, Interval 3 also pinches out at Owl Canyon.

Interval 4: Fining upward, horizontally bedded (Facies 2) to tabular cross-bedded (Facies 1A) sandstones dominate the succession in Interval 4. Thin carbonate beds of mainly carbonate mudstones (Facies 7) interfinger with horizontally bedded sandstone units (Facies 2) or thin conglomeratic sandstone units (Facies 4) in the northernmost sections (Core R114, Red Mountain, Red Nose) of this interval and are absent further south. The southernmost occurrence of Interval 4 is in Bellvue Dome (Figure 7A).

Interval 5: Interval 5 contains a higher amount of mud-supported carbonates (Facies 7) than all underlying intervals. A general lateral transition is observed throughout this interval, from fine-grained carbonates (Facies 7) in the north to coarse-grained carbonates (Facies 8 and 9) in the south. The carbonates transition into sandstones of Facies 1A and 2 in the measured section at Bellvue Dome. This interval pinches out towards the south, and also marks the southernmost occurrence of carbonates at Bellvue Dome.

Interval 6: Interval 6 is distinguished from other intervals by its wide lateral extent. This is notably the only interval that comprises trough cross-bedded (Facies 1B) and gently climbing ripple-laminated (Facies 5C) sandstones. Tabular cross-bedded sandstones (Facies 1A), horizontally bedded sandstones (Facies 2), conglomeratic sandstones (Facies 4) and siliciclastic mudstones (Facies 6) also occur prominently in this interval. This is the only interval can be traced from the northernmost (Core 18-4) to the southernmost (Carter Lake) sections of the study area.

Interval 7: Fine-grained carbonate mudstones (Facies 7) dominate the succession in Interval 7. In two of the measured sections where this interval is observed (Core R114 and Red Nose outcrop), the fine-grained carbonates are intercalated with thin sandstone beds belonging to Facies 2 or 3, and are separated from them by sharp contacts. The southernmost outcrop of this interval is at Owl Canyon.

Interval 8: Lithology of Interval 8 is dominated by fossiliferous carbonate grainstone beds (Facies 9B). This interval is documented only at the northernmost section (Core 18-4) and does not extend laterally across the study area. Thin beds of horizontally bedded (Facies 2) to tabular cross bedded (Facies 1A) sandstones interfinger with the fossiliferous carbonate grainstones (Facies 9B) and are separated from them by sharp contacts.

The eight stratigraphic intervals identified based on the northeast-southwest transect are not well-defined in the easternmost section of this study (Core 1-Upper Ferch). Based on general trends, Intervals 1 to 4 are recognized in Core 1-Upper Ferch (Figure 7B). Nevertheless, the upper 45 meters of this measured section is a thick carbonate mudstone unit that cannot be correlated to lithological assemblages observed westward.

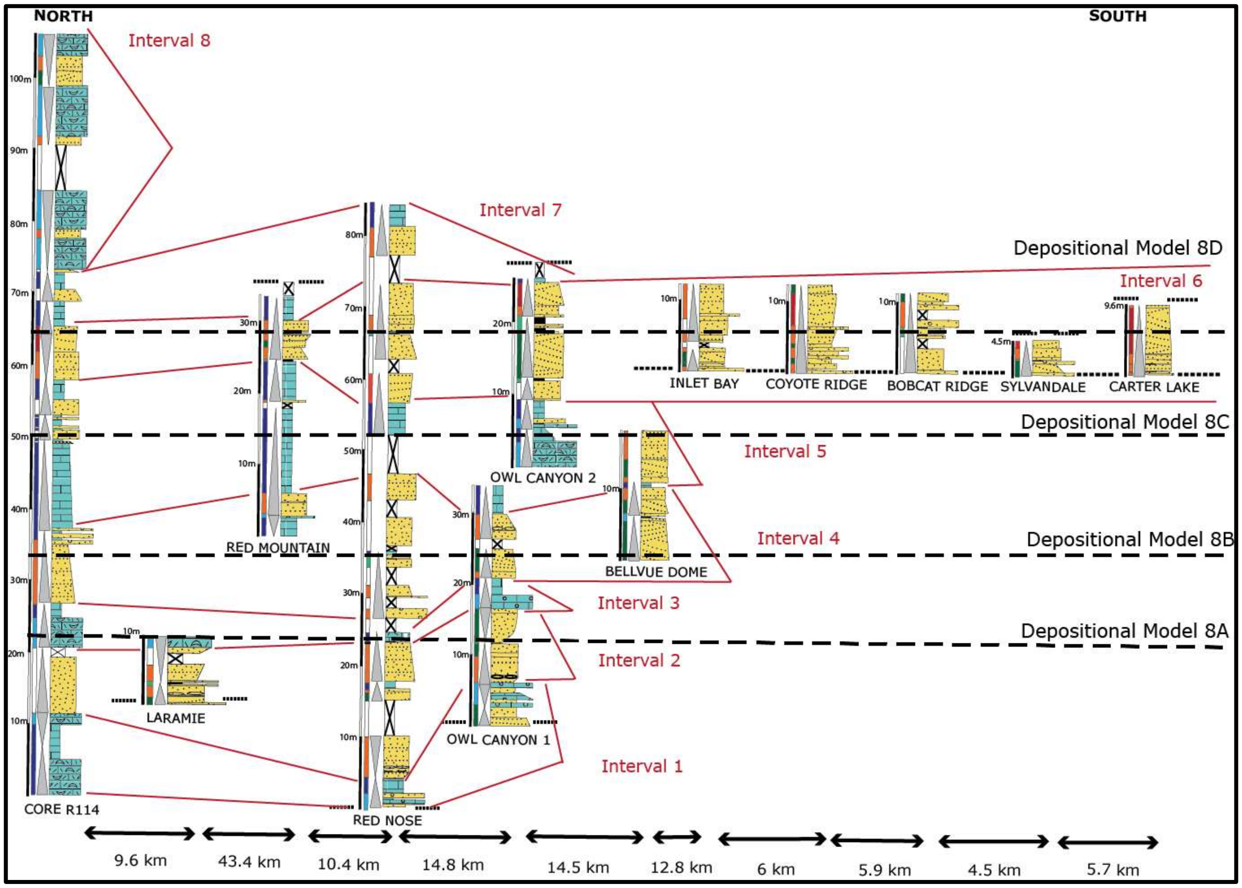

Figure 7A: North-South correlation chart for Ingleside/Casper Formation. Eight broad time intervals are identified based on lithological changes across the stratigraphic successions. Dashed lines define the transects used to construct 2-D depositional models (Figure 8)

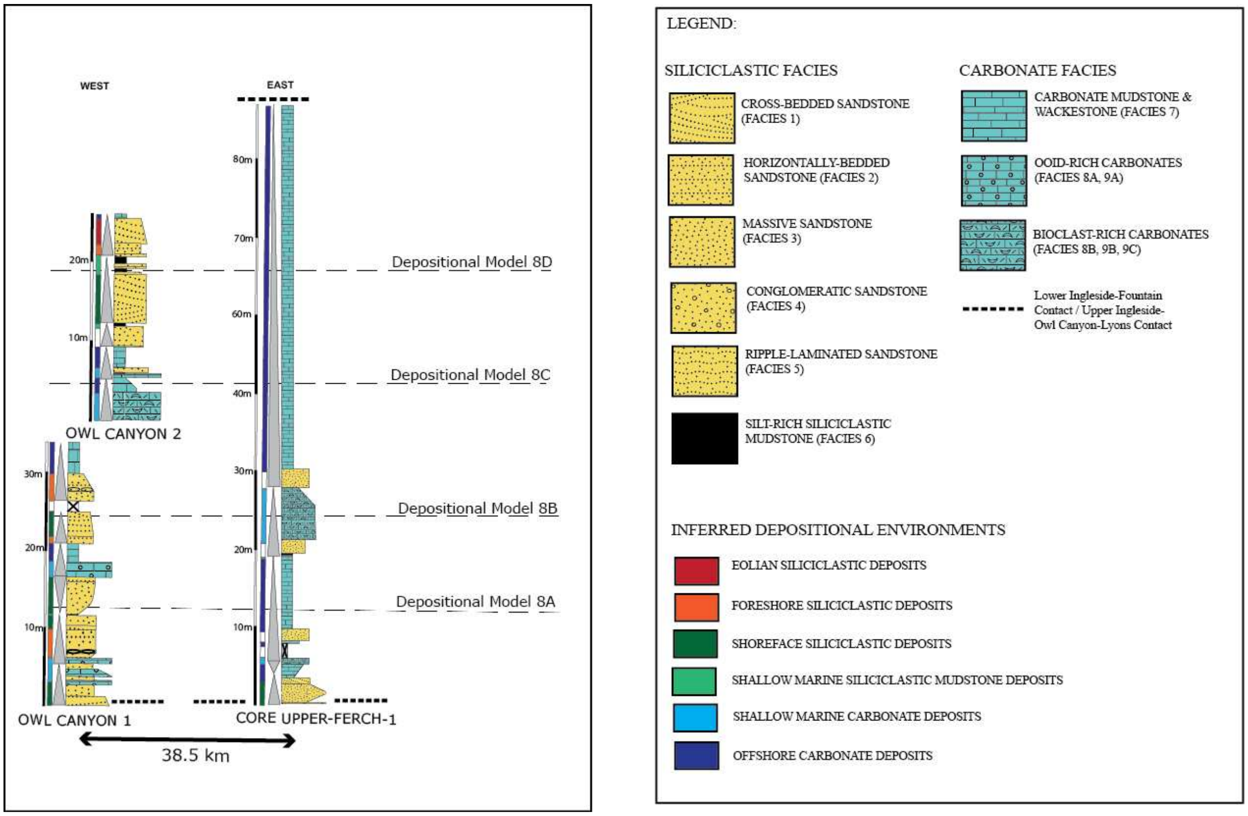

Figure 7B: West-East correlation chart for Ingleside/Casper Formation. Interval 1-4 are identified in the easternmost section (Upper Ferch) based on lithological changes across the stratigraphic sections. Dashed lines define the transects used to construct 2-D depositional models (Figure 8)

Table 1: Latitude-Longitude of measured sections used for N-S and E-W transects across the study area

Measured Section	Latitude	Longitude
Core R114	41°35’7.24’’	-105°50’9.41’’
Laramie	41°16'23.57"	105°29'13.34"
Red Mountain	40°57'37.22"	105°10'23.51"
Red Nose	40°53'10.91"	105°14'57.81"
Owl Canyon	40°45'47.01"	105°10'49.03"
Bellvue Dome	40°37'53.27"	105°10'5.46"
Inlet Bay	40°30'56.57"	105° 9'49.24"
Coyote Ride	40°29'23.46"	105° 9'18.65"
Bobcat Ridge	40°27'39.04"	105°13'2.13"
Sylvandale	40°25'13.12"	105°13'3.34"
Carter Lake	40°22'9.57	105°13'3.60"
Core Upper Ferch-1	40°63'6.52"	104°75'59.13"

DEPOSITIONAL MODEL

The succession of the Ingleside/Casper Formation is interpreted to record deposition from an offshore carbonate ramp (Facies 7,8,9) in the distal reaches of this sedimentary system to a sand-dominated nearshore environment (Facies 1A,2,5A,5B) that was, in places, fed by small fluvial systems (Facies 4). The model, as presented below, is a reflection of the facies succession depicted in the North-South transect (Figure 7A) running roughly parallel to the NW-SE-trending Ancestral Front Range Mountains (Kluth and Coney, 1981) but nevertheless recording all crucial facies changes that are relevant for this sedimentary system.

The facies architecture shows that the Ingleside/Casper Formation was a mixed carbonate-siliciclastic depositional system with dominantly carbonates deposited in the north and east, and siliciclastics in the south (Figure 7A). Based on the fossil content of brachiopods and crinoids (Bottjer and Jablonski, 1987; Tapanila, 2005), the carbonates represent marine sediments. Sedimentary structures such as cross-bedding and ripple marks indicate that the siliciclastics likely reflect both marine as well as terrestrial conditions. The increase in the amount of carbonate sediment to the north and east suggests that the marine incursions came from this direction, whereas siliciclastic input likely originated from the south.

The facies architecture shows that this mixed carbonate-siliciclastic ramp system exhibited two very different facies successions during transgressions and regressions: during transgressions, following the general concept of Vail (1987), little to no siliciclastic input occurred, and sedimentation of carbonates prevailed. In contrast, regressions transported plenty of siliciclastic debris towards the shelf, and the sedimentary system switched to siliciclastic deposition. Eolian dunes are present exclusively during one stratigraphic interval (here termed stratigraphic interval 6, see below), and they are not present during either siliciclastic or carbonate deposition in the rest of the succession.

In the following, the depositional transect will be described from its proximal riverine and foreshore to the most distal environment represented by the carbonate mudstones regardless of whether carbonates or siliciclastics dominated this sedimentary system.

The Terrestrial Setting

The terrestrial environment is interpreted to show exclusively fluvial facies in all stratigraphic intervals except interval 6, which also contains eolian facies.

The eolian depositional system was likely dominated by small crescent dunes (cf. Scherer, 2000), the remnants of which are still present as up to one meter-thick laterally discontinuous beds of trough cross-bedded sandstones (F1B). It seems most probable that the dunes formed an erg system on the continental side of this mixed carbonate-siliciclastic ramp during the duration of interval 6. As the sandstone interpreted to be eolian in origin are documented along the entire north-south transect it is likely that for a restricted period of time this erg system extended across an area of over 120km in the north-south direction.

This eolian erg was locally cut by small rivers that likely originated in the Ancestral Rocky Mountains to the west of the study area and transported their sandy and gravelly sediment load into the shallow sea in the northeast and east. The sediment probably originated in the highlands of the Ancestral Rocky Mountains which, considering the coarse grain size, must have been relatively close to the study area. As these gravelly sandstone lenses interpreted as fluvial channels are just decimeter-thick it is likely that they were relatively shallow (Bridges and Demicco 2008); their width is estimated to be only in the range of tens of meters as reflected by the width of the gravelly sandstone lenses in outcrop. Towards the east and north, the channel facies pinches out laterally against sandstones interpreted to be shallow-marine in origin. It is therefore likely that these fluvial systems were located close to the coast, and represent the distal reaches of streams just before entering the sea (cf. McGowen and Groat, 1971).

The Marine Setting

The interfingering of carbonate and siliciclastic sediments throughout the Ingleside/Casper Formation succession shows that both lithologies must have been deposited simultaneously in laterally adjacent but still different environments. Nevertheless, sedimentation during the eight stratigraphic intervals was dominated by either carbonates or siliciclastic sediments as seen in the predominance of one of these two lithologies in each of the intervals. Even though both environments occur in time-equivalent successions and existed likely parallel to each other along the Ingleside/Casper Formation coast (Figure 8), the interpretation will be kept separate for a carbonate and a siliciclastic transect. Whether a carbonate or a siliciclastic coastline developed in a specific place depended most of all on the local siliciclastic sediment input. Close to fluvial systems that shed sand into the marine realm, siliciclastic sedimentary systems developed; carbonate deposition prevailed in areas without clastic sediment input.

i. Carbonate Deposition

The most proximal of the carbonate facies were likely the grainstones reflecting constant water movement above normal wave base. The size of the grains in combination with the lack of micrite reflects high-energy deposition, likely in oolitic shoals similar to the modern ooid shoals form the Bahama bank (Shinn, 1988; Rankey et al., 2006). A shallow-marine setting is also indicated by their interfingering with planar bedded and cross-bedded sandstones (Facies 1) that are interpreted as foreshore and shoreface sediments. Similarly, a shallow-marine environment is likely indicated by the skeletal grainstones (Facies 9B and 9C) as they – similar to the oolitic grainstones - are devoid of micrite, and their grain size indicates constant water agitation. Nevertheless, the grain size of most of the skeletal grainstones in the Ingleside/Casper Formation varies significantly, suggesting that these sediments were deposited in slightly deeper water than the oolites. Anderson (1972) and Holloway (1983) propse a similar position for skeletal grainstones interpreted as being deposited as shallow skeletal sand banks and shell shoals. Nevertheless, in places the oolites and the skeletal grainstones occur in close association, and likely represent shallow-water shoal complexes similar to carbonate sand bodies from modern ramps such as the Persian Gulf (Loreau and Purser, 1973) and Yucatan Shelf (Logan et al., 1969).

Both packstone facies most likely occupied a position seaward of the grainstones, likely in a transitional to an uppermost offshore environment. The micrite content in both facies indicates that despite the large skeletal grains and ooids that reflect high-energetic conditions, there had to be some tranquil time in order to deposit the carbonate mud. The highly bimodal distribution of this facies (grains and carbonate mud) is therefore interpreted to reflect changing high- and low-energy conditions in the transition zone between shoreface and offshore. During storms, the ooids and skeletal grains get transported offshore and into an area that would normally deposit mud. Nevertheless, likely because of the size of the grains, transport path of grains towards offshore remained short, and resulted in the mixing of the grains being deposited during storms, and the mud reflecting lower energy, likely fairweather conditions. The sand grains in the packstone facies likely reflect a proximity to the nearest siliciclastic environment and probably also indicate offshore transport of siliciclastics during high-energy events. The offshore environment is exclusively composed of carbonate mudstones (Facies 7), and only locally exhibits wackestones. The carbonate mud could either represent settling out of the water column (Flügel, 2004), and/or it was formed by bed load transport as described by Schieber et al. (2013) from flume experiments. The wackestones likely represent the only traces of storm deposition in these fine-grained carbonate rocks, which is likely a function of the lack of coarse carbonate grains in the upper offshore environment of the Ingleside/Casper Formation.

ii. Siliciclastic Deposition

The Ingleside/Casper succession is exclusively composed of siliciclastic sediment in the south and shows a gradual decrease in siliciclastic deposits towards the north and east. It is inferred that siliciclastic sediment was likely sourced from the south, presumably from eolian and fluvial systems in the terrestrial realm.

The horizontally-bedded sandstones (Facies 2) are the highest energy deposits of the entire succession and therefore likely formed the most proximal of all nearshore siliciclastic facies documented in this study. They are interpreted to represent beach/foreshore sedimentation (Sallenger, 1979; Cheel and Middleton, 1986) at the interface of the terrestrial and the marine realm. These horizontally-bedded sands graded seawards into shallow-marine dunes that are interpreted to be deposited in a shoreface environment (Sutton, 1969). The fine to medium-grained sand forming these deposits was most likely sourced from fluvial systems that delivered sand into the marine environment. Nevertheless, the larger particles such as granule-sized grains and coarse-grained sand present in both the foreshore and shoreface sediments have likely been shed onto the shelf from these nearby fluvial systems. The coarse-grained sediments suggest that these foreshore and shoreface siliciclastics were likely deposited in close proximity to the small deltas delivering this sediment onto the shelf as otherwise marine processes would have completely reworked the larger grains.

The shoreface sandstones most likely graded into an offshore mudstone belt represented by the thin siliciclastic mudstone beds of facies 6. They are interpreted to represent deposition below normal wave base – deeper water than the shoreface sandstones, but still in relative proximity to the shoreface deposits as indicated by their sand and silt content. This environment could be termed the "dirt skirt" of these small deltas formed by the rivers draining the Ancestral Rocky Mountains. The mudstone setting is the environment that captured much of the fine-grained suspended and intermittently suspended material shed into the marine realm from these rivers. Nevertheless, it also reflects deposition from traction currents as reflected in its sand and silt content. It is therefore likely that advective flows operated still in this offshore realm and may be responsible for the deposition of at least some of the clay-rich sediments, too. In a distal direction, the siliciclastic mudstones likely graded into carbonate mudstones, equivalent to the ones forming the most distal setting of the carbonate depositional transect. It is envisioned that once the suspended sediment such as the clay settled out, or was transported into the offshore environment by flows (e.g. as liquid mud, see Ralston et al. 2013), the water cleared, and carbonate deposition set in, an environment typical for tropical shallow seas (Schlager, 2016).

Depositional History

The regular changes from intervals dominated by carbonate lithologies and back to siliciclastics that are laterally traceable for many tens of kilometers through northern Colorado and southern Wyoming are most likely related to relative changes in sea level, as proposed for time-equivalent late Pennsylvanian to early Permian successions elsewhere (Krainer and Lucas, 2004; Jordan and Mountney, 2012; Labaj and Pratt, 2016). These sea-level fluctuations are envisioned to be triggered by the growing and melting of ice sheets in Gondwana (e.g. Fielding et al., 2008) and are therefore considered glacioeustatic in origin.

With a few exceptions, the carbonate and siliciclastic successions recognized in this study dominantly display deepening-upwards trends, implying that all stratigraphic sections in this study preserve transgressive portions of the succession better than regressive parts. It is most likely that the difference in preservation is closely linked to the high amplitude sea-level changes, combined with an only gentle relief of the study area. During sea-level falls, the potentially exposed regressive part of the succession would be more easily eroded than the underlying transgressive portion of each cycle protected by overlying regressive strata (Catuneanu, 2002). Nevertheless, evidence of exposure could be easily eroded by any of the subsequent transgressions prior to depositing the transgressive part of each cycle.

Deepening upward trends in both carbonate and siliciclastic successions are interpreted to represent the gradual rise of sea level. An increase in detrital sediment influx is identified as the fundamental reason for carbonate-dominated deposits being laterally or vertically replaced by siliciclastic dominated sediments. The small-scale cycles represented by these deepening-upward successions are superimposed by a larger-scale sea level curve that is identified based on the extent of the onlap of successive mud-rich carbonates, which are here interpreted as the only units that represent true sea-level highstands across the study area. The southernmost carbonate mudstone bed is documented at Bellvue Dome, implying that at least one sea level highstand, recorded in Interval 5, extended as far south as this location. Highstand deposits recorded across all northeast-southwest stratigraphic successions indicate that a gradual large-scale sea level rise occurred between Intervals 1 and 5, followed by a sea level fall between Intervals 5-7.

From the data at hand it is unclear whether any climate fluctuations go hand in hand with these sea-level changes, and the sedimentary patterns observed do not call for a climatic driver to explain the lithological variations. Nevertheless, interval 6 differs from all other sandstone-dominated units: As it contains exclusively siliciclastics interpreted as eolian sediments, developed in a dry eolian system, this unit is indeed interpreted to have been caused by a change in overall climate to dryer conditions that allowed for the development of the erg system. So while there are no clearly developed cycles of more humid versus more arid conditions preserved in the Ingleside/Casper Formation, one interval does reflect a distinct change in overall climate in these rocks.

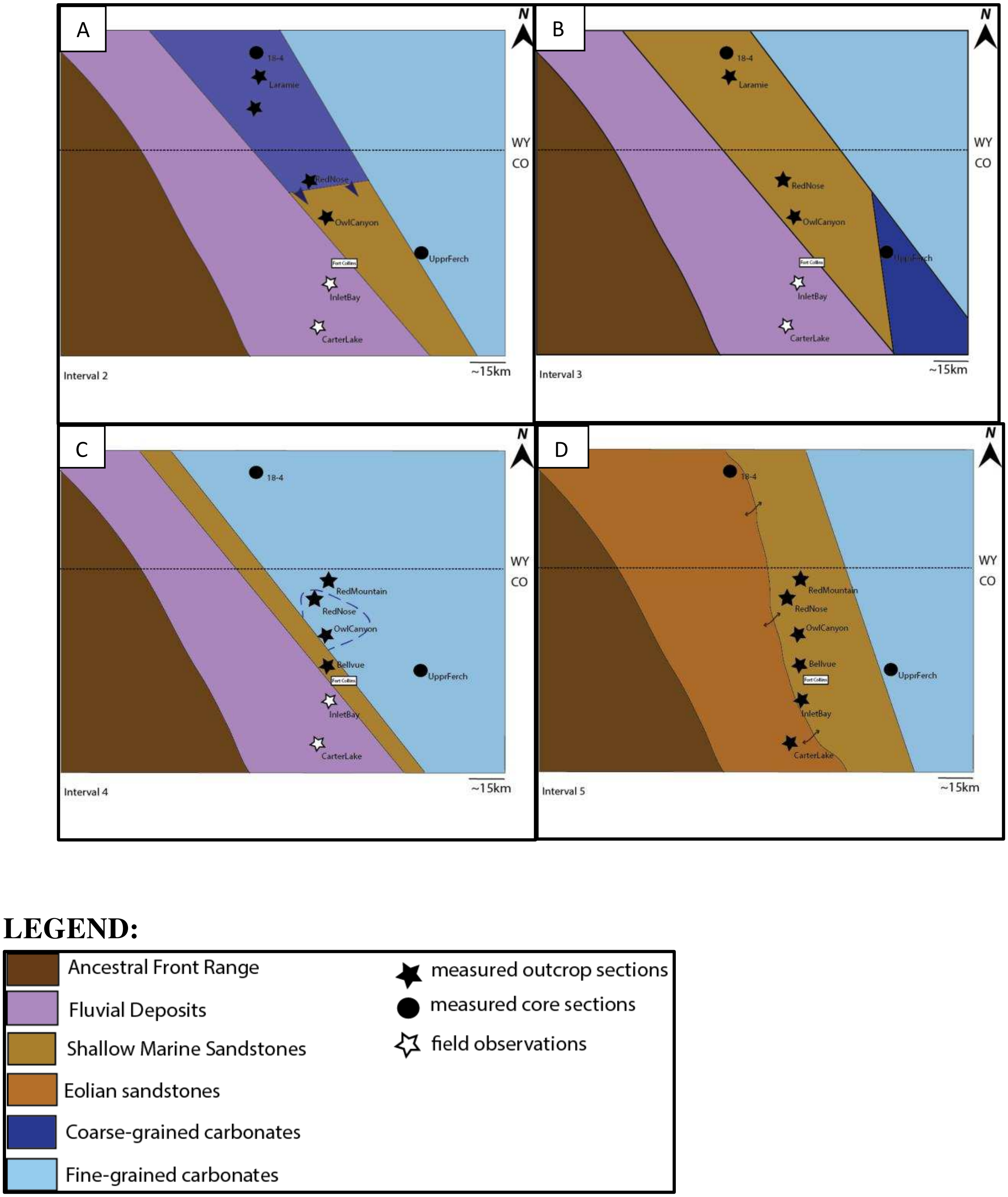

Figure 8: Schematic view of stratigraphic intervals in the Ingleside/Casper Formation. (A) Coarse carbonate deposition expands over time through Interval 2 and extends to Owl Canyon. (B) Siliciclastic deposition dominates Interval 3 and extends through the NE-SW transect. (C) Fine-carbonate deposition dominates Interval 4, dashed blue line represents a diminishing coarse-carbonate depositional environment. (D) Eolian and shallow marine sandstone deposition observed across the NE-SW transect of the study area. Brown arrows display intermixing of shallow marine and eolian sand

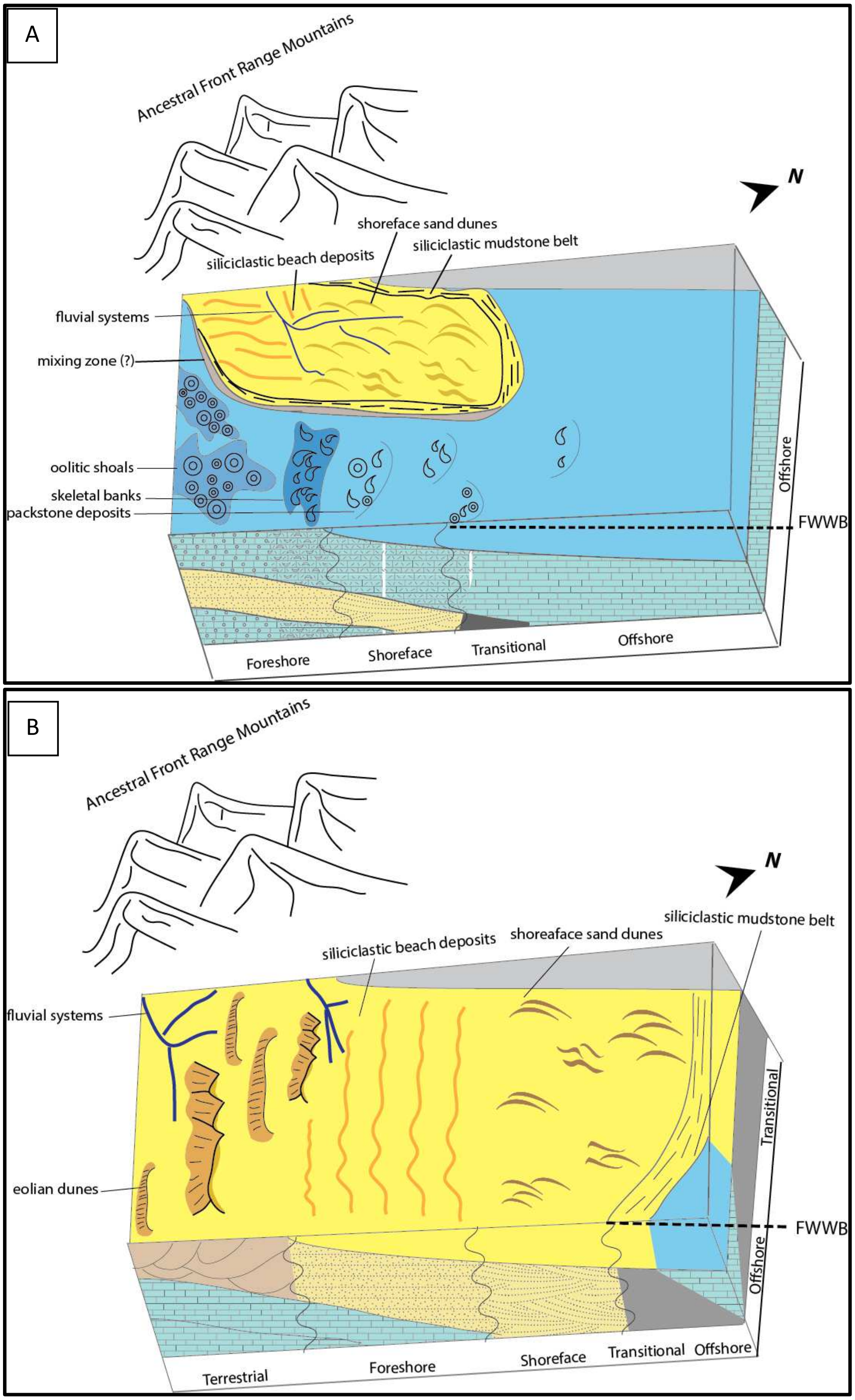
A
Ancestral Front Range Mountains
N
shoreface sand dunes
siliciclastic mudstone belt
siliciclastic beach deposits
fluvial systems
mixing zone (?)
oolitic shoals
skeletal banks
packstone deposits
Offshore
FWWB
Foreshore
Shoreface
Transitional
Offshore
B
Ancestral Front Range Mountains
N
siliciclastic mudstone belt
siliciclastic beach deposits
shoreaface sand dunes
fluvial systems
eolian dunes
Transitional
FWWB
Offshore
Terrestrial
Foreshore
Shoreface
Transitional
Offshore

Legend:

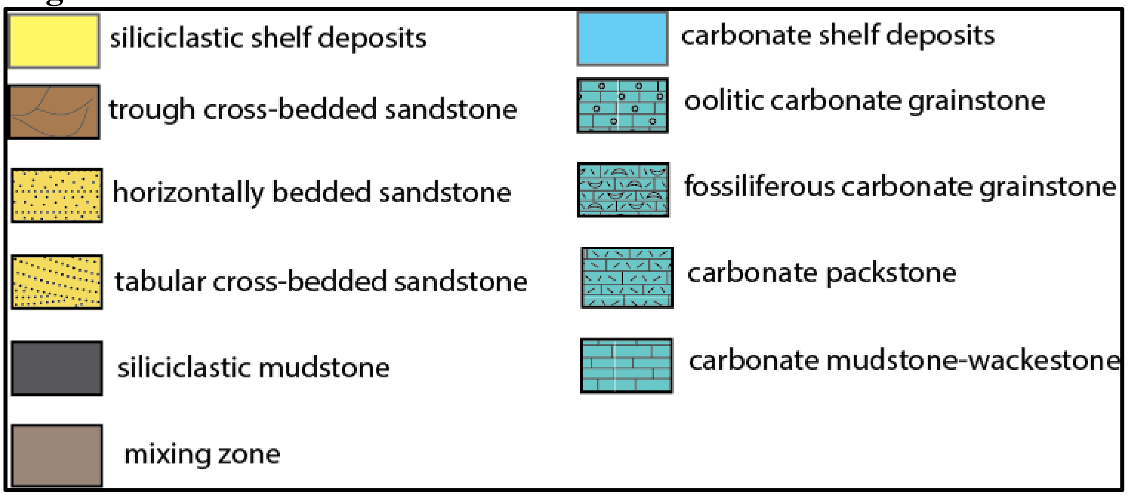

Figure 9: (A) Schematic depositional model for the Ingleside/Casper Formation display nearshore carbonate and siliciclastic facies deposited adjacent to each other. Both nearshore environments grade into fine-grained carbonates in the distal direction. (B) Schematic depositional model for the Ingleside/Casper Formation during Interval 6, when eolian dunes are observed across the study area and carbonate production ceases.

DISCUSSION

I. Correlation of Owl Canyon and Core Upper-Ferch 1 sections

The present study proposes that the type section of the Ingleside Formation at Owl Canyon is largely time-equivalent to the easternmost section of the study area represented by Core Upper Ferch-1 (Figure 7B). This lithological correlation, though lacking biostratigraphic data, shows, at least in the lower part of the Ingleside succession, stratigraphic sections that are either dominated by siliciclastics, or by carbonates, and are therefore correlated to what has been assigned to Intervals 1-4 throughout the N-S transect. Nevertheless, the upper part of the measured section in core Upper-Ferch 1, overlying Interval 4, comprises a 47 m-thick homogenous carbonate mudstone (Facies 7) unit that is not subdivided into stratigraphic intervals and has little in common with any of the other sections across the study area. This section, interpreted to represent the most distal part of the basin fill in the study area, must have been largely cut off from sediment supply whereas the lower part of the succession in the Upper-Ferch 1 core did still receive some siliciclastic input even though the distance to the shoreline must have been approximately the same throughout deposition of the Ingleside/Casper Formation. It is therefore most likely that the main siliciclastic source of the unit, the Ancestral Rocky Mountains located in the west and south of the study area, ceased to supply sediment far into the basin towards the east. Even though sea-level lowstands, especially from high-amplitude glacioeustatic fluctuations produced by the melting and growing of glaciers in Gondwana (Crowell, 1978) are likely to have helped distribute sediments far out into the basin it seems likely that a change in the source area was ultimately responsible for the observed absence of siliciclastic sediments in the upper portion of core Upper-Ferch 1. It is likely that the relief of the Ancestral Rocky Mountains was significantly lowered during the time the Ingleside/Casper Formation was deposited, which may be directly recorded in the sediment patterns, particularly in how far siliciclastic sediment is transported into the basin. Hence, it seems likely that tectonic activity must have subdued towards the end of Ingleside/Casper deposition compared the beginning, thereby confirming Ancestral Rocky Mountain uplift times, and the cessation of the uplift as suggested by Dickinson and Lawton (2003). Apart from a total lack of siliciclastic sediments, coarse-grained carbonates are also missing in the upper part of the succession in the Upper-Ferch 1 core. Together with the missing siliciclastics, the complete absence of nearshore facies in this stratigraphic part of the succession (Interval 5-8) implies that sea-level lowstands did not impact this easternmost basinal part of the study area. As the transition from Interval 4 to 5 is marked by a distinct transgression throughout the study area it is likely that this sea-level rise flooded the foremost exposed shelf, and established offshore conditions and the deposition of mostly carbonate mud for much of the basin.

II. The Ingleside/Casper Formation Erg System

This study suggests the presence of a coastal erg system in the Ingleside/Casper Formation for a restricted period of time during Interval 6. Based on the small thicknesses and trough cross-bedded nature of the eolian units recognized here, the erg system is described as being dominated by small crescentic dunes. During this stratigraphically thin interval, eolian units are present throughout the study area, suggesting that despite its limited thickness and discontinuous nature, this erg system likely extended through a significant part of northeastern Colorado. Nevertheless, due to the lateral discontinuity and limited thickness of eolian facies, the scale and character of this erg system remains unclear. In order to clarify the character of the eolian systems in the Ingleside/Casper Formation, this suggested erg is compared to eolain systems across midcontinent North America (e.g. Kerr and Dott, 1986; Chan and Kocurek, 1986; Kocurek et al., 2000), those examples being among the best-studied ergs worldwide.

Similar to other eolian strata in midcontinent North America, the Ingleside/Casper Formation sediments are well sorted and consist of fine- to very fine-grained sandstones, and eolian beds are generally trough cross-bedded (Facies 1B), or show climbing ripples (Facies 5C). One of the striking characteristics of these eolian deposits is the absence of large-scale bedforms, or the superimposition of trough cross-beds by different bedforms such as tabular cross-beds which makes it likely that these strata reflect deposition in a compound dune field based on the classification of Kerr and Dott (1986). The paleowind direction derived from trough cross-bed foresets at Owl Canyon display a dominantly south- and east-directed sediment transportation direction (average direction calculated to be 107^{o}, Figure 2C). These data suggests that the erg system was dominated by offshore, and in places coast-parallel winds. This reconstruction from the Ingleside/Casper Formation at Owl Canyon at least partly overlaps with reconstructions for the Late Paleozoic that documents paleo-wind directions coming from the northwest (northerlies) and the northeast (easterlies; Poole, 1962). The winds are thought to represent seasonal shifts of high pressure cells over what is now the central part of North America, and effects of monsoonal circulation (Parrish and Peterson, 1988; Loope et al., 2004).

The dominant wind directions would have allowed eolian sediments to form from marine deposits when the wind was coming from the north and east, and therewith towards land. Nevertheless, the differences in grain sizes do not directly show a close link between the eolian and the marine environments. The same holds true for a periodic flooding of the dune fields (e.g. during storms), or time of high water level. Such events are often seen as a significant process for supplying marine sediment to eolian systems (Chan and Kocurek, 1986). Nevertheless, deposits from such floods are generally preserved as thick water-lain interdune deposits (Ahlbrandt and Fryberger, 1981). The complete absence of interdune deposits in our study area, however, supports the idea that either flooding was likely not a common process, or the investigated sections were located too far inland to be affected by such floods. As no unequivocal marine sediments are documented that are time-equivalent to the eolian sediments, this question has to remain open. There is a high likelihood, however, that dominant northerly and easterly wind directions transported sand from extensive sand blankets documented across North America during this time (Poole, 1962; Blanchard et al., 2016) Another major sediment source that may have yielded the sand which would be in agreement with the reconstructed paleo-wind direction is therefore the area of the Ancestral Rocky Mountains.

Considering that probably no floods reached the eolian depositional sites documented in this study during interval 6, this eolian erg was most likely characterized by dry conditions and deposited without much or any influence from flowing water. This interpretation of a mostly dry system is further corroborated by the absence of deflation surfaces or polygonal surface fractures, typical of wet or damp sand deposition (Kocurek and Hunter, 1986). Dry sand is known to display much higher mobility than wet sand (Chan and Kocurek, 1986; Wiggs et al., 2004), and near-continuous sediment transportation (Thomas and Wiggs, 2008). Therefore, the wide lateral extent of this erg throughout the study area may be a direct function of this eolian system's dry nature.

Another aspect of this eolian system that is rather typical of dry systems but has not been discussed for the Ingleside/Casper Formations is the predominance of relatively thin, only meter-thick beds, and the absence of large cross-beds, as documented for much of the well-known Jurassic Navajo Sandstone in Utah (Freeman and Visher, 1975). Thin beds are thought to reflect low water tables, as the position of the water table is seen as the baseline of erosion, and hence preservation of eolian strata (Crabaugh and Kocurek, 1993). Wet eolian systems such as the Entrada Sandstone in Utah (Kocurek, 1980), in contrast, display thick beds of significant lateral continuity. The lateral discontinuity of the Ingleside/Casper Formation beds representing this erg system is therefore likely a result of poor preservation, and corroborates the dry nature of this dune field.

III. Climatic Implications of the Ingleside/Casper Erg System

This study describes an erg system during one particular time interval (interval 6). This erg is interpreted to be a dry eolian system and displays no signs of being influenced by marine waters or groundwater. It is therefore suggested that sea level and water table levels during this time were not elevated enough to impact eolian dune deposits. In this study, we interpret deposition of the eolian system to record a widespread sea-level lowstand that can be documented across the north-south transect of the basin. This continuous lowstand during interval 6 is further corroborated by the absence of carbonate deposits that would have required at least some flooding, or the record of siliciclastic highstand deposits during this time. However, apart from a rise in sea level, the position of the water table can also be a function of climate and/or tectonism (Kocurek et al., 2001). As three parameters, sea-level, climate, and tectonism could have played a role in controlling the water table across the terrestrial part of the study area, especially as sea-level and climate are typically interlinked (Tandon and Gibling, 1994; Smith and Read, 2000). It remains difficult to distinctly attribute the apparent cyclicity in the Ingleside/Casper Formation to exclusively one of these possible causes. Nevertheless, as the very distinct drawdown of sea-level is coupled with the exclusive appearance of eolian strata in interval 6, this portion of the succession most likely reflects a significant change in climate.

Several studies have linked alternating glacial and non-glacial intervals recorded in Gondwana to fluctuating climatic conditions during the Pennsylvanian across midcontinent North America (Heckel, 2008). However, the correlation between types of climate and sea level position remains controversial. Most commonly, low-latitude arid climate is proposed to coincide with glacial lowstands, and humid climate with interglacial highstands (Rankey, 1997; Olszewski and Patzkowsky, 2003; Soreghan et al., 2007). Nevertheless, some authors have suggested a reverse model (Miller et al., 1996; Cecil et al., 2003). The mechanism by which sediment supply increases in the present study area remains unclear. However, the stratigraphic distribution of wind-derived siliciclastics in Late Paleozoic strata of the Midland Basin (Sur et al., 2010) and the Paradox Basin (Soreghan, 1992) suggest a general increase in aridity and sediment availability during lowstands. In most successions, shallow water tables in eolian depositional environments seem to rise in association with humid conditions, and are therefore associated with highstands (Crabaugh and Kocurek, 1993). Indications of humid conditions are generally thought of as preserved deflation surface in eolian strata (Kocurek and Lancaster, 1999) -- a record that is absent in the Ingleside/Casper erg system studied here.

It is therefore suggested that arid climatic conditions coupled with sea level lowstands, as observed in the Sahara during the Quaternary (Wilson, 1973; Kocurek, 1998), was likely responsible for development of the Ingleside/Casper erg system.

IV. Age of the Ingleside Formation

Traditionally, the Ingleside Formation is interpreted as representing entirely Wolfcampian-age deposits (Hoyt, 1962; Maughan et al., 1985). The only age datum for this units stems from a single, well-preserved specimen of *Triticites ventricosus* from the base of the Ingleside Formation at Owl Canyon that was assigned a Wolfcampian age (Hoyt and Chronic, 1961). However, recent developments in fusuline research (Langer and Hottinger, 2000; Groves and Hue, 2009) and the Pennsylvanian-Permian transition are not in agreement with the traditional stratigraphic interpretation put forward by this study.

Robust fusulinid data from a large part of the Casper Formation in Wyoming assigns ages of latest Virgilian to early Missourian (Latest Pennsylvanian) to limestone strata based on the occurrences of fusuline assemblages that include *T. ventricosus* (Burns and Nestell, 2009). This particular study also uses drill cores from a location in the close vicinity of core-R114 considered for the present sedimentological study. Since the lower part of the Ingleside Formation is considered as being time-equivalent to at least the southern extent of the Casper Formation in Wyoming, it seems reasonable to assign a Virgilian to Missourian age to the Ingleside Formation

Whether the Pennsylvanian-Permian transition lies within the uppermost Ingleside/Casper succession was previously unknown, especially since no age data exist from the youngest limestone and sandstone units in these successions. Nevertheless, it is suggested here that significant sea-level and climatic signals characterizing the Pennsylvanian-Permian transition are also present in the stratigraphic record of the Ingleside/Casper Formation.

Recent studies suggest a dramatic expansion of glacial ice across much of Gondwana spanning the Gzhelian – Wolfcampian boundary (Late Pennsylvanian – Early Permian) (Isbell et al., 2003; Fielding et al., 2008). This glacial expansion is also supported by stable isotope records from Late Pennsylvanian - Early Permian marine carbonates and organic-rich facies around the world (Grossman et al., 2008; Birgenheier et al., 2010). Carbonate ramps such as the one where the Ingleside/Casper Formation was deposited, are especially sensitive indicators of eustatic changes, and also reflect the onset of this major Gonwanan glaciation phase during the Late Paleozoic (Heckel, 2008). In many areas across the United States Midcontinent (e.g. Permian Basin, Texas, and the Orogrande Basin, New Mexico), earliest Permian (Asselian) strata show a gradual overall drop in relative sea-level (Koch and Frank, 2011). It is suggested in this study that the carbonate mudstones represent highstand deposits, and their general distribution in the upper portion of the

Ingleside/Casper Formation reflects a regression that is culminating in the overlying tidal flat deposits of the Owl Canyon Formation (Peterson, 1972), and the eolian deposits of the Lyons Formation (Adams and Patton, 1979).

Additionally, a general trend towards increased aridity in the Latest Pennsylvanian-Early Permian has been well-established in recent studies (Tabor and Montañez, 2004; Tabor and Poulsen, 2008). A regional shift to more arid conditions is observed in the Ingleside/Casper succession in the present study and in other studies of the Casper Formation in adjacent Wyoming (Steidtmann, 1974; Ahlbrandt and Fryberger, 1982). It is therefore inferred from the present study that the general increase in aridity mirrored especially in the upper portion of the Ingleside/Casper Formation records the same changing climatic conditions observed across the entire area of equatorial Pangea during the Latest Pennsylvanian-Early Permian.

It is unclear whether the uppermost parts of the Ingleside/Casper Formation contain earliest Permian deposits. It is, however, reasonable to suggest a Late Pennsylvanian age for most of the Ingleside deposition.

CONCLUSIONS

Measured sections of the Ingleside/Casper Formation investigated in this study extends across an area of over 120 km in a north-south direction, and over 35km in an east-west direction from northern Colorado into southeastern Wyoming. It consists of an intercalation of carbonates and siliciclastics. The succession shows an increase in carbonate lithologies towards the north and east, and south of the Bellvue outcrop near Fort Collins, Colorado, the formation consists exclusively of siliciclastics . The succession is subdivided into ten facies that include three carbonates and seven siliciclastics.

The three carbonate facies (Facies 7; Facies 8A and 8B; Facies 9A, 9B, and 9C) are distinguished based on dominant carbonate components. They are: (i) carbonate grainstone (carbonate grainstone with non-skeletal grains, carbonate grainstone with bioclasts), (ii) carbonate packstone (carbonate packstone with non-skeletal grains, carbonate packstone with bioclasts), and (iii) carbonate mudstone - wackestone.

The seven siliciclastic facies (Facies 1A and 1B; Facies 2; Facies 3; Facies 4; Facies 5A, 5B, and 5C; Facies 6) are identified based on sedimentary structures, grain size, and sorting. They are: (i) cross-bedded sandstones (tabular cross-bedded sandstones, (ii) trough cross-bedded sandstones), (iii) horizontally-bedded sandstones, (iv) massive sandstones, (v) conglomeratic sandstones, (vi) ripple-laminated sandstones (asymmetric current ripples, moderately-steeply climbing ripples, gently climbing ripples), and (vii) silt-rich siliciclastic mudstone.

Based on the facies, this study divides the Ingleside/Casper Formation into 8 stratigraphic intervals, with each interval displaying a distinct lithological assemblage that is either dominated by carbonates, or by siliciclastics. Typically, all 8 intervals show fining-upwards trends, and very few coarsening-upwards trends are observed.

The Ingleside/Casper Formation is interpreted to represent a mixed carbonate-siliciclastic ramp environment that developed along the Ancestral Front Range during the Late Paleozoic. Lateral and vertical intergrading of siliciclastic and carbonate facies indicate that the deposition alternated between dominantly carbonate and dominantly siliciclastic settings. During deposition in a carbonate-dominated environment, carbonate facies occupied distinct positions on the ramp, with carbonate grainstones representing the most proximal facies and carbonate mudstones the most distal facies belts. Siliciclastic deposits are suggested to have dominated the study area during times when siliciclastic input into the shallow marine environment was high and largely shut down carbonate production in the proximal realm. During dominantly siliciclastic deposition, the foreshore consisted of horizontally bedded sandstones, dune deposits dominated in the shoreface environment, and silt-rich siliciclastic mudstones were deposited in a low-energy offshore setting. The facies architecture of the Ingleside/Casper Formation indicates that both carbonate-dominated and siliciclastic-dominated environments graded into carbonate mudstones in the most distal settings. Therefore, carbonate mudstone units overlying any other strata are regarded as the only facies transition that records significant increases in sea-level, regardless whether the underlying environment was carbonate or siliciclastic. Besides these small-scale changes that are recorded eight times in the Ingleside/Casper Formation, the overall trend with carbonates showing a more wide-spread distribution in the middle portion of the formation than at the top or bottom indicates an overall transgression in the lower part of the unit followed by a regression in the upper part.

The development of an eolian environment exclusively during one interval (Interval 6) across the study area suggests an important shift in sea level and climate during the deposition of the Ingleside/Casper Formation. It is inferred that for a period of time, a dry eolian system extended across the entire western part of the study area. This significant increase in aridity coupled with a sharp sea level drop was mirrored in the development of the eolian dunes. It is likely that this basin-wide trend was caused by glacial expansion across much of Gondwana immediately prior to the Pennsylvanian-Permian transition. For this reason, the Ingleside Formation, traditionally described as Permian in age, is here reassigned to be likely Late Pennsylvanian in age. This reassignment is also based on the correlation of the Casper Formation, known to be of Late Pennsylvanian age from fussuline data, to the Ingleside Formation.

REFERENCES

Adams, J., and J. Patton, 1979, Sebkha-dune deposition in the Lyons Formation (Permian), northern Front Range, Colorado: Mountain Geologist, v. 16, p. 47-57.

Agatston, R. S., 1954, Pennsylvanian and Lower Permian of Northern and eastern Wyoming: Bulletin of the American Association of Petroleum Geologists, v. 38, p. 508-583.

Ahlbrandt, T. S., and S. G. Fryberger, 1981, Sedimentary features and significance of interdune deposits: Special Publication - Society of Economic Paleontologists and Mineralogists, p. 293-314.

Algeo, T. J., and P. H. Heckel, 2008, The Late Pennsylvanian Midcontinent Sea of North America; a review: Palaeogeography, Palaeoclimatology, Palaeoecology, v. 268, p. 205-221, doi: 10.1016/j.palaeo.2008.03.049

Allen, J. R. L., 1972, Instability of an upper-phase plane bed; a test of Bagnold's criterion: Sedimentary Geology, v. 8, p. 309-316.

Allen, J. R. L., 1982, Sedimentary structures, their character and physical basis; I: Netherlands, Elsevier Sci. Publ. Co. : Amsterdam, Netherlands.

Allen, J. R. L., 1984, Parallel lamination developed from upper stage plane beds; a model based on the larger coherent structures of the turbulent boundary layer: Sedimentary Geology, v. 39, p. 227-242.

Anderson, E. J., 1972, Sedimentary structure assemblages in transgressive and regressive calcarenites: International Geological Congress, Abstracts--Congres Geologique Internationale, Resumes, v. 24, p. 179-179.

Berger, W. H., A. A. Ekdale, and P. P. Bryant, 1979, Selective preservation of burrows in deep-sea carbonates: Marine Geology, v. 32, p. 205-230.

Bigarella, J. J., 1972, Eolian environments; their characteristics, recognition, and importance: Special Publication - Society of Economic Paleontologists and Mineralogists, v. 16, p. 12-62.

Birgenheier, L. P., C. R. Fielding, M. C. Rygel, T. D. Frank, and J. Roberts, 2009, Evidence for dynamic climate change on sub-10 (super 6) -year scales from the late Paleozoic glacial record, Tamworth

Belt, New South Wales, Australia: Journal of Sedimentary Research, v. 79, p. 56-82, doi: 10.2110/jsr.2009.013

Birgenheier, L. P., T. D. Frank, C. R. Fielding, and M. C. Rygel, 2010, Coupled carbon isotopic and sedimentological records from the Permian system of eastern Australia reveal the response of atmospheric carbon dioxide to glacial growth and decay during the late Palaeozoic ice age: Palaeogeography, Palaeoclimatology, Palaeoecology, v. 286, p. 178-193, doi: 10.1016/j.palaeo.2010.01.008

Blakey, R. C., 2008, Pennsylvanian-Jurassic sedimentary basins of the Colorado Plateau and Southern Rocky Mountains Sedimentary basins of the world, v. 5: Netherlands, Elsevier : Amsterdam, Netherlands, p. 245-296, doi: 10.1016/S1874-5997(08)00007-5

Blakey, R. C., and E. N. Eastwood, 2004, From outcrop to paleogeography; reconstructing the Permian Hermit Formation and related rocks, Colorado Plateau: Abstracts with Programs - Geological Society of America, v. 36, p. 402-402.

Blakey, R. C., and L. T. Middleton, 1983, Permian shoreline eolian complex in central Arizona; dune changes in response to cyclic sea level changes Developments in sedimentology, v. 38: Netherlands, Elsevier Sci. Publ. Co. : Amsterdam, Netherlands, p. 551-581.

Blanchard, S., C. R. Fielding, T. D. Frank, J. E. Barrick, and S. Lokier, 2016, Sequence stratigraphic framework for mixed aeolian, peritidal and marine environments; insights from the Pennsylvanian subtropical record of western Pangaea: Sedimentology, v. 63, p. 1929-1970, doi: 10.1111/sed.12285

Boggs, S., Jr., 1987, Principles of sedimentology and stratigraphy: United States, Merrill Publ. Co. : Columbus, OH, United States, 688p

Bottjer, D. J., M. L. Droser, and D. Jablonski, 1987, Bathymetric trends in the history of trace fossils: Field Trip Guidebook - Pacific Section, Society of Economic Paleontologists and Mineralogists, v. 52, p. 57-65.

Bridge, J. S., and R. V. Demicco, 2008, Earth surface processes, landforms and sediment deposits: United

Kingdom, Cambridge University Press : Cambridge, United Kingdom.

Brookfield, M. E., 1977, The origin of bounding surfaces in ancient aeolian sandstones: Sedimentology, v. 24, p. 303-332.

Burchette, T. P., and V. P. Wright, 1992, Carbonate ramp depositional systems: Sedimentary Geology, v. 79, p. 3-57.

Burns, D. M., and M. K. Nestell, 2009, Using fusulinids to evaluate the periodicity of cycles in a sequence stratigraphic section of Pennsylvanian-Permian strata and to suggest possible support for low-frequency Milankovitch perturbations; Casper Formation, southeastern Wyoming: Special Publication - Society for Sedimentary Geology, v. 93, p. 253-267.

Carozzi, A. V., 1964, Complex ooids from Triassic lake deposit, Virginia: American Journal of Science, v. 262, p. 231-241.

Cecil, C. B., F. T. Dulong, R. R. West, R. G. Stamm, B. R. Wardlaw, and N. T. Edgar, 2003, Climate controls on the stratigraphy of a Middle Pennsylvanian cyclothem in North America: Special Publication - Society for Sedimentary Geology, v. 77, p. 151-180.

Chan, M. A., and G. Kocurek, 1988, Complexities in eolian and marine interactions; processes and eustatic controls on erg development: Sedimentary Geology, v. 56, p. 283-300.

Cheel, R. J., and G. V. Middleton, 1986a, Horizontal laminae formed under upper flow regime plane bed conditions: Journal of Geology, v. 94, p. 489-504.

Cheel, R. J., and G. V. Middleton, 1986b, Horizontal laminae formed under upper flow regime plane bed conditions: Journal of Geology, v. 94, p. 489-504.

Clark, D. N., 1986, The distribution of porosity in Zechstein carbonates: Geological Society Special Publications, v. 23, p. 121-149.

Crabaugh, M., and G. Kocurek, 1993, Entrada Sandstone; an example of a wet aeolian system: Geological Society Special Publications, v. 72, p. 103-126.

Crowell, J. C., 1978, Gondwanan glaciation, cyclothems, continental positioning, and climate change: American Journal of Science, v. 278, p. 1345-1372.

Curtis, B. F., 1958, Pennsylvanian paleotectonics of Colorado and adjacent areas: United States, Rocky Mt. Assoc. Geol. : Denver, Colorado, United States, p. 9-12.

Dahanayake, K., 1978, Sequential position and environmental significance of different types of oncoids: Sedimentary Geology, v. 20, p. 301-316.

De Voto, R. H., 1980, Pennsylvanian stratigraphy and history of Colorado: United States, Rocky Mount. Assoc. Geol. : Denver, CO, United States, p. 71-101.

Dickinson, W. R., and T. F. Lawton, 2003, Sequential intercontinental suturing as the ultimate control for Pennsylvanian ancestral Rocky Mountains deformation: Geology [Boulder], v. 31, p. 609-612.

Dumas, S., R. W. C. Arnott, and J. B. Southard, 2005, Experiments on oscillatory-flow and combined-flow bed forms; implications for interpreting parts of the shallow-marine sedimentary record: Journal of Sedimentary Research, v. 75, p. 501-513, doi: 10.2110/jsr.2005.039

Eardley, A. J., 1951, Structural geology of North America.

Egenhoff, S., C. Cassle, J. Maletz, A. M. Frisk, J. O. R. Ebbestad, and K. Stuebner, 2010, Sedimentology and sequence stratigraphy of a pronounced Early Ordovician sea-level fall on Baltica; the Bjorkasholmen Formation in Norway and Sweden: Sedimentary Geology, v. 224, p. 1-14, doi: 10.1016/j.sedgeo.2009.12.003

Egenhoff, S. O., and N. S. Fishman, 2013, Traces in the dark-sedimentary processes and facies gradients in the upper shale member of the Upper Devonian-Lower Mississippian Bakken Formation, Williston Basin, North Dakota, U.S.A: Journal of Sedimentary Research, v. 83, p. 803-824, doi: 10.2110/jsr.2013.60

Fielding, C. R., T. D. Frank, and J. L. Isbell, 2008, The late Paleozoic ice age; a review of current understanding and synthesis of global climate patterns: Special Paper - Geological Society of America, v. 441, p. 343-354, doi: 10.1130/2008.2441(24)

Flügel, E., 2004, Microfacies of carbonate rocks; analysis, interpretation and application: Germany, Springer : Berlin, Federal Republic of Germany, 975p

Freeman, W. E., and G. S. Visher, 1975, Stratigraphic analysis of the Navajo Sandstone: Journal of

Sedimentary Petrology, v. 45, p. 651-668.

Fryberger, S. G., and C. J. Schenk, 1988, Pin stripe lamination; a distinctive feature of modern and ancient eolian sediments: Sedimentary Geology, v. 55, p. 1-15.

Grossman, E. L., T. E. Yancey, T. E. Jones, P. Bruckschen, B. Chuvashov, S. J. Mazzullo, and H.-s. Mii, 2008, Glaciation, aridification, and carbon sequestration in the Permo-Carboniferous; the isotopic record from low latitudes: Palaeogeography, Palaeoclimatology, Palaeoecology, v. 268, p. 222-233, doi: 10.1016/j.palaeo.2008.03.053

Heckel, P. H., 1972, Recognition of ancient shallow marine environments: Special Publication - Society of Economic Paleontologists and Mineralogists, v. 16, p. 226-286.

Heckel, P. H., 1986, Sea-level curve for Pennsylvanian eustatic marine transgressive-regressive depositional cycles along Midcontinent outcrop belt, North America: Geology [Boulder], v. 14, p. 330-334.

Heckel, P. H., 2008, Pennsylvanian cyclothems in Midcontinent North America as far-field effects of waxing and waning of Gondwana ice sheets: Special Paper - Geological Society of America, v. 441, p. 275-289, doi: 10.1130/2008.2441(19)

Holloway, S., 1983, The shell-detrital calcirudites of the Forest Marble Formation (Bathonian) of Southwest England: Proceedings of the Geologists' Association, v. 94, p. 259-266.

Howe, D. M., 1970, Post-Casper-Ingleside unconformity and related sediments of southeastern Wyoming and northcentral Colorado, United States.

Hoyt, J. H., and B. J. Chronic, Jr., 1961, Wolfcampian fusulinid from Ingleside Formation, Owl Canyon, Colorado: Journal of Paleontology, v. 35, p. 1089-1089.

Hunter, R. E., 1981, Stratification styles in eolian sandstones; some Pennsylvanian to Jurassic examples from the Western Interior U.S.A: Special Publication - Society of Economic Paleontologists and Mineralogists, p. 315-329.

Isbell, J. L., M. F. Miller, K. L. Wolfe, and P. A. Lenaker, 2003, Timing of late Paleozoic glaciation in Gondwana; was glaciation responsible for the development of Northern Hemisphere cyclothems?:

Special Paper - Geological Society of America, v. 370, p. 5-24.

Joeckel, R. M., 1999, Paleosol in Galesburg Formation (Kansas City Group, Upper Pennsylvanian), northern Midcontinent, U.S.A.; evidence for climate change and mechanisms of marine transgression: Journal of Sedimentary Research, v. 69, p. 720-737.

Jordan, O. D., and N. P. Mountney, 2010, Styles of interaction between aeolian, fluvial and shallow marine environments in the Pennsylvanian to Permian lower Cutler beds, south-east Utah, USA: Sedimentology, v. 57, p. 1357-1385, doi: 10.1111/j.1365-3091.2010.01148.x

Jordan, O. D., and N. P. Mountney, 2012, Sequence stratigraphic evolution and cyclicity of an ancient coastal desert system; the Pennsylvanian-Permian lower Cutler beds, Paradox Basin, Utah, U.S.A: Journal of Sedimentary Research, v. 82, p. 755-780, doi: 10.2110/jsr.2012.54

Kerr, D. R., E. H. Konopka, R. H. Dott, Jr., and S. G. Driese, 1986, Late Carboniferous (Pennsylvanian) eustasy and siliciclastic-carbonate sedimentation, Northern Rocky Mountains, United States: Australia, Bureau of Mineral Resources, Geol. and Geophys. : Canberra, Australia, p. 161-161.

Kluth, C. F., and P. J. Coney, 1981, Plate tectonics of the ancestral Rocky Mountains: Geology [Boulder], v. 9, p. 10-15.

Knight, S. H., 1929, The Fountain and the Casper formations of the Laramie Basin; a study on genesis of sediments: Wyoming Univ. Pub. Sci. Geology, v. 1, p. 1-82.

Koch, J. T., and T. D. Frank, 2011, The Pennsylvanian-Permian transition in the low-latitude carbonate record and the onset of major Gondwanan glaciation: Palaeogeography, Palaeoclimatology, Palaeoecology, v. 308, p. 362-372, doi: 10.1016/j.palaeo.2011.05.041

Kocurek, G., and R. E. Hunter, 1986, Origin of polygonal fractures in sand, uppermost Navajo and Page sandstones, Page, Arizona: Journal of Sedimentary Petrology, v. 56, p. 895-904.

Kocurek, G., N. I. Robinson, and J. M. Sharp, 2001, The response of the water table in coastal aeolian systems to changes in sea level: Sedimentary Geology, v. 139, p. 1-13.

Kocurek, G. A., 1980, Significance of bounding surfaces, interdune deposits, and dune stratification types in ancient erg reconstruction, United States.

Krainer, K., and S. G. Lucas, 2004, The Upper Pennsylvanian Red Tanks Member of the Bursum Formation at Carrizo Arroyo, central New Mexico; transition from shallow marine to nonmarine facies: Bulletin - New Mexico Museum of Natural History and Science, v. 25, p. 53-70.

Labaj, M. A., and B. R. Pratt, 2016, Depositional dynamics in a mixed carbonate-siliciclastic system; Middle-Upper Cambrian Abrigo Formation, southeastern Arizona, U.S.A: Journal of Sedimentary Research, v. 86, p. 11-37.

Leary, R. J., P. Umhoefer, M. E. Smith, and N. Riggs, 2017, A three-sided orogen; a new tectonic model for ancestral Rocky Mountain uplift and basin development: Geology [Boulder], v. Pre-Issue Publication, doi: 10.1130/G39041.1

Lee, W. T., 1927, Correlation of geologic formations between east-central Colorado, central Wyoming, and southern Montana, United States, U. S. Geological Survey : Reston, VA, United States.

Lehrmann, D. J., Y. Wan, J. Wei, Y. Yu, and J. Xiao, 2001, Lower Triassic peritidal cyclic limestone; an example of anachronistic carbonate facies from the Great Bank of Guizhou, Nanpanjiang Basin, Guizhou Province, South China: Palaeogeography, Palaeoclimatology, Palaeoecology, v. 173, p. 103-123.

Logan, B. W., 1969, Carbonate sediments and reefs, Yucatan shelf, Mexico: Memoir - American Association of Petroleum Geologists, p. 1-198.

Loope, D. B., 1984, Eolian origin of upper Paleozoic sandstones, southeastern Utah: Journal of Sedimentary Petrology, v. 54, p. 563-580.

Loreau, J. P., and B. H. Purser, 1973, Distribution and ultrastructure of Holocene ooids in the Persian Gulf: Kingston Geological Review, v. 73, p. 8-8.

Mallory, W. W., 1960, Outline of Pennsylvanian stratigraphy of Colorado: United States, Rocky Mtn. Assoc. Geologists: Denver, CO, United States, p. 23-33.

Margolis, S., and R. W. Rex, 1971, Endolithic algae and micrite envelope formation in Bahamian oolites as revealed by scanning electron microscopy: Geological Society of America Bulletin, v. 82, p. 843-851.

Marshak, S., K. E. Karlstrom, and J. M. Timmons, 2000, Inversion of Proterozoic extensional faults; an explanation for the pattern of Laramide and ancestral Rockies intracratonic deformation, United States: Geology [Boulder], v. 28, p. 735-738, doi: 10.1130/0091-7613(2000)028

Maughan, E. K., 1993, The ancestral Rocky Mountains in Wyoming: Memoir - Geological Survey of Wyoming, v. 5, p. 188-207.

McGowen, J. H., and C. G. Groat, 1971, Van Horn sandstone, west Texas; an alluvial fan model for mineral exploration, United States, University of Texas at Austin, Bureau of Economic Geology : Austin, TX, United States.

McKee, E. D., 1966, Structures of dunes at White Sands National Monument, New Mexico (and a comparison with structures of dunes from other selected areas), International, Blackwell: Oxford-Boston, International.

Miall, A. D., 1985, Architectural-element analysis; a new method of facies analysis applied to fluvial deposits: SEPM Short Course, v. 19, p. 33-81.

Miller, A. K., and H. D. Thomas, 1936, The Casper Formation (Pennsylvanian) of Wyoming and its cephalopod fauna: Journal of Paleontology, v. 10, p. 715-738.

Olszewski, T. D., and M. E. Patzkowsky, 2003, From cyclothems to sequences; the record of eustasy and climate on an icehouse epeiric platform (Pennsylvanian-Permian, North American Midcontinent): Journal of Sedimentary Research, v. 73, p. 15-30.

Parrish, J. T., and F. Peterson, 1988, Wind directions predicted from global circulation models and wind directions determined from eolian sandstones of the Western United States; a comparison: Sedimentary Geology, v. 56, p. 261-282.

Ralston, D. K., W. R. Geyer, P. A. Traykovski, and N. J. Nidzieko, 2013, Effects of estuarine and fluvial processes on sediment transport over deltaic tidal flats: Continental Shelf Research, v. 60, p. S40-s57.

Rankey, E. C., S. L. Reeder, W. L. Watney, and A. P. Byrnes, 2006, Spatial trend metrics of ooid shoal complexes, Bahamas; implications for reservoir characterization and prediction: Papers presented at the Gulf Coast Section, Society of Economic Paleontologists and Mineralogists Foundation Annual Bob F. Perkins Research Conference, v. 26, p. 849-873.

Scherer, C. M. S., 2000, Eolian dunes of the Botucatu Formation (Cretaceous) in southernmost Brazil; morphology and origin: Sedimentary Geology, v. 137, p. 63-84.

Schieber, J., J. Southard, and K. Thaisen, 2007, Accretion of mudstone beds from migrating floccule ripples: Science, v. 318, p. 1760-1763, doi: 10.1126/science.1147001

Schieber, J., J. B. Southard, P. Kissling, B. Rossman, and R. Ginsburg, 2013, Experimental deposition of carbonate mud from moving suspensions; importance of flocculation and implications for modern and ancient carbonate mud deposition: Journal of Sedimentary Research, v. 83, p. 1025-1031, doi: 10.2110/jsr.2013.77

Schlager, W., 2000, Sedimentation rates and growth potential of tropical, cool-water and mud-mound carbonate systems: Geological Society Special Publications, v. 178, p. 217-227.

Schwarz, E., G. D. Veiga, G. A. Trentini, and L. A. Spalletti, 2016, Climatically versus eustatically controlled, sediment-supply-driven cycles; carbonate-siliciclastic, high-frequency sequences in the Valanginian of the Neuquen Basin (Argentina): Journal of Sedimentary Research, v. 86, p. 312-335, doi: 10.2110/jsr.2016.21

Shinn, E. A., 1988, The geology of the Florida Keys: Oceanus [Woods Hole], v. 31, p. 46-53.

Simons, D. B., E. V. Richardson, and C. F. Nordin, Jr., 1965, Bedload equation for ripples and dunes, United States, U. S. Geological Survey : Reston, VA, United States, p. H1-h9.

Smith, L. B., Jr., and J. F. Read, 2000a, Rapid onset of late Paleozoic glaciation on Gondwana; evidence from Upper Mississippian strata of the Midcontinent, United States: Geology [Boulder], v. 28, p. 279-282.

Smith, L. B., Jr., and J. F. Read, 2000b, Rapid onset of late Paleozoic glaciation on Gondwana; evidence from Upper Mississippian strata of the Midcontinent, United States: Geology [Boulder], v. 28, p. 279-282.

Soreghan, G. S., 1992, Preservation and paleoclimatic significance of eolian dust in the ancestral Rocky

Mountains province: Geology [Boulder], v. 20, p. 1111-1114.

Soreghan, G. S., D. E. Sweet, K. R. Marra, C. F. Eble, M. J. Soreghan, R. D. Elmore, S. A. Kaplan, and M. D. Blum, 2007, An exhumed late Paleozoic canyon in the Rocky Mountains: Journal of Geology, v. 115, p. 473-481, doi: 10.1086/518075

Sur, S., G. S. Soreghan, M. J. Soreghan, W. Yang, and A. H. Saller, 2010, A record of glacial aridity and Milankovitch-scale fluctuations in atmospheric dust from the Pennsylvanian tropics: Journal of Sedimentary Research, v. 80, p. 1046-1067, doi: 10.2110/jsr.2010.091

Tabor, N. J., and I. P. Montanez, 2004, Morphology and distribution of fossil soils in the Permo-Pennsylvanian Wichita and Bowie Groups, north-central Texas, USA; implications for western equatorial Pangean palaeoclimate during icehouse-greenhouse transition: Sedimentology, v. 51, p. 851-884, doi: 10.1111/j.1365-3091.2004.00655.x

Tabor, N. J., and C. J. Poulsen, 2008, Palaeoclimate across the Late Pennsylvanian-Early Permian tropical palaeolatitudes; a review of climate indicators, their distribution, and relation to palaeophysiographic climate factors: Palaeogeography, Palaeoclimatology, Palaeoecology, v. 268, p. 293-310, doi: 10.1016/j.palaeo.2008.03.052

Tandon, S. K., and M. R. Gibling, 1994, Calcrete and coal in Late Carboniferous cyclothems of Nova Scotia, Canada; climate and sea-level changes linked: Geology [Boulder], v. 22, p. 755-758.

Tapanila, L., 2005, Palaeoecology and diversity of endosymbionts in Palaeozoic marine invertebrates; trace fossil evidence: Lethaia, v. 38, p. 89-99.

Tenney, C. S., 1966, Pennsylvanian and Lower Permian deposition in Wyoming and adjacent areas: Bulletin of the American Association of Petroleum Geologists, v. 50, p. 227-250.

Tweto, O., 1980, Summary of Laramide Orogeny in Colorado: United States, Rocky Mount. Assoc. Geol.: Denver, CO, United States, p. 129-134.

Vail, P. R., 1987, Seismic stratigraphy interpretation using sequence stratigraphy; Part 1, Seismic stratigraphy interpretation procedure: AAPG Studies in Geology, v. 27, p. 1-10.

Wilkinson, B. H., R. M. Owen, and A. R. Carroll, 1985, Submarine hydrothermal weathering, global eustasy, and carbonate polymorphism in Phanerozoic marine oolites: Journal of Sedimentary Petrology, v. 55, p. 171-183.

Williams, J. S., 1962, Pennsylvanian System in central and northern Rocky Mountains, United States, p. 159-187.

Wilson, M. E. J., 2008, Global and regional influences on equatorial shallow-marine carbonates during the Cenozoic: Palaeogeography, Palaeoclimatology, Palaeoecology, v. 265, p. 262-274.

Wilson, M. E. J., E. C. Eewah, S. Dorobek, and P. Lunt, 2013, Onshore to offshore trends in carbonate sequence development, diagenesis and reservoir quality across a land-attached shelf in SE Asia: Marine and Petroleum Geology, v. 45, p. 349-376, doi: 10.1016/j.marpetgeo.2013.03.011

Appendix A: Ingleside/Casper Formation Stratigraphic Sections

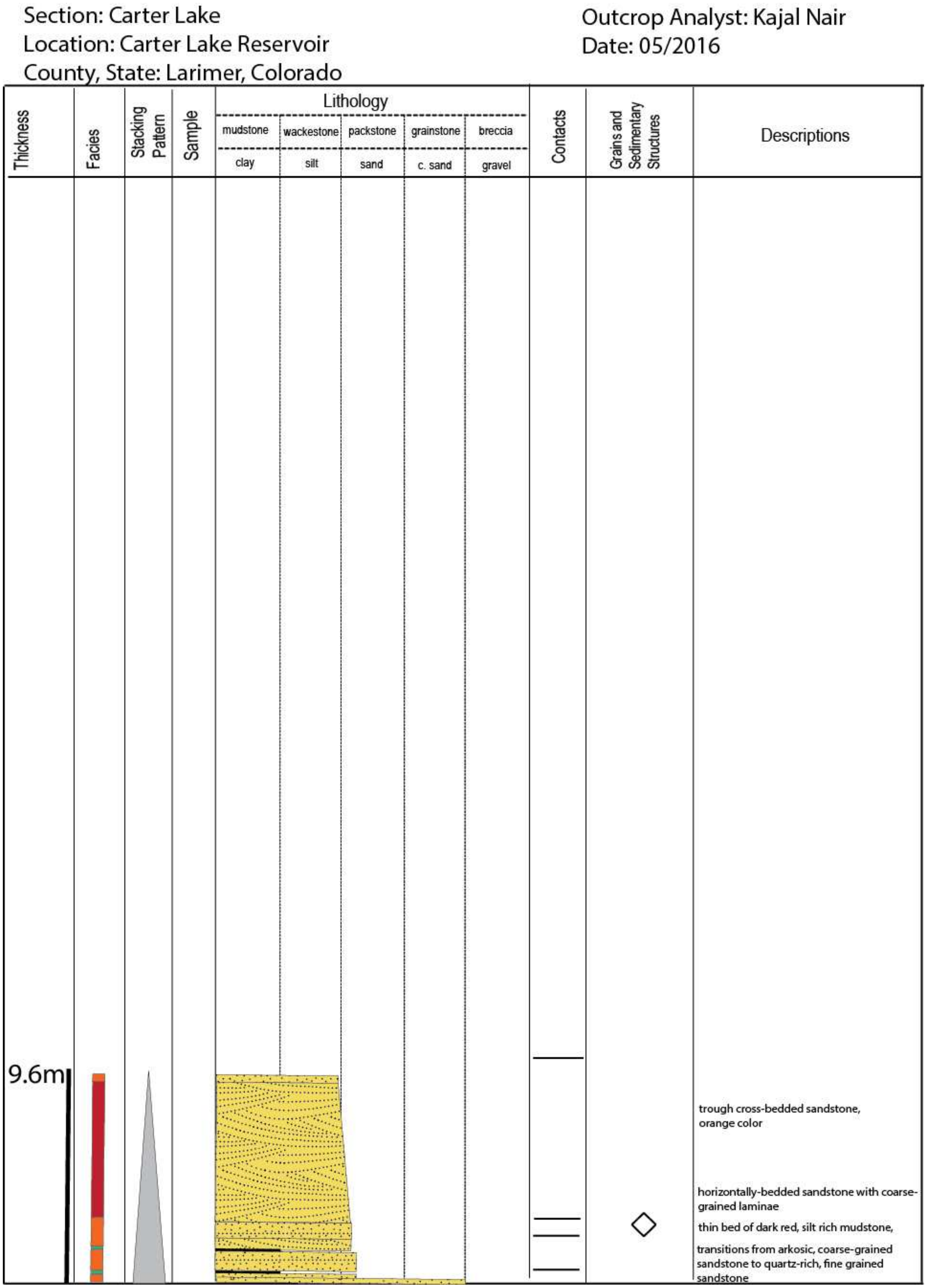

Section: Sylvandale
Location: Sylvandale Ranch
County, State: Larimer, Colorado

Outcrop Analyst: Kajal Nair
Date: 05/2016

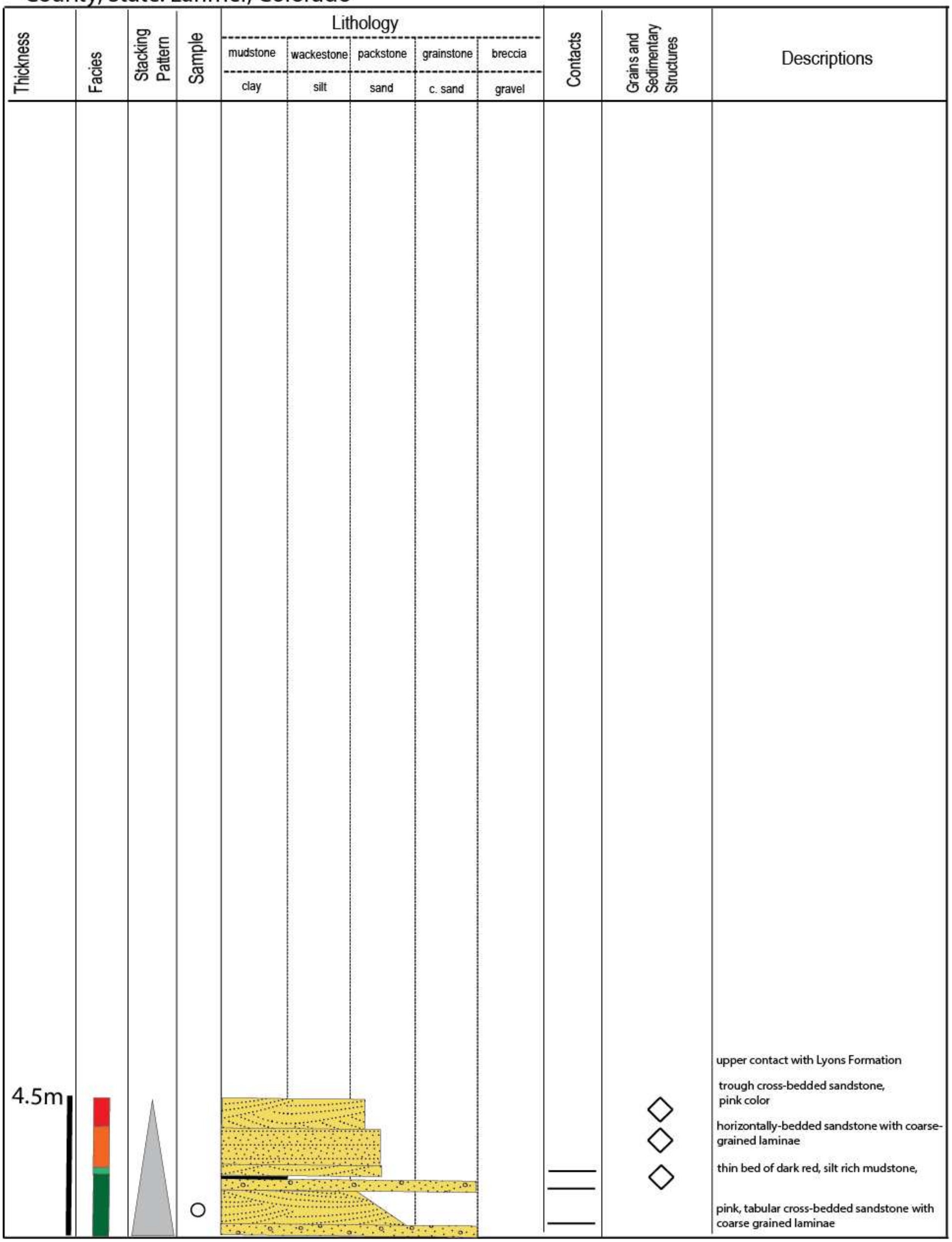

Section: Coyote Ridge
Location: Coyote Ridge
County, State: Larimer, Colorado

Outcrop Analyst: Kajal Nair
Date: 05/2016

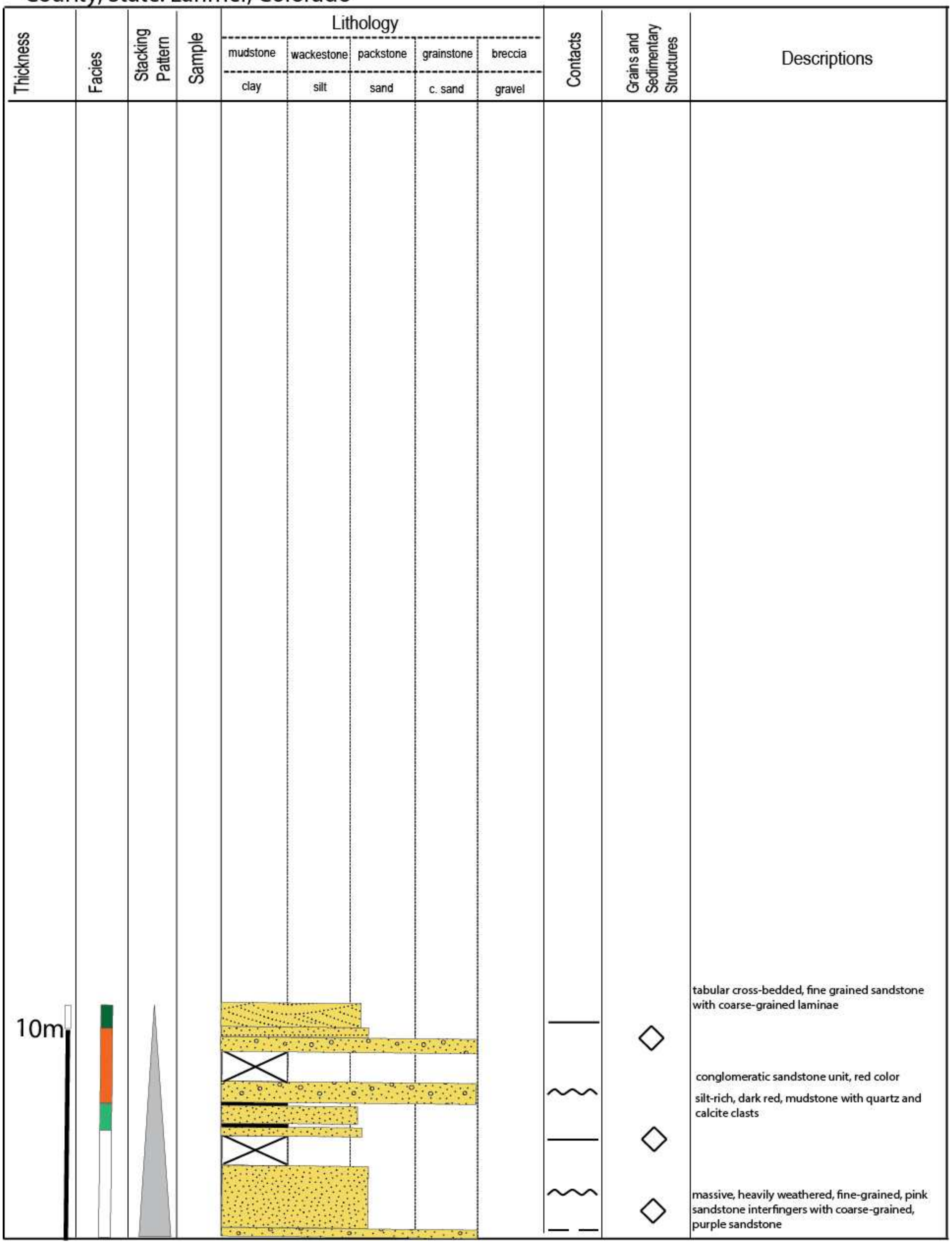

Section: Coyote Ridge
Location: Coyote Ridge
County, State: Larimer, Colorado

Outcrop Analyst: Kajal Nair
Date: 05/2016

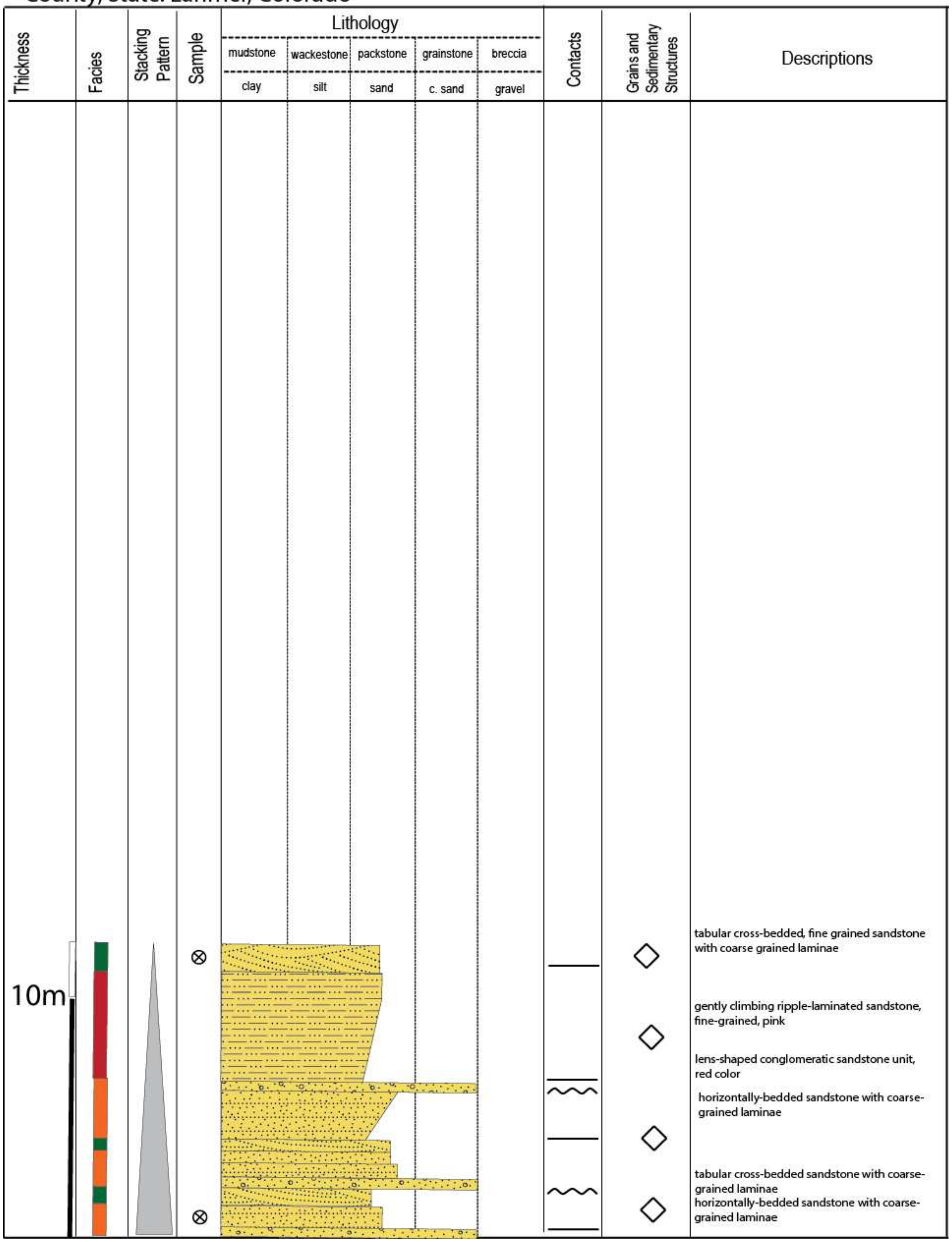

Location: Inlet Bay
County, State: Larimer, Colorado

Outcrop Analyst: Kajal Nair
Date: 05/2016

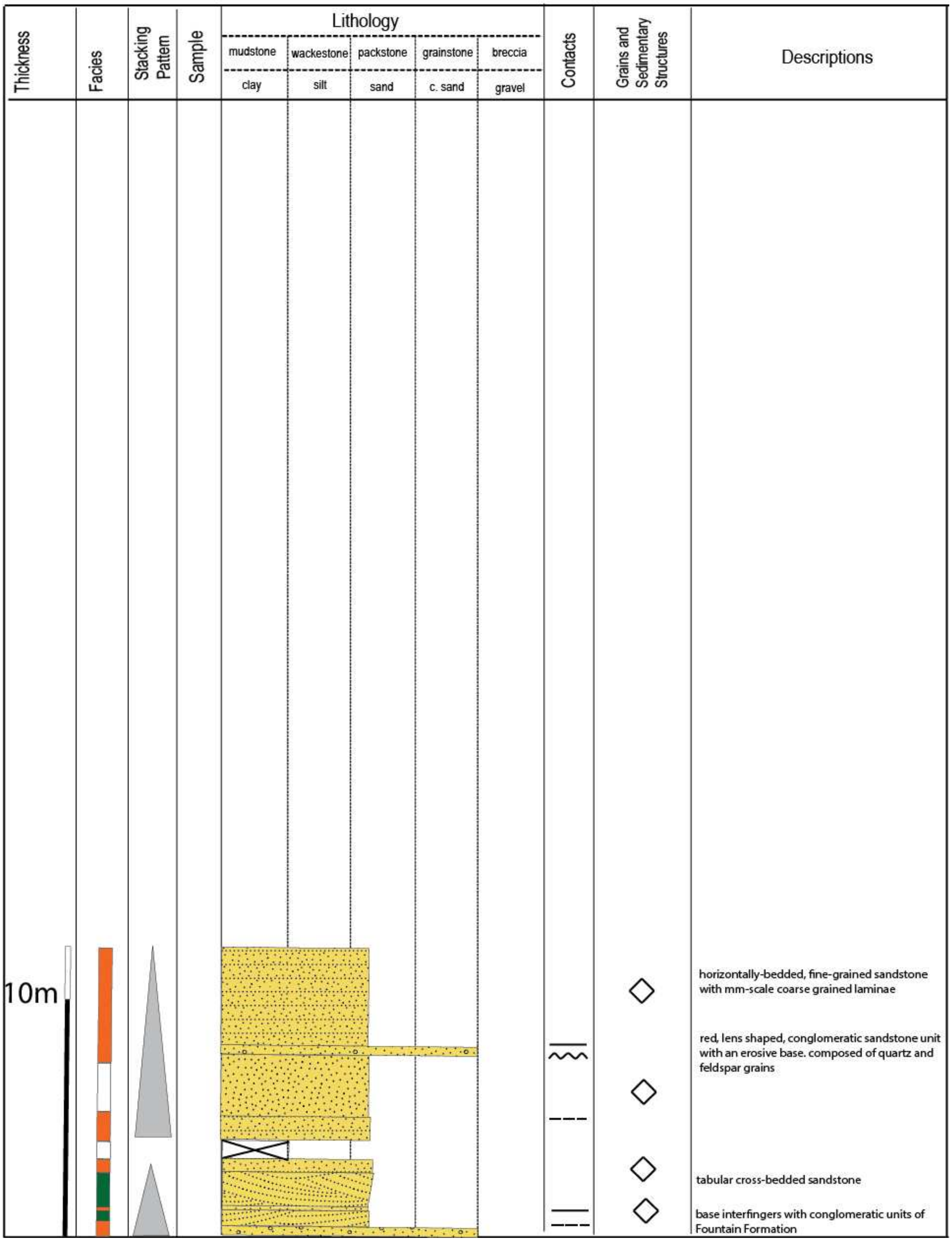

Section: Bellvue
Location: Bellvue
County, State: Larimer, Colorado

Outcrop Analyst: Kajal Nair
Date: 06/2016

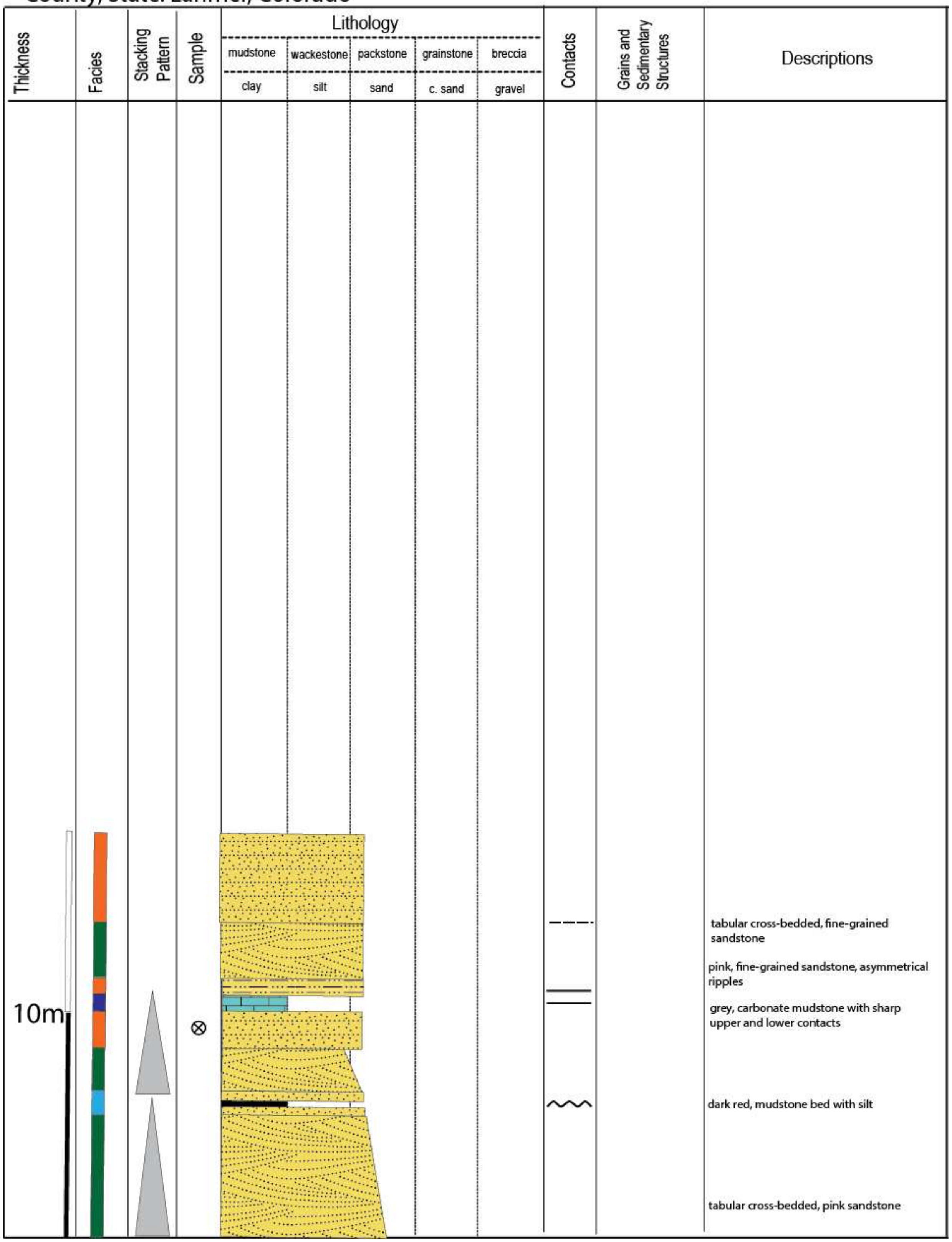

Section: Owl Canyon 1
Location: Owl Canyon
County, State: Larimer, Colorado

Outcrop Analyst: Kajal Nair
Date: 06/2016

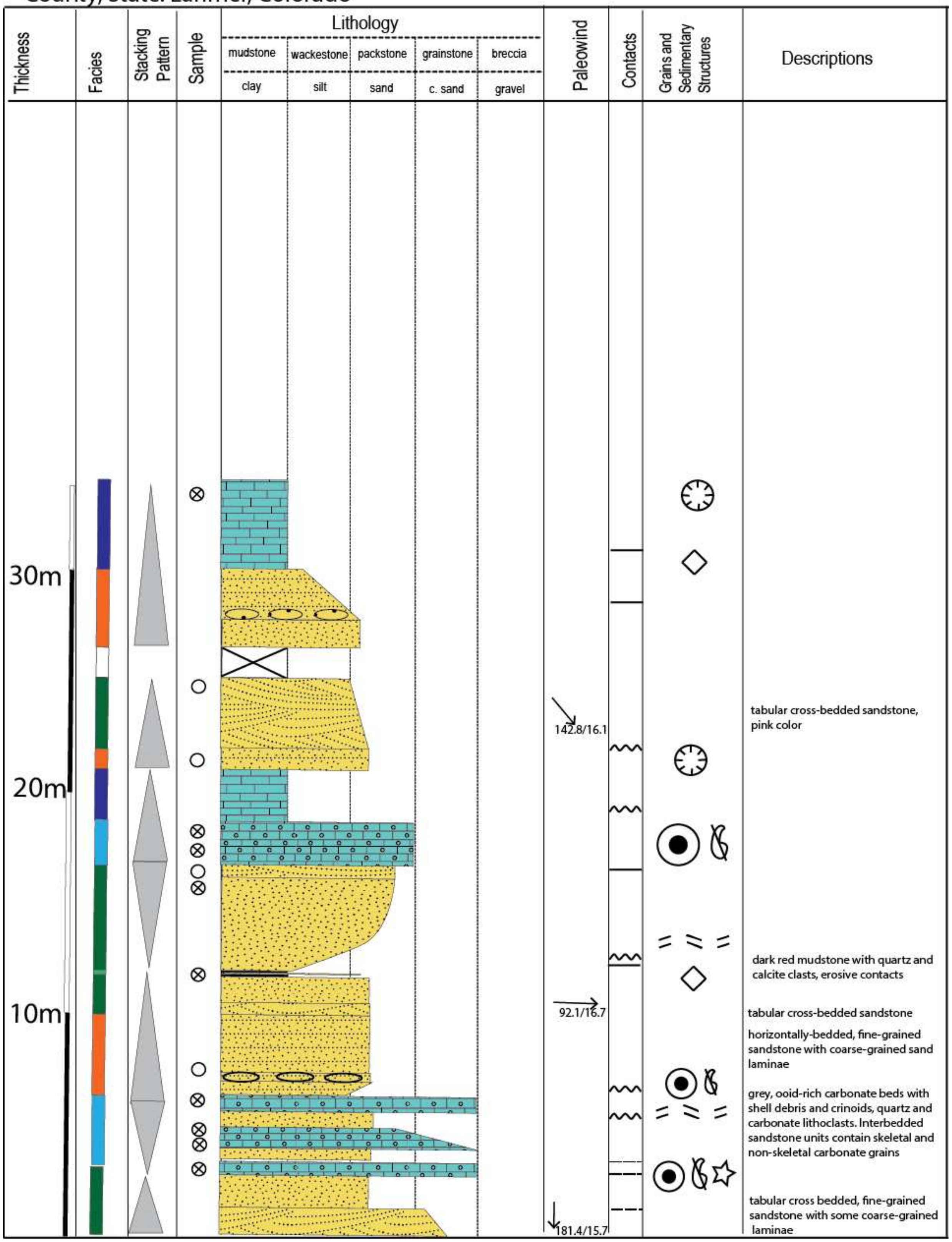

Section: Owl Canyon 1
Location: Owl Canyon
County, State: Larimer, Colorado

Outcrop Analyst: Kajal Nair
Date: 06/2016

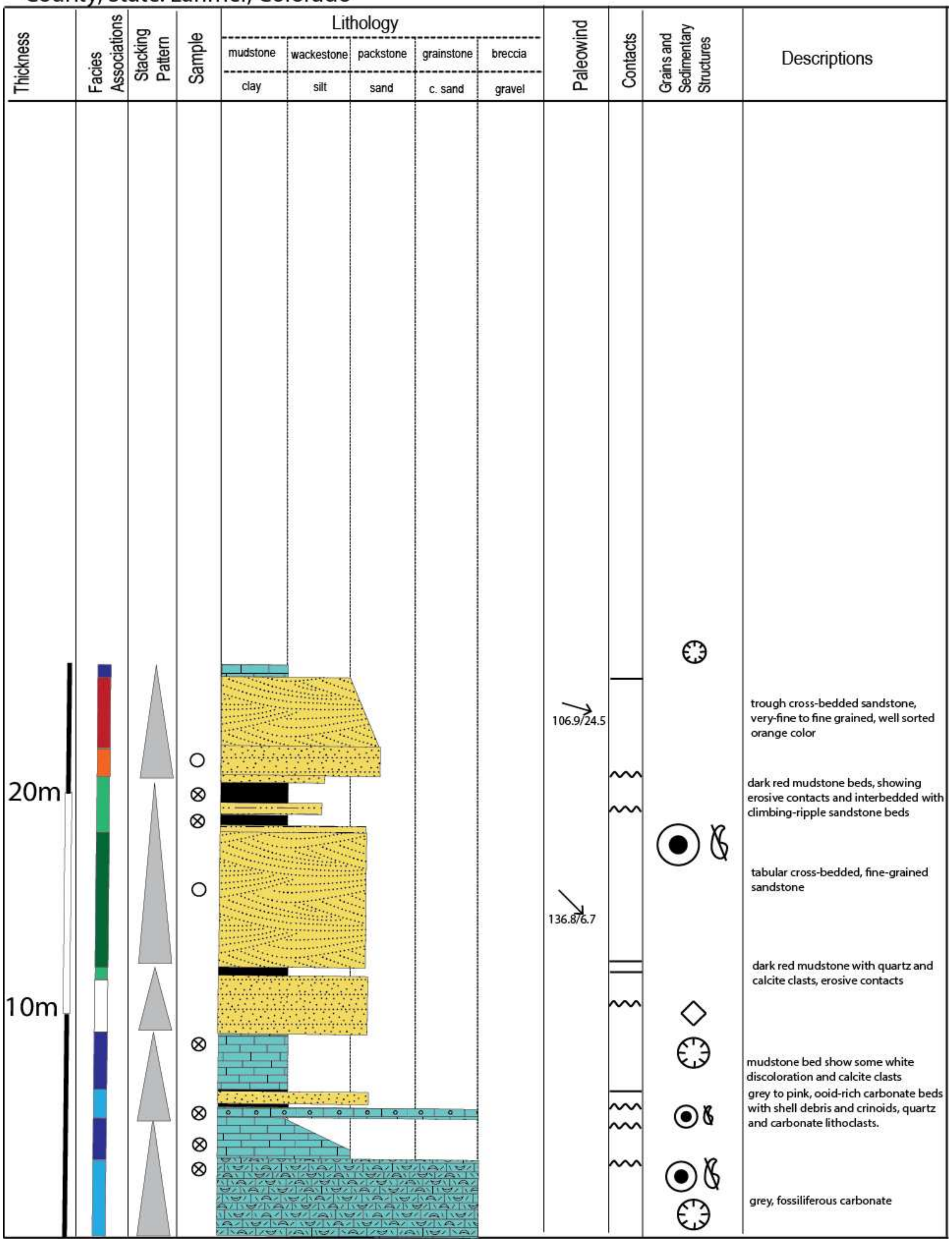

Section: Red Nose
Location: Red Nose
County, State: Larimer, Colorado

Outcrop Analyst: Kajal Nair
Date: 05/2016

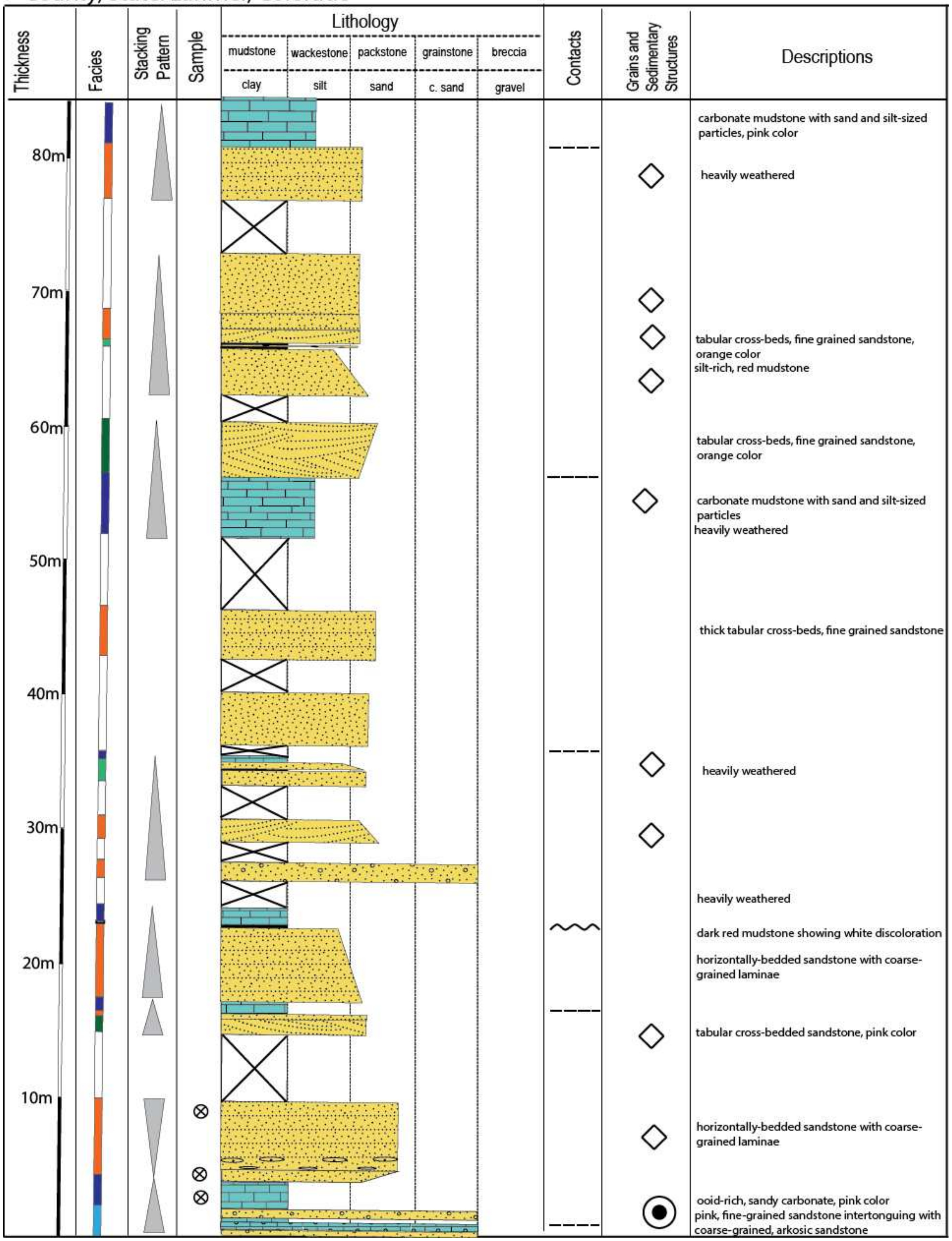

Location: Red Mountain
County, State: Larimer, Colorado

Outcrop Analyst: Kajal Nair
Date: 07/2016

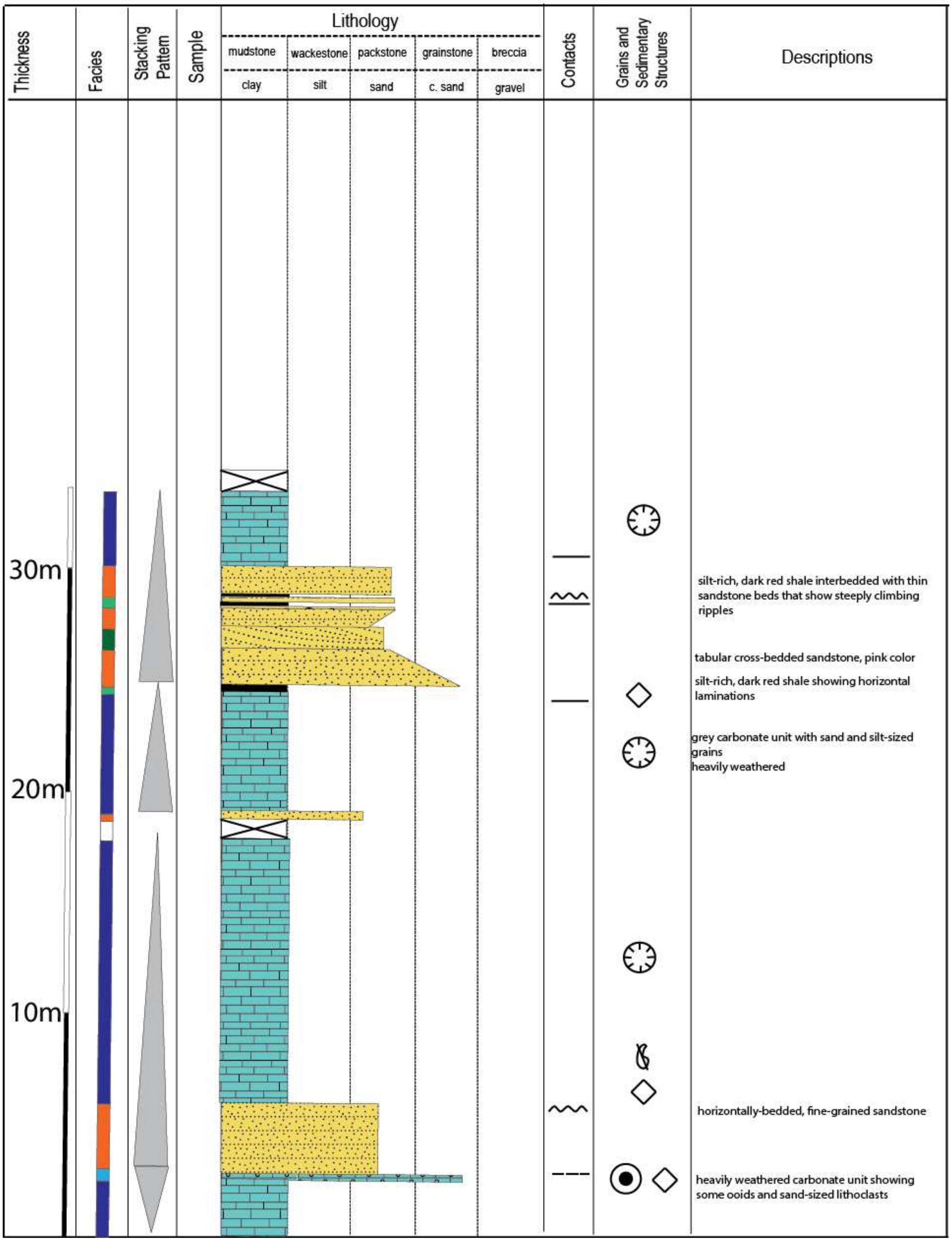

Location: Laramie
County, State: Laramie, Wyoming

Outcrop Analyst: Kajal Nair
Date: 07/2016

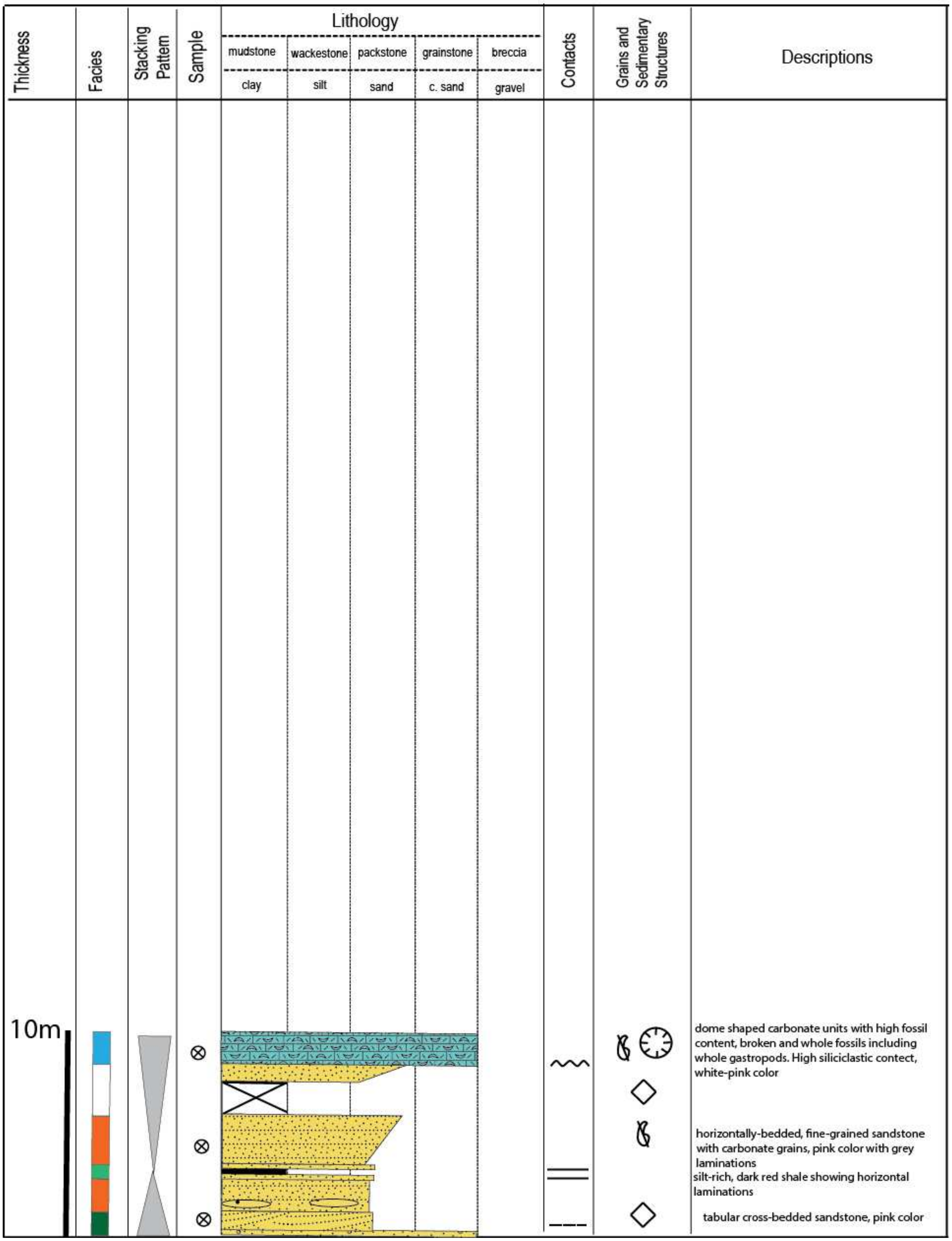

Section: R114 Well Name: 18-4
Stratigraphic Interval: Casper Formation
County, State: Albany, Wyoming

Core Analyst: Kajal Nair
Date: 10/2016

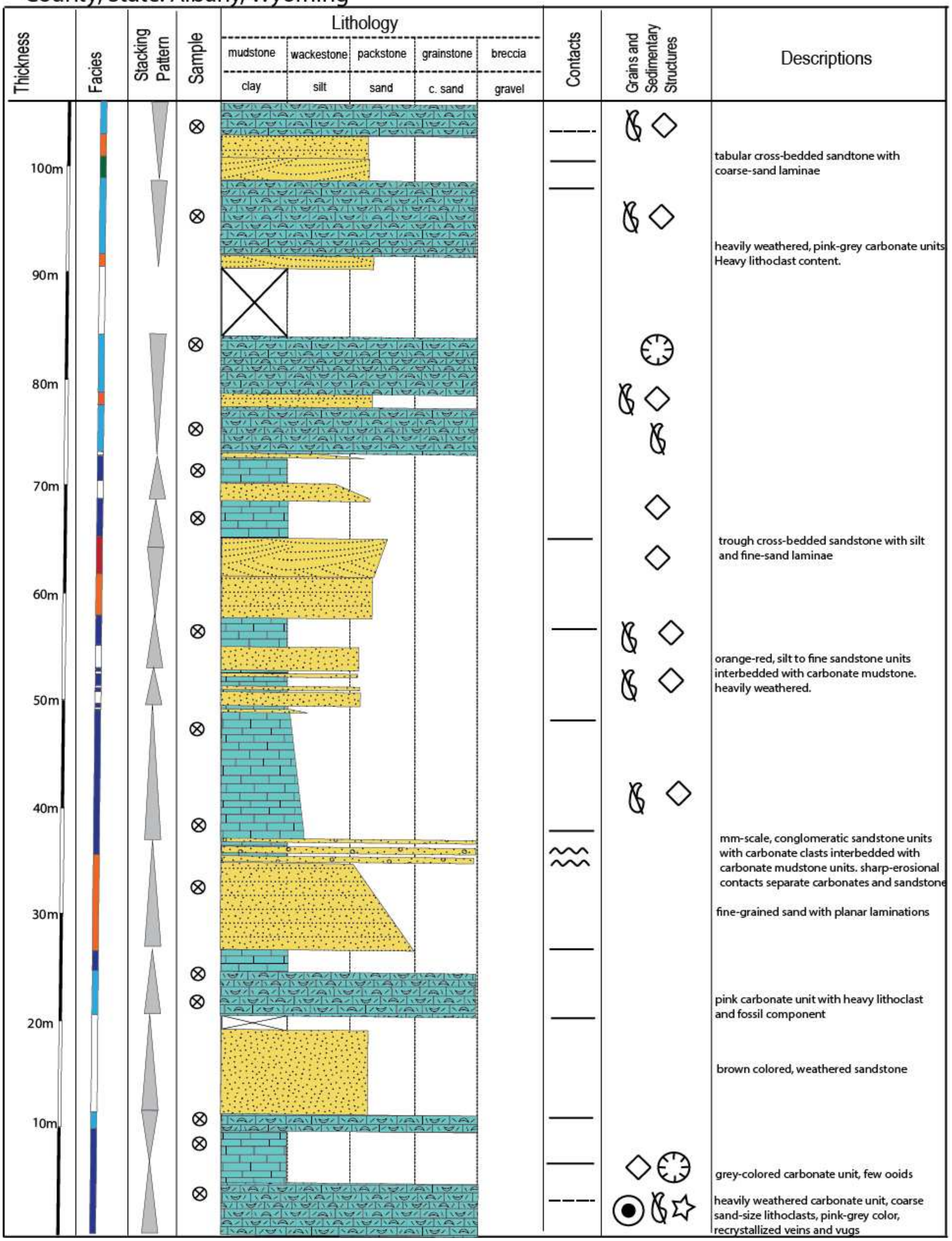

Section: Upper Ferch Well Name: 1-UPRR FERCH
Stratigraphic Interval: Ingleside Formation
County, State: Weld, Colorado

Core Analyst: Kajal Nair
Date: 10/2016

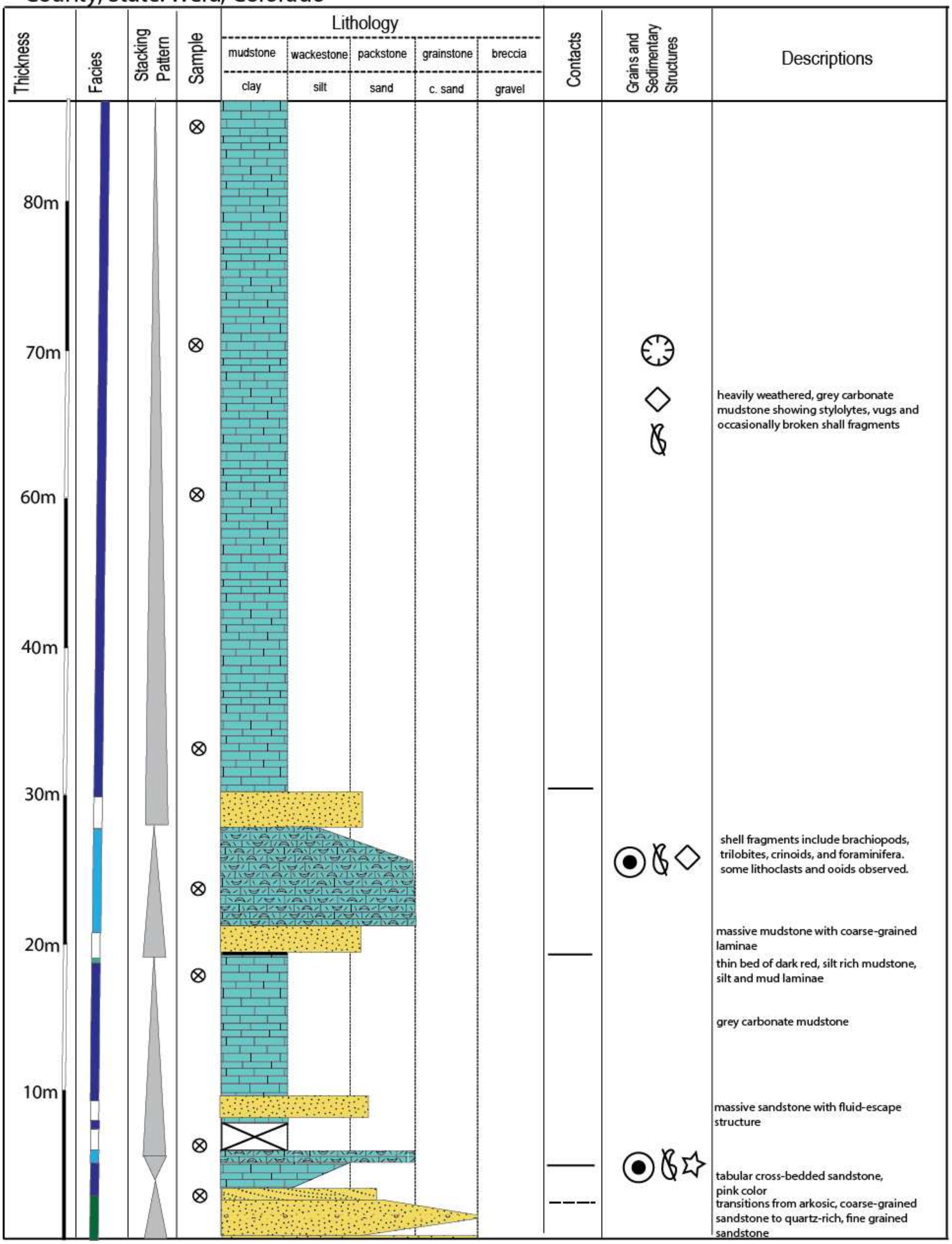

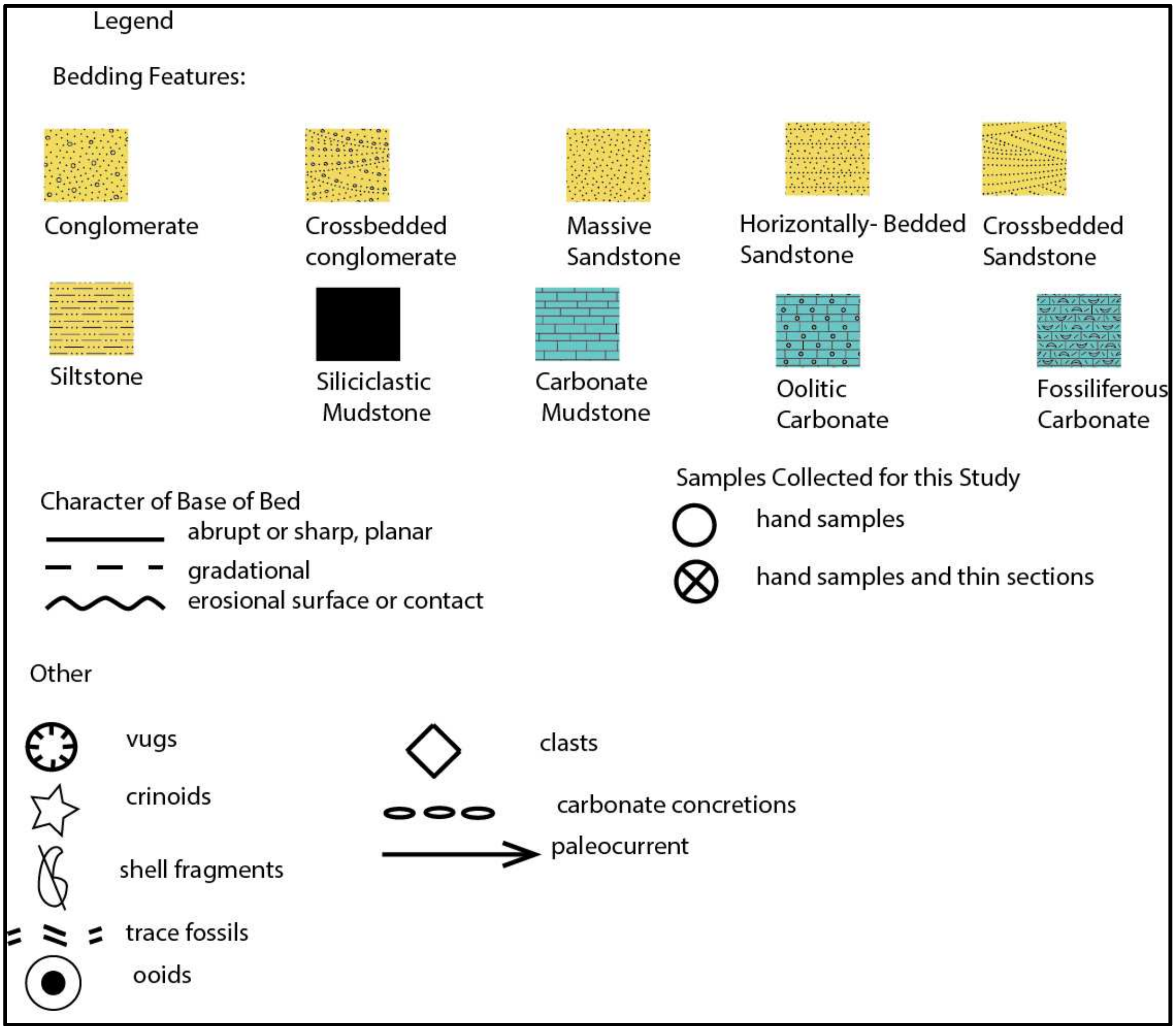
Legend
Bedding Features:
Conglomerate
Crossbedded conglomerate
Massive Sandstone
Horizontally- Bedded Sandstone
Crossbedded Sandstone
Siltstone
Siliciclastic Mudstone
Carbonate Mudstone
Oolitic Carbonate
Fossiliferous Carbonate
Character of Base of Bed
abrupt or sharp, planar
gradational
erosional surface or contact
Samples Collected for this Study
hand samples
hand samples and thin sections
Other
vugs
crinoids
shell fragments
trace fossils
ooids
clasts
carbonate concretions
paleocurrent

PART 2: DETRITAL ZIRCON GEOCHRONOLOGY OF THE INGLESIDE FORMATION

INTRODUCTION

U-Pb ages of detrital zircon grains in sandstone are commonly used as a guide to sediment provenance. Established detrital zircon reference curves for western North America provide enhanced characterizations of the age of magmatic assemblages and a robust means to distinguish the provenance of detrital zircon grains that accumulated along western Laurentia (Gehrels and Pecha, 2014). Detrital zircon ages from Paleozoic sandstones in the Grand Canyon record a major shift in provenance beginning in the Mississippian (Gehrels et al., 2011). This change is defined by the appearance of a significant population of Paleozoic-aged zircon grains interpreted to have been shed from the central Appalachian orogen. Distinct Paleozoic peaks from detrital zircon ages are well documented in the Mississippian Surprise Canyon Formation of the Grand Canyon and generally increase in frequency through younger Pennsylvanian and Early Permian strata (Gehrels et al., 2011).

Other studies have also identified detrital zircon populations shed from the Appalachian orogen in Paleozoic sedimentary strata across western United States (Figure 1). The oldest stratigraphic unit in Colorado that detects this age population is the Early Pennsylvanian loessite deposits of the Molas Formation in southwestern Colorado (Evans and Soreghan, 2015). Paleozoic detrital zircons are also documented in the Early Pennsylvanian Amsden Formation in southern Montana and Tensleep Formation in northern Wyoming (May et al., 2013), Middle Pennsylvanian Hailey Member of the Wood River Formation in south-central Idaho (Link et al., 2014), Early Permian Cedar Mesa Member of the Cutler Formation in southeastern Utah (Dickinson and Gehrels, 2003; Figure 1). Further east, detrital zircon populations from the central Appalachian orogen have been documented in the Cretaceous Dakota Formation in western Iowa and eastern Nebraska (Finzel, 2014), Middle Pennsylvanian Warrensburg and Moberly channel sandstones in central Missouri (Chapman, 2016), and the Permian Wellington Formation in southern Oklahoma (Thomas et al., 2016; Figure 1). These studies indicate that Appalachian-derived sediment was widely distributed across western United States by the Early Pennsylvanian. Appalachian detrital zircon populations are also widely detected through Early Triassic and Middle Jurassic sandstones along the Front Range and in southeastern Colorado (Hagadorn et al., 2016).

The arrival of Appalachian-sourced zircons across western North America has major paleogeographic implications for western Laurentia during Paleozoic time. Transcontinental sediment transport may have primarily been driven by major river systems carrying sediment westward from southern and central Appalachians (Blakey, 2009; Gehrels et al., 2011; Chapman, 2016). An increasingly arid climate, starting in the Middle Pennsylvanian, resulted in strong northeasterly and southeasterly wind systems (Parrish and Peterson, 1988; Soreghan et al., 2002) that further transported and reworked Appalachian-sourced sediments into local eolian units.

Various studies recording detrital zircon ages for Paleozoic and Mesozoic sandstones in Colorado collectively recognize a broad range of age populations defined by discrete peaks of age-frequency plots, reflecting local and transcontinental sediment sources (Duncan et al., 2013; Siddoway and Gehrels, 2014; Evans and Soreghan, 2015; Hagadorn et al., 2016). Local sources for Colorado Paleozoic sandstones include Yavapai-Mazatzal provinces (1800-1600 Ma) in the basement-cored Ancestral Rockies, Granite-Rhyolite province (1480-1340 Ma) in the southern midcontinent, and Pikes Peak batholith (1080 Ma) in the Ute Pass uplift. More distant sources include Archean basement (3015-2500 Ma) of the Laurentian shield, Grenville basement (1300-1000 Ma), Iapetan synrift (760-530 Ma), Peri-Gondwanan terranes (750-500 Ma); and Taconic (490-440 Ma), Acadian (430-350 Ma), and Alleghanian (330-270 Ma) synorogenic rocks.

The main objective of this study is to compare detrital zircon age populations from potentially time-equivalent upper Paleozoic Ingleside, Molas, and Hermosa sandstones with published detrital zircon U-Pb data from underlying and overlying sedimentary units in order to determine the timing of the arrival of exotic Appalachian zircons into two Ancestral Rocky Mountain basins across Colorado. Further, deposition of the Ingleside and Hermosa Formations mark a shift from terrestrial to shallow marine environments along the Ancestral Front Range and the Uncompahgre uplifts. Our study assesses whether the significant shift in depositional environments across two Ancestral Rocky Mountain uplifts also corresponds with a shift in sediment source.

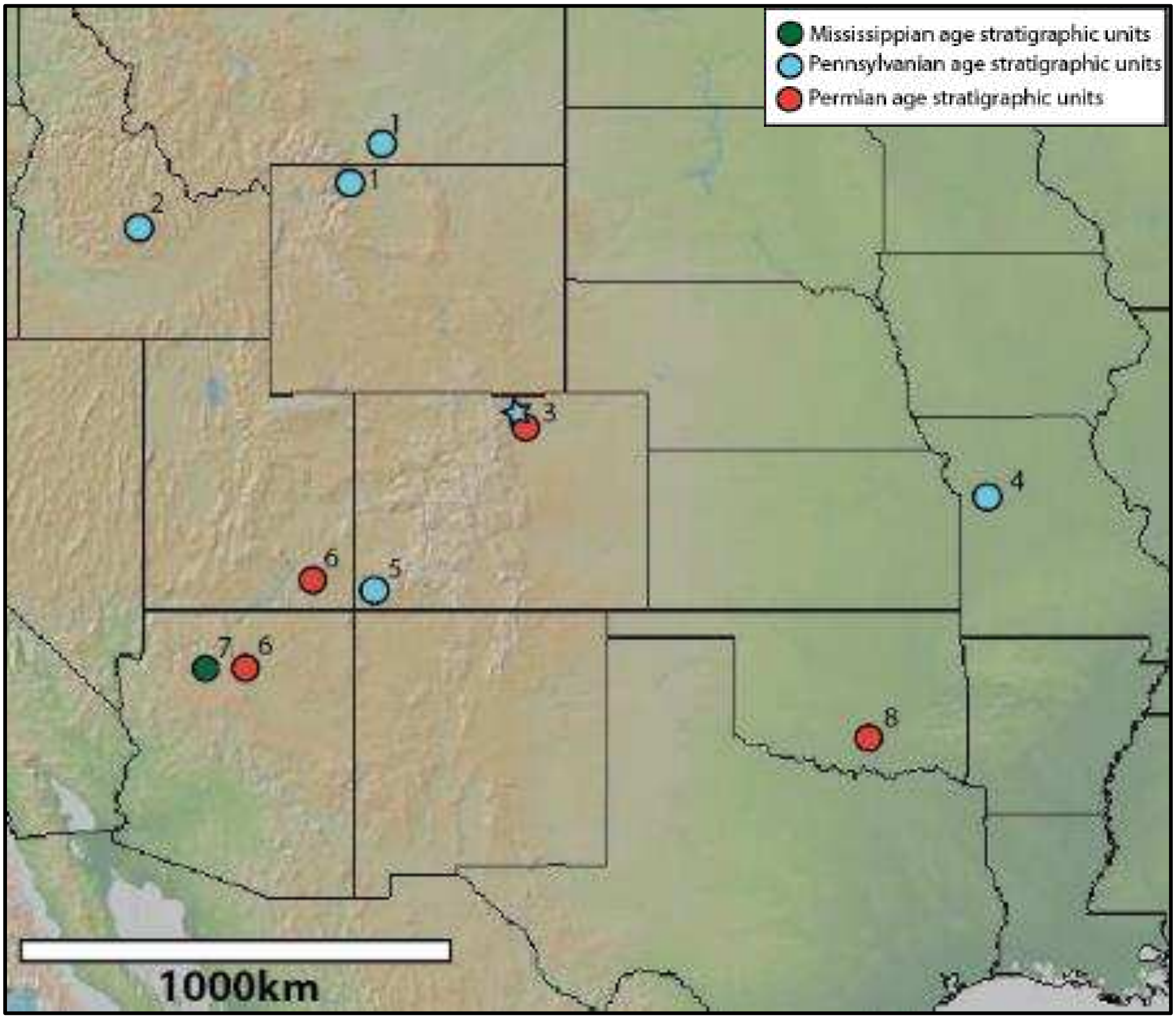

Figure 1: Locations of Appalachian-derived grain populations previously identified in Late Paleozoic sandstones (May et al., 2013[1] ; Link et al., 2014[2]; Holm-Denoma, unpublished[3]; Chapman, 2016[4]; Evans and Soreghan, 2015[5]; Dickinson and Gehrels, 2003[6]; Gehrels et al., 2011[7]; Thomas et al., 2016[8]. Location of Ingleside Formation analyzed in this study is marked by the star. Location of Molas and Hermosa Formations analyzed in this study overlaps location of Evans and Soreghan, 2015[5] ages). Base map from http://www.geomapapp.org.

GEOLOGICAL BACKGROUND

The Ancestral Rocky Mountain (ARM) system developed in an intraplate setting and consists of NW-trending basement-cored uplifts and sedimentary basins extending from Utah and Colorado to Texas. The deformation that resulted in the amagmatic ARM uplifts remains poorly understood. Various models invoke stresses along the Ouachita-Marathon belt, transpressional convergence along the Sonora margin, and reactivation of pre-existing basement faults to explain ARM deformation (Kluth and Coney, 1981; Dickinson and Lawton, 2003; Leary et al., 2017; Marshak et al., 2000).

Uplifts of ARM structures began in early Pennsylvanian and continued into early Permian time (e.g Kluth and Coney, 1981; Dickinson and Lawton, 2003). In present day Colorado, ARM uplifts developed during this time have been identified as the Ancestral Front Range highland, Apishapa highland, and Uncompahgre highland (Figure 2). These uplifted areas were rapidly denuded of older Paleozoic sedimentary rocks, and Proterozoic crystalline basement shed sedimentary debris into adjacent lowlands (Blakey, 2009). Pennsylvanian-Permian sedimentary rocks subsequently deposited in the low platforms are characterized by cyclic stratal sequences and are linked to Gondwanian glaciation in the southern hemisphere (Heckel, 1986; Blakey, 2008).

The early Pennsylvanian in western Colorado is characterized by the widespread deposition of the Molas Formation, a regolithic to marine deposit developed during a period of extensive subaerial weathering (Mallory, 1960). Potentially coeval with Molas deposition, vigorous uplift of the Ancestral Front Range highland in eastern Colorado resulted in widespread deposition of coalescing alluvial fans and fluvial deposits, collectively identified as the Fountain Formation (Knight, 1929).

The Ancestral Front Range, Uncompahgre highlands, and adjacent basins most likely reached their maximum tectonic expression in the late-middle Pennsylvanian time (Mallory, 1960; Blakey, 2008). Marine waters invaded the ARM basins during the middle-late Pennsylvanian, resulting in partial erosion of underlying rocks and Pennsylvanian-Permian deposition of the Hermosa and Cutler Formations in the Paradox basin, west of the Uncompahgre highland, and the Ingleside and Lyons Formations in the low-lying regions east of the Ancestral Front Range Highland. Late Paleozoic cyclic stratal sequences in both basins are characterized by a gradual transition from humid with alternating semi-arid intervals to more arid conditions (Blakey, 2009).

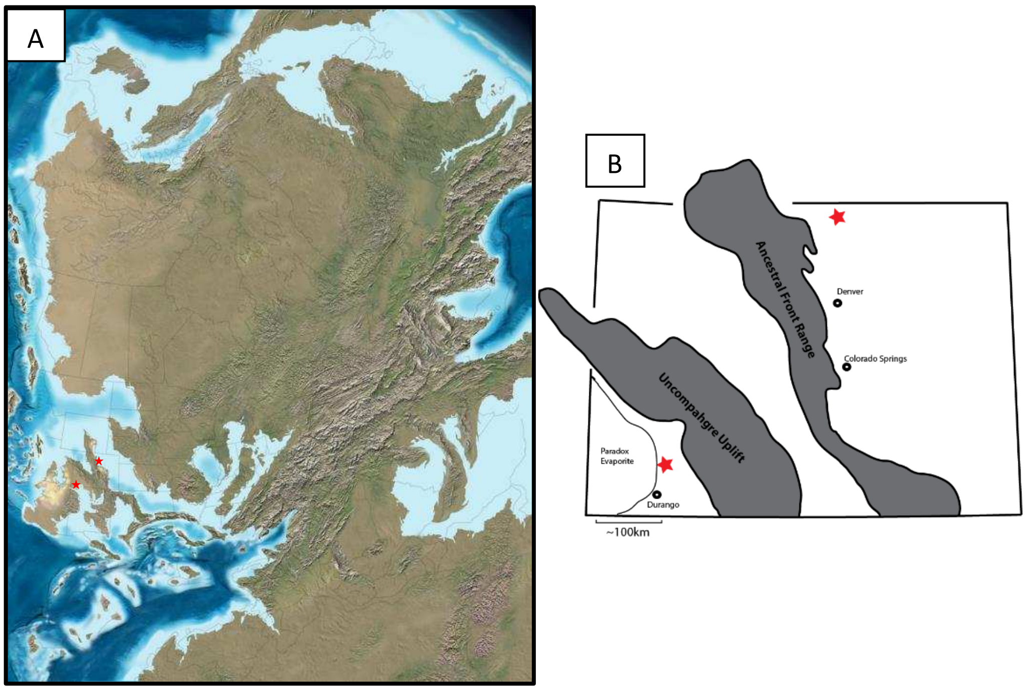

Figure 2: (A) Paleogeographic reconstruction of North America during the Late Pennsylvanian (Reference: Blakey, 2015). (B) Paleogeographic reconstruction of Ancestral Rocky Mountain uplift in Colorado (Halka and Chronic, 2014). Stars mark locations of samples analyzed in this study

METHODS

Sandstone samples were collected from the Ingleside Formation, Molas Formation, and Hermosa Formation for this study. The Ingleside Formation type-locality outcrop located at Owl Canyon in northern Colorado was logged for detailed sedimentological observations and paleocurrent analyses (Figures 2, 3, 4). Two representative fine-grained, quartz-rich sandstone samples were collected from the lower and upper portion of the Ingleside Formation at this section (Figure 2). A silt-rich sandstone sample from the upper Molas Formation and a fine-grained sandstone sample from the lower Hermosa Formation were collected across the Molas-Hermosa contact near Molas Lake in southwestern Colorado (Figure 2).

Zircons were separated using conventional methods that included crushing, lightly panning, sieving below 300 µm, magnetic separation, and heavy liquid separation. Representative splits of the final zircon yields were mounted in epoxy plugs and polished. Cathodoluminescence (CL) images were generated for all four samples and the images were used to pick 120+ laser spots in homogeneous portions of crystals in each sample (Figure 4, Appendix B).

U-Pb detrital zircon data reported here were generated at the U.S. Geological Survey (USGS) in Denver using laser ablation-inductively coupled plasma-mass spectrometry (LA-ICP-MS). All ages >1300 Ma are reported as $^{207}Pb/^{206}Pb$ ages, whereas $^{206}Pb/^{238}U$ ages were used for <1300 Ma grains. Two separate discordance filters were used to generate probability-density plots for our data and for calculating statistically significant age populations. In Figure 4B and 4D, data with >20% discordance or >5% reverse discordance were rejected. In Figure 4A and 4C, data with >30% discordance or >10% reverse discordance were rejected.

Figure 6 displays the results generated in comparing our samples with each other and with other published samples from throughout the broader region. Published samples compared here include data from the Lyons Formation (Holm-Denoma C., 2016, unpublished), Fountain Formation (Siddoway and Gehrels, 2014), and lower Molas Formation (Evans and Soreghan, 2015). A general >20% discordance or <5% reverse discordance is applied to all samples compared in this figure, and all age spectra are normalized so the areas under the curve are equivalent, regardless of number of analyses.

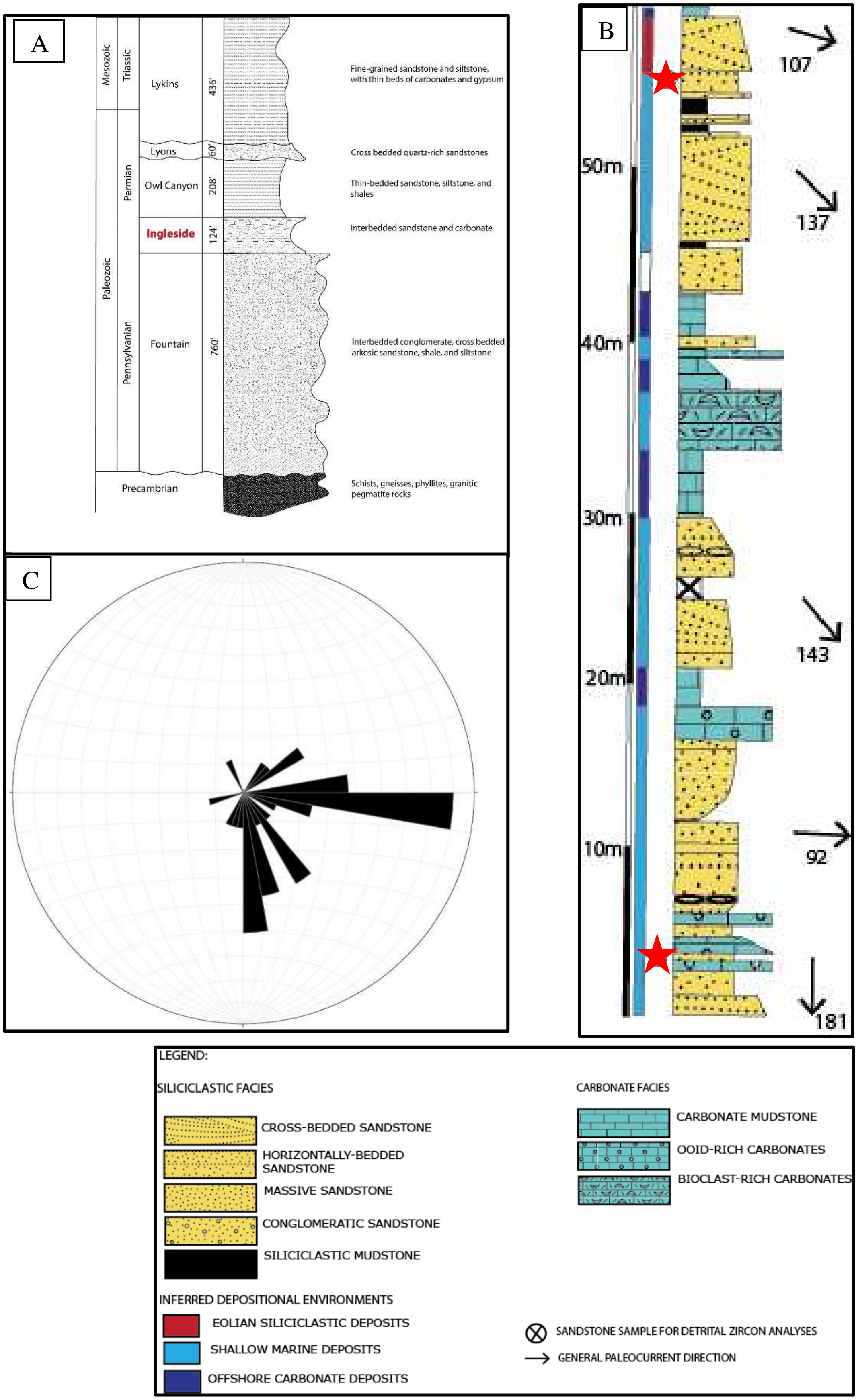
A
Mesozoic
Triassic
Lykins
436'
Fine-grained sandstone and siltstone, with thin beds of carbonates and gypsum
Lyons
60'
Cross bedded quartz-rich sandstones
Permian
Owl Canyon
208'
Thin-bedded sandstone, siltstone, and shales
Ingleside
124'
Interbedded sandstone and carbonate
Paleozoic
Pennsylvanian
Fountain
760'
Interbedded conglomerate, cross bedded arkosic sandstone, shale, and siltstone
Precambrian
Schists, gneisses, phyllites, granitic pegmatite rocks
B
50m
40m
30m
20m
10m
107
137
143
92
181
C
LEGEND:
SILICICLASTIC FACIES
CROSS-BEDDED SANDSTONE
HORIZONTALLY-BEDDED SANDSTONE
MASSIVE SANDSTONE
CONGLOMERATIC SANDSTONE
SILICICLASTIC MUDSTONE
CARBONATE FACIES
CARBONATE MUDSTONE
OOID-RICH CARBONATES
BIOCLAST-RICH CARBONATES
INFERRED DEPOSITIONAL ENVIRONMENTS
EOLIAN SILICICLASTIC DEPOSITS
SHALLOW MARINE DEPOSITS
OFFSHORE CARBONATE DEPOSITS
SANDSTONE SAMPLE FOR DETRITAL ZIRCON ANALYSES
GENERAL PALEOCURRENT DIRECTION

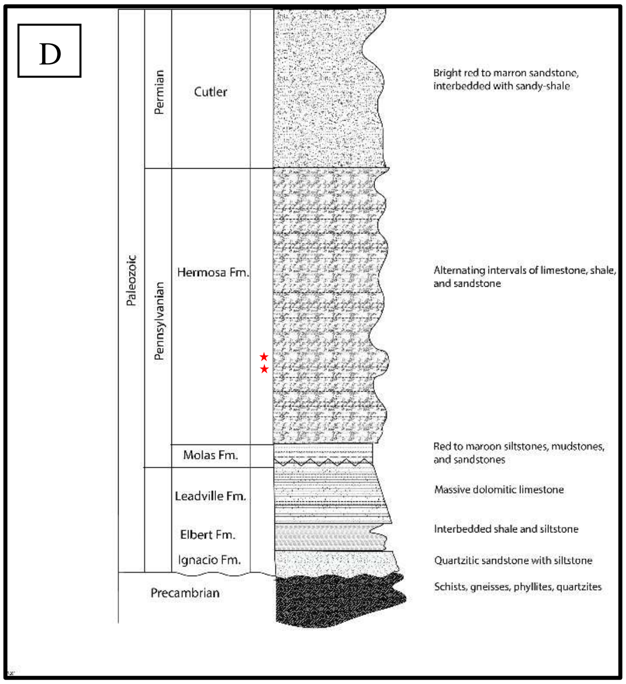

Figure 3: (A) Generalized stratigraphic column of Northern Colorado. (B) Type section of the Ingleside Formation at Owl Canyon displays a mixed carbonate-siliciclastic facies distribution, with inferred shallow marine and eolian depositional environments. (C) Thirty-three paleocurrent analyses from the Ingleside Formation at Owl Canyon show a dominantly S- and E- sediment transportation direction. (D) Generalized stratigraphic column of Southwestern Colorado, stars mark approximate location of samples analyzed for Upper Molas and Lower Hermosa Formations.

Table 1: UTM coordinates, location, and description for samples analyzed

Sample	Stratigraphic Units	Location	UTM Coordinates			Sample Description
			Grid Zone	Easting	Northing	
OC-DZ1-2.8	Lower Ingleside	Owl Canyon, N. CO	13S	0484790	4512465	tabular cross-bedded, pink, fine-grained sandstone overlying a carbonate unit and 2.8m above the Fountain-Ingleside contact
OC-DZ2-56	Upper Ingleside	Owl Canyon, N. CO	13S	0485041	4512595	horizontally-bedded, fine-grained sandstone, 56m above the Fountain-Ingleside contact
MP-DZ1	Molas	Molas Pass, SW. CO	13S	4180618	4180618	massive, silt-rich, very fine-grained sandstone, dark red color, (~20m from the base of the Molas Formation
MP-DZ2	Hermosa	Molas Pass, SW. CO	13S	4180740	4180740	horizontally-bedded, medium-grained sandstone, gray-brown color, overlying a carbonate unit and ~4m above the Molas-Hermosa contact

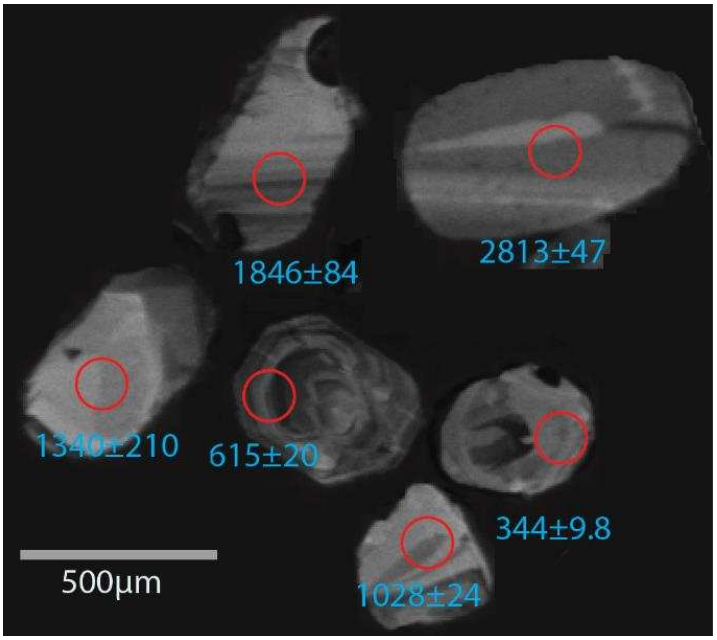

Figure 4: Representative CL images of zircons from prominent age distribution peaks at 330-490 Ma, 515-700 Ma, 990-1200 Ma, 1600-1800 Ma, 2500-3500 Ma.

RESULTS

I. Description

The detrital zircon U-Pb data collected from the Ingleside, Molas, and Hermosa Formations (Table 1) reveal a wide spread of age populations, with prominent age distribution peaks at 330-490 Ma, 515-700 Ma, 990-1200 Ma, 1340-1500 Ma, 1600-1800 Ma, and 2500-3500 Ma (Figure 5 and 6).

Detrital zircon data from the Ingleside Formation sandstone are compared to data from the underlying Fountain Formation (Siddoway and Gehrels, 2014; Duncan et al., 2013) and overlying Lyons Formation in the Colorado Front Range (Holm-Denoma et al., 2016, unpublished) (Figure 7). The youngest population of grains recorded (330-490 Ma) is first detected in the Lower Ingleside Formation where Paleozoic-aged zircons range between 331 and 448 Ma and make up 10% of the total concordant ages (<20% discordance or <5% negative discordance). The Upper Ingleside displays a Paleozoic age population between 376 and 498 Ma, comprising 5% of the total concordant ages. Results from Lyons Formation sandstone collected near Park Creek Reservoir, Colorado (Holm-Denoma et al., 2016, unpublished) show an increase in Paleozoic-aged zircons, with U-Pb ages ranging between 330 and 457 Ma and comprising ~14% of the total concordant ages. While the Lower Ingleside, Upper Ingleside, and overlying Lyons Formation show similar age peaks, they vary significantly from the underlying Fountain Formation. Detrital zircon ages from the Fountain Formation near Manitou Springs record a dominant age peak at 1600-1800 Ma, which comprises 44% of the total concordant ages. Other prominent age peaks in the Fountain Formation are observed at 990-1200 Ma and 1340-1500 Ma (Siddoway and Gehrels, 2014; Duncan et al., 2013).

Detrital zircon data collected from the Molas and Hermosa Formation sandstone near the eastern margin of the Paradox Basin show age distributions that are similar to the Ingleside and Lyons Formations (Figure 7). We also compare our U-Pb ages to data presented by Evans and Soreghan (2015) from two underlying Molas loessite samples collected in the same general area in the Paradox Basin (Molas Lake) (Figure 8). Paleozoic zircons dated in the Molas Formation sandstone range between 430 and 500 Ma, and comprise

10% of the total concordant ages. The overlying Hermosa Formation displays a smaller abundance of Paleozoic zircons that range between 415 and 467 Ma, and comprise 4% of the total analyses. Interestingly, notable differences are observed between the Molas and Hermosa samples in age peaks that lie between 990-1200, 1340-1500, and 1600-1800 Ma (Figure 9). The 990-1200 Ma population makes up a dominant peak in the Molas Formation analyses, whereas the 1340-1500 Ma and 1600-1800 Ma age peaks increase significantly in the Hermosa Formation. It is interesting to note that the two Molas loessite samples dated by Evans and Soreghan (2015) display a minor population of younger zircons (between 281-400 Ma) that is absent in the overlying Molas and Hermosa sandstone samples from this study. Paleozoic-aged zircons in the loessites are more abundant than the overlying Molas and Hermosa samples collected for this study, comprising 11% and 17% of the total concordant ages.

Detrital zircons in the Ingleside, Molas, and Hermosa Formations dominantly record U/Th ratios greater than 10, which are compatible with an igneous origin (e.g. Kirkland et al., 2015; Figure 10). A few miscellaneous zircons in the 990-1200 Ma and 2500-3500 Ma age populations record U/Th ratios <10, suggesting a metamorphic origin.

Paleocurrent analyses from the Ingleside Formation at Owl Canyon display a dominantly south- and east-directed sediment transport direction (Figure 3B). In comparison, the Fountain Formation near Manitou Springs, Colorado displays similar south- and east- dominated sediment transport direction in the upper sandstone strata and north- and east- dominated paleocurrent directions in the lower sandstone strata (Sweet and Soreghan, 2010)

II. Interpretation

Paleozoic sandstones from the Colorado Front Range in north-central Colorado and the eastern Paradox Basin in southwestern Colorado display a diversity of age populations that record several different source regions. Local zircon sources are primarily reflected in the 1600-1800 Ma age peak that is derived from the Yavapai province and 1340-1500 Ma age peak that is may be derived from local igneous units within Yavapai province (Whitmeyer and Karlstrom, 2007). The southern Rocky Mountains in general record a long history of 1800-1400 Ma tectonism, and identifying Proterozoic subprovinces within Colorado has been difficult. Reed (1987) identified three Yavapai subprovinces and suggested that the age of the subprovinces decreases southward. Closer to the Ingleside and Lyons Formation sample locations, Yavapai basement rocks are likely characterized by pluton ages greater than 1750 Ma (Reed, 1987). Closer to the Hermosa and Molas Formation sample locations, pluton and metavolcanic ages of 1760-1600 Ma are common (Bickford et al., 1986 Bickford et al., 2008). Zircons belonging to these age ranges are interpreted to have been supplied from basement rocks that are truly local to our sample locations.

Extensive Mesoproterozoic magmatism resulted in emplacement of igneous complexes in a belt that spanned southwestern Laurentia. Several of these igneous complexes are located close to the outcrops analyzed in this study. Specifically, the Sherman Granite pluton (1415-1435 Ma) in north-central Colorado and southeastern Wyoming is located ~17 km northwest of the Lyons Formation sample location and ~21 km northwest of the Ingleside Formation sample location (Nyman et al., 1994; Frost et al., 1999). The location of this batholith and its close proximity to our Front Range sandstone outcrops make it a likely source for a fraction of Mesoproterozoic zircons in our data. South- and east- directed sediment transport directions, as observed from our paleocurrent analyses of the Ingleside Formation, also support the presence of local sediment source to the north and west of our study area. Similarly, the closest Mesoproterozoic plutons to the Molas and Hermosa sandstone samples location is ~15 km south in the Needle Mountains, where plutonic rocks make up the Electra Lake Gabbro and Eolus Gabbro (1442-1435 Ma) (Gonzales et al., 1996). Based on their close proximity, these plutonic rocks are suggested to be a likely source for a portion of Mesoproterozoic zircons in the Molas and Hermosa sandstone.

A wide age peak centered at 990-1200 Ma is interpreted to reflect grains shed directly from the Grenville orogeny. Grenvillian basement rocks occupy an elongate belt that were exposed in the Taconic-Acadian tectonic belts in northeastern North America and the southeastern flank of Laurentia. Locally derived sediment from the Pikes Peak Batholith within the Rocky Mountain Region is suggested as an alternative source for a narrow subset of these grains that center on 1100 Ma (Van Schmus and Bickford, 1993). Due to its local setting and the presence of narrow U-Pb peaks at ~1100 Ma that superimpose the broader 990-

1200 Ma peak, the Pikes Peak Batholith likely did contribute Mesoproterozoic zircons to both sedimentary basins studied here. However, the wide range of Grenvillian-age zircons suggest that sediments were also derived from other Grenvillian-age provinces outside the Ancestral Rocky Mountain province. The specific Grenville terrane that contributed sediments to Ancestral Rocky Mountain basins is unclear. Similar to Jurassic eolianites across the Colorado Plateau (Dickinson and Gehrels, 2003), it is suggested that the Appalachians were a likely source for Grenville –age zircons. This interpretation corresponds well with the inference of an Appalachian derivation for Paleozoic zircons.

Paleozoic zircons (330-490 Ma) record sediment shed directly from the Taconic-Acadian orogeny along the Appalachian orogenic belt. Paleozoic peaks in the Lower and Upper Ingleside can be subdivided into a 440-490 Ma population corresponding to the Taconic orogeny and a 330-420 Ma population corresponding to the Acadian orogeny. In comparison, Paleozoic age populations in the Molas silty-sandstone and Hermosa samples display only Taconic-aged zircons.

Gondwanan and peri-Gondwanan terranes contain zircons dominantly within the age range of 550-850 Ma (Wortman et al., 2000) and are a potential source for relatively small 515-700 Ma peaks. A mixture of these Neoproterozoic ages with younger Paleozoic grains likely indicate derivation from the Appalachian orogenic belt. Peri-Gondwanan terranes embedded within the Appalachians include the Avalone terrane of the northern Appalachian, the Carolina terrane of the southern Appalachians, and the Suwannee terrane in the Florida peninsula, all of which contain zircons mainly in the age range of 535-635 Ma (Wortman et al., 2000), but also extending to 765 Ma (Barr, 1993). It is likely that sediments from these terranes were transferred to mid-continent North America along the Appalachian-Ouachita orogenic margin in the Late Paleozoic (Abati et al., 2010). An alternative source area for a small portion of these grains might be the 520-540 Ma granites in the Wichita Mountains, where emplacement of synrift igneous magmas along the Southern Oklahoma fault system accompanied late stages of rifting of southeastern Laurentia (Thomas et al., 2016).

A minor zircon population between 2500-3500 Ma is present in all the sandstone samples (Figure 3) are interpreted to have originated from exposed blocks of Archean cratons or large areas of reworked Archean crust (Corrigan et al., 2005). Derivation from the nearby Wyoming Archean province, lying directly north of the Ancestral Rocky Mountain basin is inferred for this age population for both basins.

The Front Range outcrops display dominantly local sources for the Fountain Formation originating from the Yavapai-Mazatal terranes (1600-1800 Ma), local plutonic sources (1340-1500 Ma), and the Pikes Peak Batholith (1100 Ma). More widespread sediment sources are observed for the Ingleside and Lyons Formation. Both the Ingleside Formation samples analyzed for this study show similar age peaks and grain populations for different sediment sources, with a distinct increase in grains sourced from the Appalachian orogen observed in the Lyons Formation.

The eastern Paradox Basin sandstone samples show an interesting trend with a significant increase in locally derived grains (1600-1800 Ma, 1340-1500 Ma) in the Hermosa Formation. Zircon age distributions in the underlying Molas Formation show relatively greater age peaks for exotic zircons sourced from the Appalachian orogen and Grenville orogen. The Molas loessite samples display a small population of Acadian-aged zircons that is absent in the overlying Molas silty-sandstone and Hermosa samples. A general comparison between the Molas loessite and the Molas silty-sandstone samples indicates that general decrease in abundance of Paleozoic-aged (330-490 Ma) zircons.

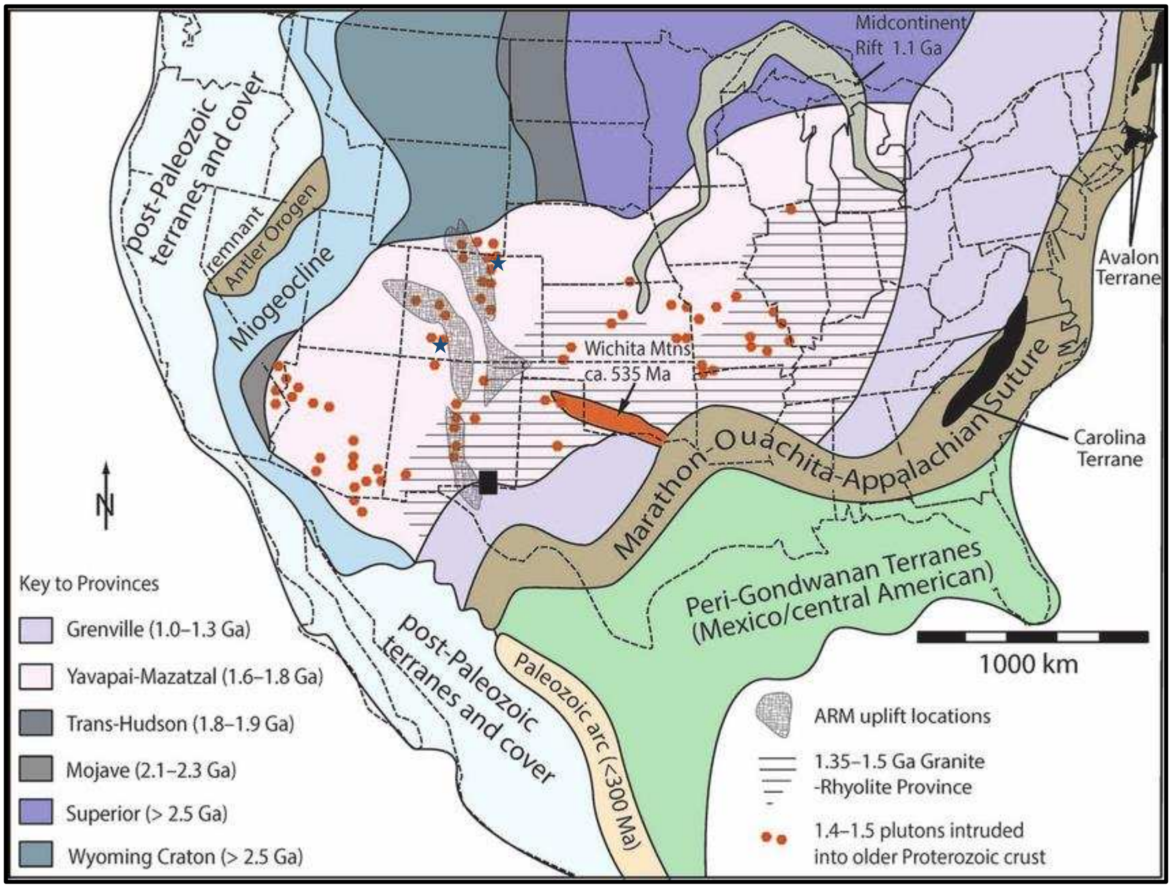

Figure 5: Map depicting the main age provinces of basement rock in North America (Soreghan and Soreghan, 2013). Stars mark locations of samples analyzed for this study.

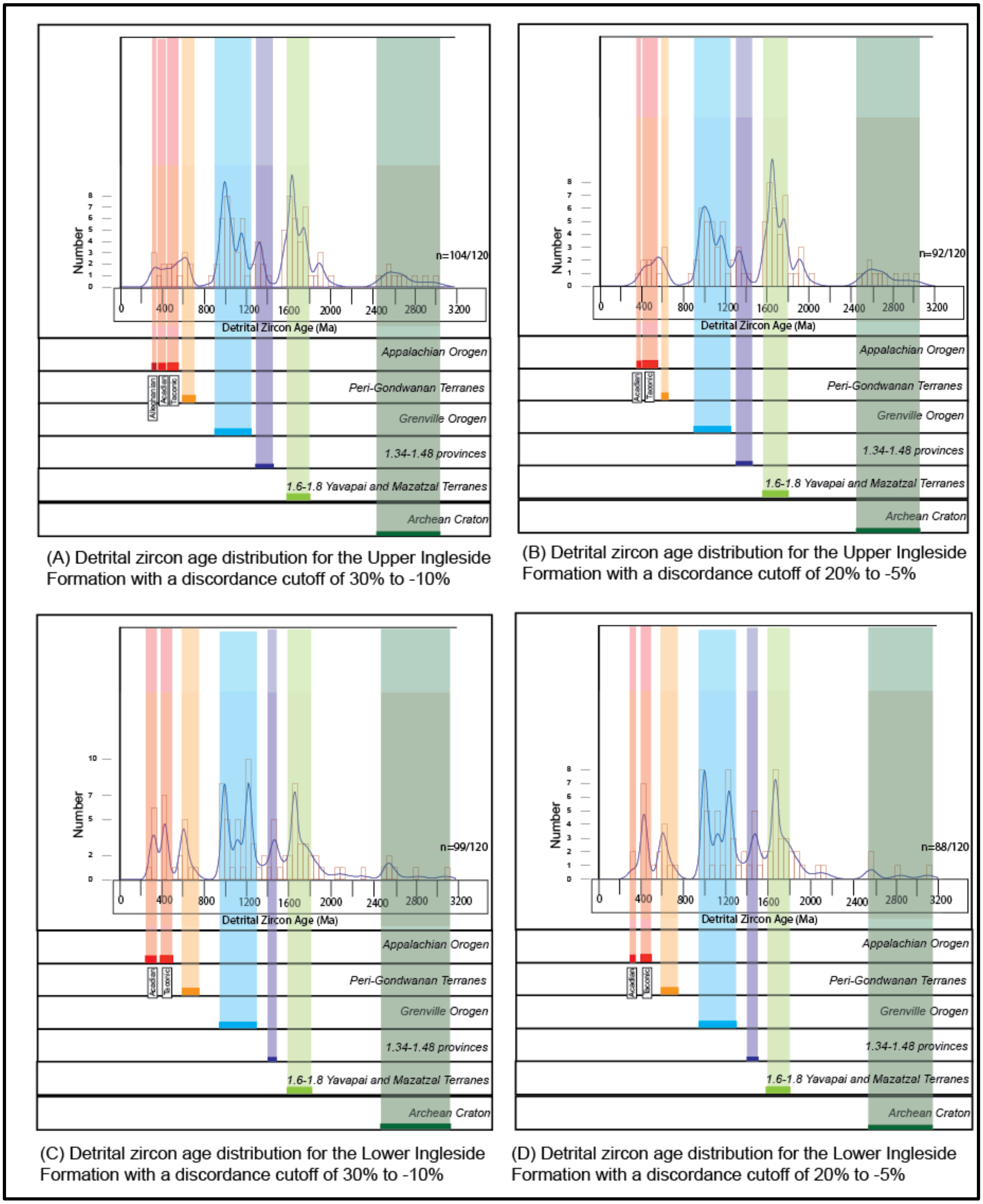

(A) Detrital zircon age distribution for the Upper Ingleside Formation with a discordance cutoff of 30% to -10%

(B) Detrital zircon age distribution for the Upper Ingleside Formation with a discordance cutoff of 20% to -5%

(C) Detrital zircon age distribution for the Lower Ingleside Formation with a discordance cutoff of 30% to -10%

(D) Detrital zircon age distribution for the Lower Ingleside Formation with a discordance cutoff of 20% to -5%

Figure 6: Probability density plots showing U-Pb ages of detrital zircons from fine-grained sandstones from the Ingleside Formation. Information on the lower right of the diagram gives number of ages plotted/number of ages determined.

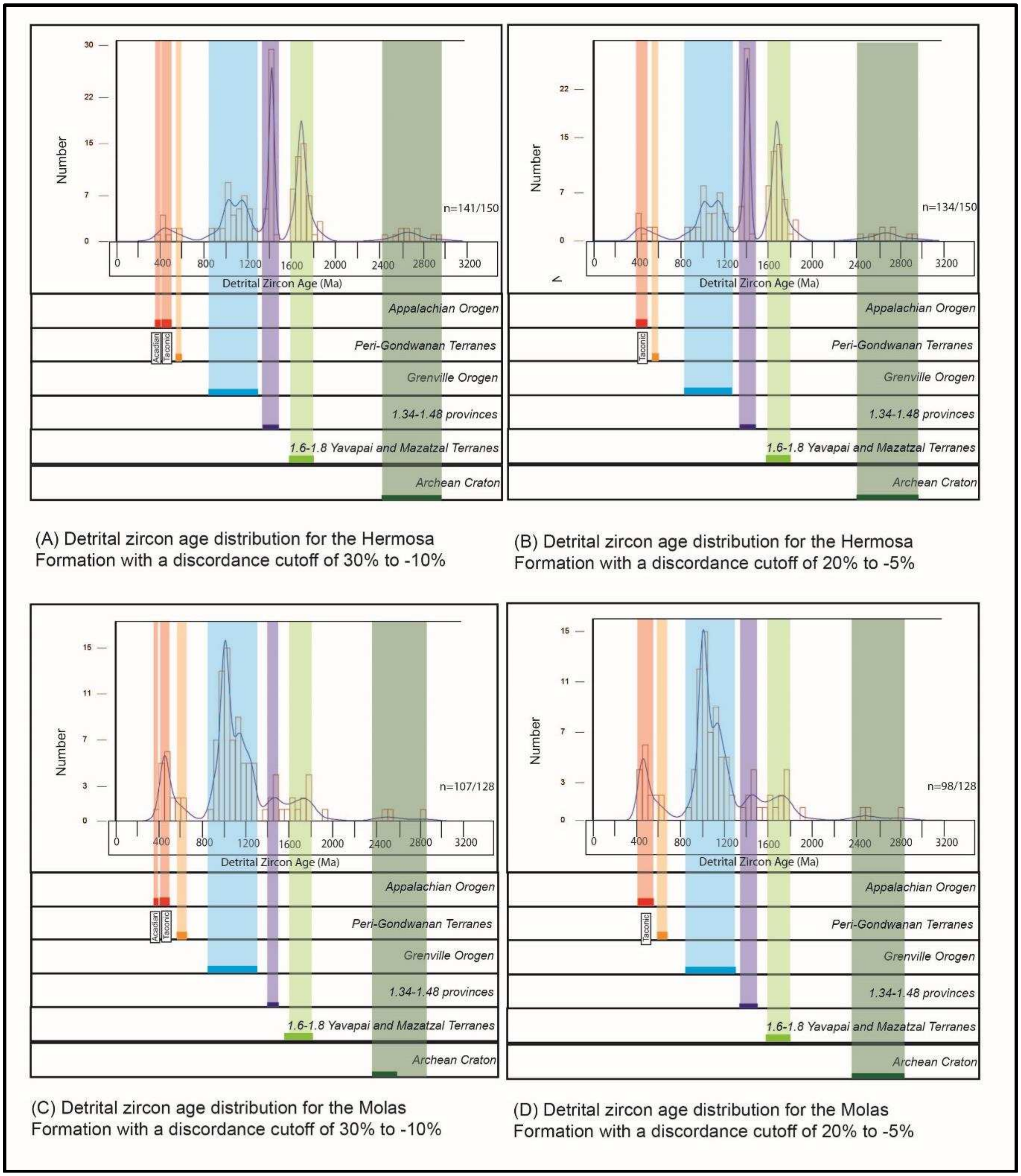

Figure 7: Probability density plots showing U-Pb ages of detrital zircons from fine-grained sandstones from the Molas and Hermosa Formations. Information on the lower right of the diagram gives number of ages plotted/number of ages determined.

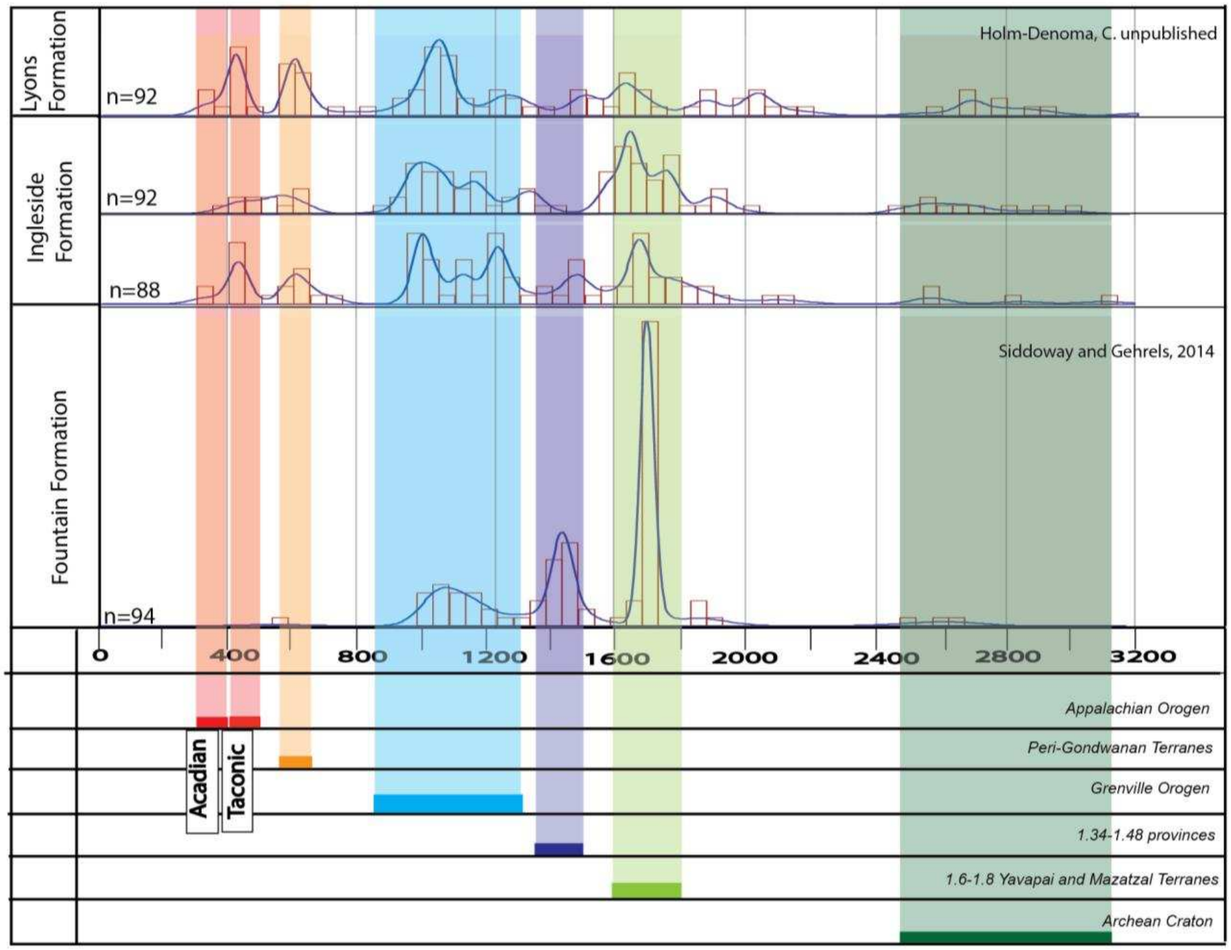

Figure 8: Probability density plots comparing U-Pb ages of detrital zircons from the Ingleside Formation analyzed in this study to published data from the underlying Fountain Formation (Siddoway and Gehrels, 2014) and data from the overlying Lyons Formation (Holm-Denoma, unpublished).

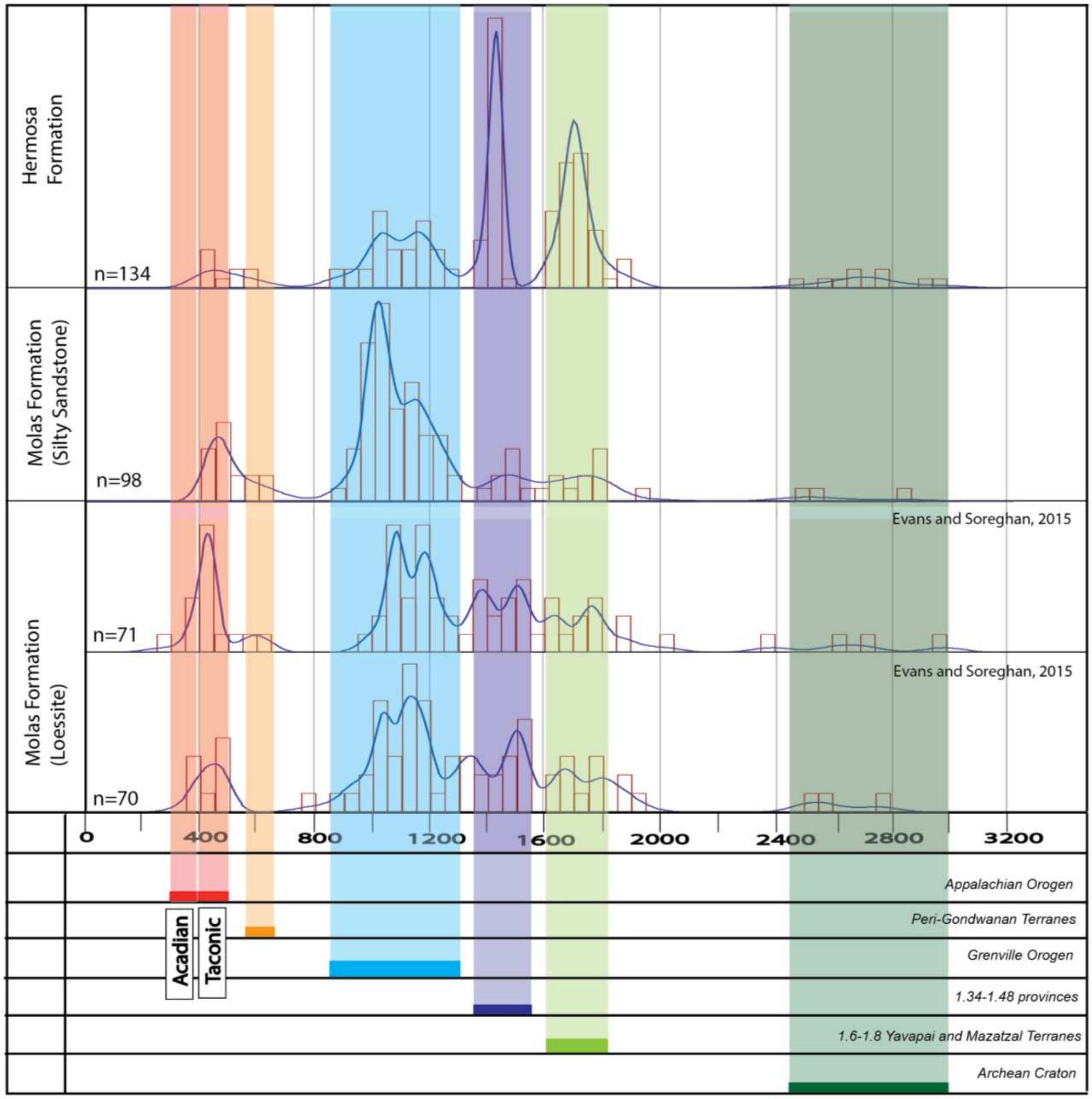

Figure 9: Probability density plots comparing U-Pb ages of detrital zircons from the Molas and Hermosa Formations analyzed in this study to published data from the underlying Molas loessite (Evans and Soreghan, 2015).

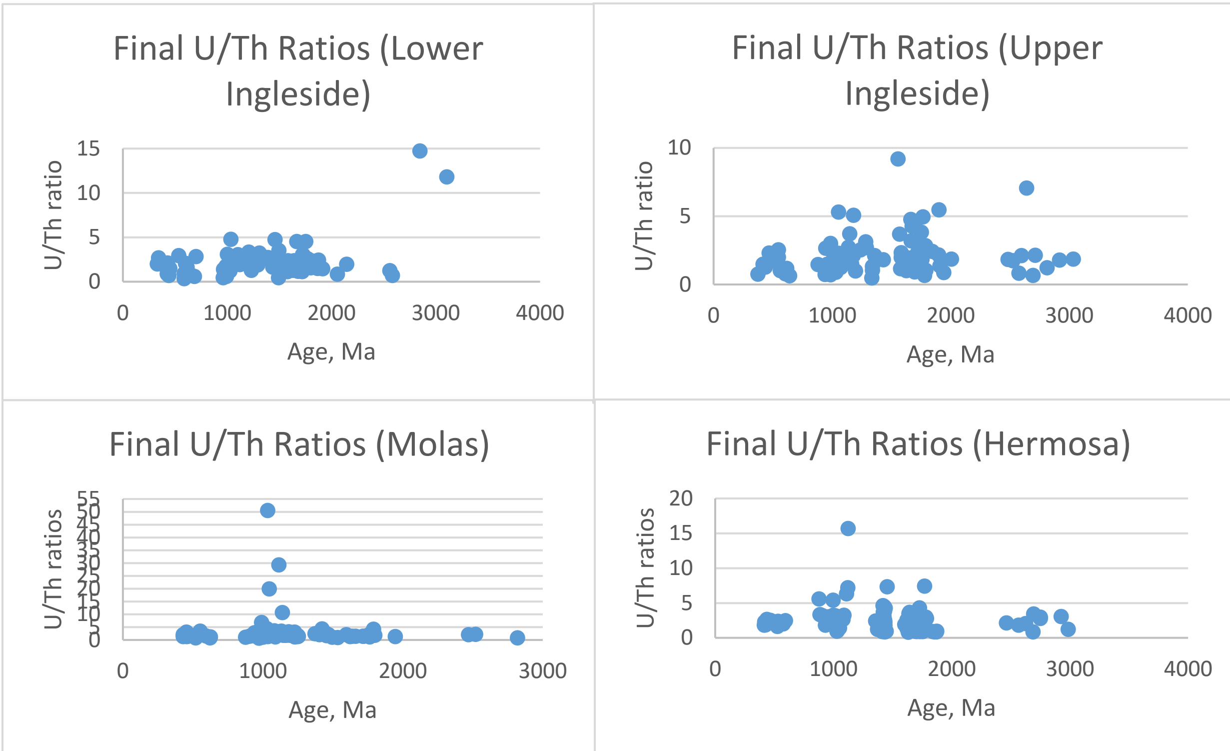

Figure 10: U/Th ratios for all analyzed samples are dominantly <10

DISCUSSION

Detrital zircon data from Late Paleozoic sandstone analyzed here provides new information for tracking of sediment dispersal paths. Specifically, this study documents the first appearance of Paleozoic-aged zircons along the Front Range in the Ingleside Formation. Our comparison of detrital zircon signatures of the Molas and Hermosa Formations also allows us to make significant paleogeographic interpretations. The source of sediment for all Paleozoic detrital zircon population (330-490 Ma), a fraction of Neoproterozoic Peri-Gondwanan-sourced zircons (515-700 Ma), and a fraction of Mesoproterozoic Grenville basement-sourced zircons (990-1200 Ma) is identified as the distant Appalachian orogen.

Similar to detrital zircon age distribution in Pennsylvanian and Lower Permian sandstones of the Grand Canyon (Gehrels et al., 2011), U-Pb data from the Ingleside and Lyons Formation document detrital zircons formed during the Acadian and Taconic orogenies, but none from the subsequent Pennsylvanian-Permian Alleghanian orogeny. An average lag time of 25 million years was documented in Upper Paleozoic strata of the Grand Canyon and support the absence of Alleghanian-aged zircons in Pennsylvanian-Early Permian sandstones in the Ancestral Rocky Mountains. Additionally, based on data from the Appalachian foreland, it is suggested that the rate of erosional unroofing of Alleghanian plutons was not far enough advanced to include these zircons in sediments that make up Pennsylvanian and Lower Permian sandstones (Thomas et al., 2004). Delayed exhumation of Alleghanian plutons likely resulted in the lack of Alleghanian-age zircons in Pennsylvanian-age sandstones in proximal sediments along the length of the Appalachian foreland basins (Thomas et al., 2004; Becker et. al., 2005) that are interpreted to characterize the headwaters of inferred dispersal paths from the Appalachians to the Grand Canyon (Thomas, 2011). Gehrels et al. (2011) suggest that transcontinental rivers from the Appalachians travelled northwestward and then southward by prevailing winds from the north, northeast, and northwest (Poole, 1962). These headwaters and fluvial systems likely also fed eolian systems prevalent in Ancestral Rocky Mountain provinces at the time.

A widespread sand-dispersal system that transported local and distant sediments into sedimentary basins along the Ancestral Rockies is also evidenced in the diverse components in our detrital zircon age data. Mixed detrital zircon signature across time-equivalent sedimentary units likely point towards an extensive sand blanket that extended across Colorado during the Late Paleozoic. Areas of significant eolian recycling have been documented in the Molas and Hermosa Formations (Evans and Reed, 2007; Jordan and Mountney, 2010) and the Ingleside (Figure 3A) and Lyons Formations (Hunter, 1981), while prominent marine incursions and relatively small fluvial systems are documented in the Hermosa Formation (Jordan and Mountney, 2010), and Ingleside Formation (Figure 3A). Facies distribution along with detrital zircon signatures across these sedimentary systems suggest that eolian sands were widespread across Ancestral Rocky Mountain Basins during the Paleozoic, and then likely redistributed interregionally through marine and fluvial systems in both basins. Similar sediment transportation system has been interpreted for Jurassic sandstones of the Colorado Plateau (Dickinson and Gehrels, 2003). In addition, a greater population of Taconic-Acadian derived zircons in Molas loessite samples in relation to our Molas sandstone sample is interpreted to be a strong indication that wind systems played an important role in the transportation of young, distally-sourced zircons during Late Paleozoic time.

The sandstone samples analyzed from the Ingleside and Hermosa Formation are shallow marine deposits, further implying that marine systems played a significant role in reworking exotic zircons into both sedimentary basins. Our paleocurrent analyses for dominantly shallow-marine sandstones and some eolian sandstones of the Ingleside Formation at Owl Canyon document a prevailing south and east sediment transport direction (Figure 3B). However, it is important to note that paleocurrent direction only yield the final transportation direction of the sediment and have no necessary local relationship to long-distance dispersal from provenance to depositional site (e.g. Thomas, 2011). We interpret our paleocurrent data to imply that erg systems located to the north and west of our study area at Owl Canyon were important sediment sources for the Ingleside and Lyons Formation and were likely reworked into Ingleside shallow marine sandstones by marine currents. The interaction of three independent dispersal processes suggested here for the presence of Appalachian-derived zircons in Ancestral Rocky Mountain basins illustrates the complexities of long-distance sediment transportation during the Late Paleozoic.

The oldest strata recording Paleozoic-aged zircons in the Grand Canyon is the Upper Mississippian Surprise Canyon Formation (Gehrels et al., 2011). The Lower Pennsylvanian Molas Formation loessites of southwestern Colorado also record Paleozoic-aged zircons (Evans and Soreghan, 2015). Based on these studies it is clear that a sand- dispersal system transporting distant Appalachian-derived zircons was present prior to the Ancestral Rocky Mountain uplift. Deposition of the Fountain Formation during the uplift of the Ancestral Front Range (Kluth and Coney, 1981) and Hermosa Formation during the uplift of the Uncompahgre Highlands (Thomas, 2007) resulted in a dominating supply of clastic sediment from the Proterozoic basement. Outwash from the Ancestral Rockies must have overwhelmed transcontinental drainage across Colorado and provided local sources of Pennsylvanian-Permian detritus as reflected in the age populations of the Fountain and Hermosa Formations. The transition is observed along the Front Range from a dominantly local Proterozoic detrital zircon signature in the Fountain Formation to a dominantly mixed Laurentian detrital zircon signature in the overlying Ingleside (Figure 6). Cessation of uplift of the Ancestral Front Range Highlands and the increased appearance of distal detrital zircons is accompanied by the onset of marine sedimentation documented by the Ingleside Formation and the termination of non-marine sedimentation documented by the underlying Fountain Formation. A subtler transition is observed in the eastern Paradox Basin, with both the Molas and the Hermosa Formation displaying a mixed Laurentian detrital zircon signature, but an increase in abundance of locally-derived detrital zircons (~1340-1500 Ma and 1600–1800 Ma) is observed in the Hermosa sandstone. We interpret this increase in abundance of locally-derived zircons to also record the initiation of uplift of the Uncompahgre highlands during the deposition of the Pennsylvanian Hermosa Formation. Pennsylvanian-age faulting associated with Uncompahgre uplift has previously been documented in the Hermosa Formation (Thomas, 2007) and ties in well with the detrital zircon signatures of Paradox Basin sandstone analyzed here. Converse to the Ancestral Front Range, initiation of the Uncompahgre uplift is accompanied by cessation of non-marine sedimentation documented by the Molas Formation and the onset of marine sedimentation documented by the Hermosa Formation (Evans and Reed, 2007).

CONCLUSIONS

We compare our detrital zircon data from the Ingleside, Molas, and Hermosa Formations with published data from other late Paleozoic sandstone units to identify the earliest appearance of Paleozoic-aged zircons in sedimentary strata across the Colorado Ancestral Rocky Mountain region. We also compare our data with published detrital zircon data from different time slices in the same location to interpret paleogeographic implications of U-Pb age populations. The earliest appearance of Paleozoic zircons is recorded in the Ingleside Formation along the Front Range in north-central Colorado and increases in abundance in the overlying Lyons Formation. The earliest record of Paleozoic zircons along the Uncompahgre Highlands in southwestern Colorado is in loessite deposits from the Molas Formation and generally decrease in abundance in the overlying silt-rich sandstone deposits of the Upper Molas Formation and in the Hermosa Formation.

We infer that Paleozoic, Peri-Gondwanan, and Grenville-age detrital zircons were primarily sourced from the Appalachian orogenic belt and were delivered to their final locations by interaction of several independent dispersal paths that include paleorivers, wind systems, and/or marine currents. Additionally, we are able to infer the general timing of cessation of Ancestral Front Range uplift and initiation of Uncompahgre uplift based on significant shifts in U-Pb age populations in the sedimentary basins flanking both highlands. The cessation of Ancestral Rocky Mountain uplift is here identified to coincide with decrease in locally-sourced zircon population and increase in distally-sourced zircon population between the Fountain and Ingleside Formations. Conversely, the initiation of the Uncompahgre uplift is likely reflected in an increase in locally-sourced zircons observed in the Hermosa Formation.

REFERENCES

Abati, J., A. M. Aghzer, A. Gerdes, and N. Ennih, 2010, Detrital zircon ages of Neoproterozoic sequences of the Moroccan Anti-Atlas belt: Precambrian Research, v. 181, p. 115-128, DOI: https://doi.org/10.1016/j.precamres.2010.05.018

Barr, S. M., M. L. Bevier, C. E. White, and R. Doig, 1993, Magmatic history of the Caledonia (Avalon) Terrane of southern New Brunswick based on U-Pb (zircon) geochronology, Canada, New Brunswick Natural Resources and Energy: Fredericton, NB, Canada, p. 10-17.

Becker, T. P., W. A. Thomas, S. D. Samson, and G. E. Gehrels, 2005, Detrital zircon evidence of Laurentian crustal dominance in the Lower Pennsylvanian deposits of the Alleghanian clastic wedge in eastern North America: Sedimentary Geology, v. 182, p. 59-86, DOI: https://doi.org/10.1016/j.sedgeo.2005.07.014

Blakey, R. C., 2008, Pennsylvanian-Jurassic sedimentary basins of the Colorado Plateau and Southern Rocky Mountains Sedimentary basins of the world, v. 5: Netherlands, Elsevier : Amsterdam, Netherlands, p. 245-296, DOI: https://doi.org/10.1016/S1874-5997(08)00007-5

Chapman, A. D., 2016, Detrital zircon geochronology of the Warrensburg-Moberly Channel sandstone, central Missouri; a paleoriver that connected the Appalachian Orogen to Grand Canyon and adjacent depocenters?: Abstracts with Programs - Geological Society of America, v. 48, p. 52.

Corrigan, D., 2005, Proterozoic crustal growth of Laurentia; insights from Lithoprobe: Abstracts with Programs - Geological Society of America, v. 37, p. 494-494.

Crowell, J. C., 1978, Gondwanan glaciation, cyclothems, continental positioning, and climate change: American Journal of Science, v. 278, p. 1345-1372.

Dickinson, W. R., and G. E. Gehrels, 2003, U-Pb ages of detrital zircons from Permian and Jurassic eolian sandstones of the Colorado Plateau, USA; paleogeographic implications: Sedimentary Geology, v. 163, p. 29-66, DOI: https://doi.org/10.1016/S0037-0738(03)00158-1

Dickinson, W. R., and G. E. Gehrels, 2009, Use of U-Pb ages of detrital zircons to infer maximum depositional ages of strata; a test against a Colorado Plateau Mesozoic database: Earth and Planetary Science Letters, v. 288, p. 115-125, DOI: https://doi.org/10.1016/j.epsl.2009.09.013

Dickinson, W. R., and T. F. Lawton, 2003, Sequential intercontinental suturing as the ultimate control for Pennsylvanian ancestral Rocky Mountains deformation: Geology [Boulder], v. 31, p. 609-612

Duncan, C. R., A. E. Hoisington, and D. P. Hawkins, 2013, Insights into the late Paleozoic geology of an ancestral Rocky Mountain range from detrital zircons in the Fountain Formation, Manitou Springs, Colorado: Abstracts with Programs - Geological Society of America, v. 45, p. 38-38.

Evans, J. E., and J. M. Reed, 2007, Integrated loessite-paleokarst depositional system, Early Pennsylvanian Molas Formation, Paradox Basin, southwestern Colorado, U.S.A: Sedimentary Geology, v. 195, p. 161-181, DOI: https://doi.org/10.1016/j.sedgeo.2006.07.010

Evans, J. E., and M. Soreghan, 2015a, Long-distance sediment transport and episodic resedimentation of Pennsylvanian dust (eolian silt) in cave passages of the Mississippian Leadville Limestone, southwestern Colorado, USA: Special Paper - Geological Society of America, v. 516, p. 263-283.

Evans, J. E., and M. Soreghan, 2015b, Long-distance sediment transport and episodic resedimentation of Pennsylvanian dust (eolian silt) in cave passages of the Mississippian Leadville Limestone, southwestern Colorado, USA: Special Paper - Geological Society of America, v. 516, p. 263-283.

Frost, C. D., B. R. Frost, K. R. Chamberlain, and B. R. Edwards, 1999, Petrogenesis of the 1.43 Ga Sherman Batholith, SE Wyoming, USA; a reducted, rapakivi-type anorogenic granite: Journal of Petrology, v. 40, p. 1771-1802.

Gehrels, G., and M. Pecha, 2013, Detrital zircon U-Pb geochronology and Hf isotope geochemistry of Paleozoic and Triassic passive margin strata of western North America: Geosphere, v. 10, p. 49-65, DOI: https://doi.org/10.1130/GES00889.1

Gehrels, G. E., R. Blakey, K. E. Karlstrom, J. M. Timmons, B. Dickinson, and M. Pecha, 2011, Detrital zircon U-Pb geochronology of Paleozoic strata in the Grand Canyon, Arizona: Lithosphere, v. 3, p. 183-200, DOI: https://doi.org/10.1130/L121.1

Gonzales, D. A., K. E. Karlstrom, and G. S. Siek, 1996, Syncontractional crustal anatexis and deformation during emplacement of approximately 1435 Ma plutons, western Needle Mountains, Colorado: Journal of Geology, v. 104, p. 215-223.

Hagadorn, J. W., K. R. Whiteley, B. L. Lahey, C. M. Henderson, and C. S. Holm-Denoma, 2016, The Permian-Triassic transition in Colorado: Field Guide [Geological Society of America], v. 44, p. 73-92.

Heckel, P. H., 1986, Sea-level curve for Pennsylvanian eustatic marine transgressive-regressive depositional cycles along Midcontinent outcrop belt, North America: Geology [Boulder], v. 14, p. 330-334.

Hunter, R. E., 1981, Stratification styles in eolian sandstones; some Pennsylvanian to Jurassic examples from the Western Interior U.S.A: Special Publication - Society of Economic Paleontologists and Mineralogists, p. 315-329.

Jordan, O. D., and N. P. Mountney, 2010, Styles of interaction between aeolian, fluvial and shallow marine environments in the Pennsylvanian to Permian lower Cutler beds, south-east Utah, USA: Sedimentology, v. 57, p. 1357-1385, DOI: 10.1111/j.1365-3091.2010.01148.x

Kirkland, C. L., R. H. Smithies, R. J. M. Taylor, N. Evans, and B. McDonald, 2015, Zircon Th/U ratios in magmatic environs: Lithos [Oslo], v. 212-215, p. 397-414.

Kluth, C. F., and P. J. Coney, 1981, Plate tectonics of the ancestral Rocky Mountains: Geology [Boulder], v. 9, p. 10-15.

Knight, S. H., 1929, The fountain and the Casper formations of the Laramie Basin; a study on genesis of sediments: Wyoming Univ. Pub. Sci. Geology, v. 1, p. 1-82.

Leary, R. J., P. Umhoefer, M. E. Smith, and N. Riggs, 2017, A three-sided orogen; a new tectonic model for ancestral Rocky Mountain uplift and basin development: Geology [Boulder], v. Pre-Issue Publication, DOI: https://doi.org/10.1130/G39041.1

Link, P. K., R. C. Mahon, L. P. Beranek, E. A. Campbell-Stone, and R. Lynds, 2014, Detrital zircon provenance of Pennsylvanian to Permian sandstones from the Wyoming Craton and Wood River basin, Idaho, U.S.A: Rocky Mountain Geology, v. 49, p. 115-136.

Mallory, W. W., 1960, Outline of Pennsylvanian stratigraphy of Colorado: United States, Rocky Mtn. Assoc. Geologists : Denver, CO, United States, p. 23-33.

Marshak, S., K. E. Karlstrom, and J. M. Timmons, 2000, Inversion of Proterozoic extensional faults; an explanation for the pattern of Laramide and ancestral Rockies intracratonic deformation, United States: Geology [Boulder], v. 28, p. 735-738.

May, S. R., G. G. Gray, L. L. Summa, N. R. Stewart, G. E. Gehrels, and M. E. Pecha, 2013, Detrital zircon geochronology from the Bighorn Basin, Wyoming, USA; implications for tectonostratigraphic evolution and paleogeography: Geological Society of America Bulletin, v. 125, p. 1403-1422, DOI: https://doi.org/10.1130/B30824.1

Nyman, M. W., K. E. Karlstrom, E. Kirby, and C. M. Graubard, 1994, Mesoproterozoic contractional orogeny in western North America; evidence from ca. 1.4 Ga plutons: Geology [Boulder], v. 22, p. 901-904.

Parrish, J. T., and F. Peterson, 1988, Wind directions predicted from global circulation models and wind directions determined from eolian sandstones of the Western United States; a comparison: Sedimentary Geology, v. 56, p. 261-282.

Poole, F. G., 1962, Wind directions in late Paleozoic to middle Mesozoic time on the Colorado Plateau; Article 163, United States, U. S. Geological Survey : Reston, VA, United States, p. D147-d151.

Smith Siddoway, C., and G. E. Gehrels, 2014, Basement-hosted sandstone injectites of Colorado; a vestige of the Neoproterozoic revealed through detrital zircon provenance analysis: Lithosphere, v. 6, p. 403-408, DOI: https://doi.org/10.1130/L390.1

Soreghan, M. J., G. S. Soreghan, and M. A. Hamilton, 2002, Paleowinds inferred from detrital-zircon geochronology of upper Paleozoic loessite, western equatorial Pangea: Geology [Boulder], v. 30, p. 695-698, DOI: https://doi.org/10.1130/0091-7613(2002)030

Sweet, D. E., and G. S. Soreghan, 2010, Late Paleozoic tectonics and paleogeography of the ancestral Front Range; structural, stratigraphic, and sedimentologic evidence from the Fountain Formation (Manitou Springs, Colorado): Geological Society of America Bulletin, v. 122, p. 575-594, DOI:

https://doi.org/10.1130/B26554.1

Thomas, W. A., 2011, Detrital-zircon geochronology and sedimentary provenance: Lithosphere, v. 3, p. 304-308, DOI: https://doi.org/10.1130/RF.L001.1

Thomas, W. A., T. P. Becker, S. D. Samson, and M. A. Hamilton, 2004, Detrital zircon evidence of a recycled orogenic foreland provenance for Alleghanian clastic-wedge sandstones: Journal of Geology, v. 112, p. 23-37.

Thomas, W. A., G. E. Gehrels, and M. C. Romero, 2016, Detrital zircons from crystalline rocks along the southern Oklahoma fault system, Wichita and Arbuckle Mountains, USA: Geosphere [Boulder, CO], v. 12, p. 1224-1234.

Van Schmus, W. R., M. E. Bickford, and K. C. Condie, 1993, Early Proterozoic transcontinental orogenic belts in the United States: Abstracts with Programs - Geological Society of America, v. 25, p. 44-44.

Whitmeyer, S. J., and K. E. Karlstrom, 2007, Tectonic model for the Proterozoic growth of North America: Geosphere, v. 3, p. 220-259, DOI: https://doi.org/10.1130/GES00055.1

Wortman, G. L., S. D. Samson, and J. P. Hibbard, 2000, Precise U-Pb zircon constraints on the earliest magmatic history of the Carolina Terrane: Journal of Geology, v. 108, p. 321-338.

APPENDIX A: U-Pb DATA FOR ANALYZED SAMPLES

Table 1- U/Pb data from Sample: OC_2.8_DZ1

Analysis #		Final207_	Final207_	Final206_	Final206_	ErrorCorre	FinalAge2	FinalAge2	FinalAge2	FinalAge2	FinalAge2	FinalAge2	%DISC	Preferred	2se	FInal_U_T	FInal_U_Th_Ratio_In
~~OC-2.8-DZ1-027~~	~~Output_1_~~	~~0.303~~	~~0.025~~	~~0.0238~~	~~0.0013~~	~~0.29489~~	~~151.4~~	~~8~~	~~315.1~~	~~9.6~~	~~1440~~	~~100~~	~~89.48611~~	~~151.4~~	~~8~~	~~3.15~~	~~0.18~~
~~OC-2.8-DZ1-041~~	~~Output_1_~~	~~0.391~~	~~0.038~~	~~0.0363~~	~~0.002~~	~~0.3641~~	~~230~~	~~13~~	~~301~~	~~18~~	~~1120~~	~~130~~	~~79.46429~~	~~230~~	~~13~~	~~0.951~~	~~0.038~~
~~OC-2.8-DZ1-047~~	~~Output_1_~~	~~0.354~~	~~0.04~~	~~0.0465~~	~~0.0027~~	~~0.19605~~	~~293~~	~~17~~	~~205~~	~~33~~	~~380~~	~~210~~	~~22.89474~~	~~293~~	~~17~~	~~2.141~~	~~0.072~~
~~OC-2.8-DZ1-088~~	~~Output_1_~~	~~0.36~~	~~0.021~~	~~0.0486~~	~~0.001~~	~~0.2955~~	~~305.8~~	~~6.3~~	~~320~~	~~11~~	~~410~~	~~100~~	~~25.41463~~	~~305.8~~	~~6.3~~	~~0.4734~~	~~0.0072~~
~~OC-2.8-DZ1-035~~	~~Output_1_~~	~~0.393~~	~~0.037~~	~~0.0491~~	~~0.0016~~	~~0.80909~~	~~308.8~~	~~9.6~~	~~342~~	~~11~~	~~429~~	~~43~~	~~28.01865~~	~~308.8~~	~~9.6~~	~~2.423~~	~~0.049~~
~~OC-2.8-DZ1-032~~	~~Output_1_~~	~~0.451~~	~~0.037~~	~~0.0493~~	~~0.0012~~	~~0.84956~~	~~310~~	~~7.4~~	~~407~~	~~16~~	~~771~~	~~36~~	~~59.79248~~	~~310~~	~~7.4~~	~~2.764~~	~~0.045~~
~~OC-2.8-DZ1-077~~	~~Output_1_~~	~~0.385~~	~~0.026~~	~~0.0505~~	~~0.0013~~	~~0.61952~~	~~317.9~~	~~8.1~~	~~327~~	~~15~~	~~415~~	~~73~~	~~23.39759~~	~~317.9~~	~~8.1~~	~~1.685~~	~~0.02~~
~~OC-2.8-DZ1-120~~	~~Output_1_~~	~~0.408~~	~~0.02~~	~~0.0517~~	~~0.0011~~	~~0.12475~~	~~325.2~~	~~6.6~~	~~327.8~~	~~8.2~~	~~532~~	~~92~~	~~38.87218~~	~~325.2~~	~~6.6~~	~~1.45~~	~~0.037~~
~~OC-2.8-DZ1-079~~	~~Output_1_~~	~~0.405~~	~~0.024~~	~~0.05179~~	~~0.00093~~	~~0.001~~	~~325.5~~	~~5.7~~	~~347~~	~~14~~	~~510~~	~~140~~	~~36.17647~~	~~325.5~~	~~5.7~~	~~2.34~~	~~0.036~~
OC-2.8-DZ1-055	Output_1_	0.398	0.037	0.0527	0.0016	0.55273	331	10	331	14	380	110	12.89474	331	10	2.011	0.063
~~OC-2.8-DZ1-070~~	~~Output_1_~~	~~0.373~~	~~0.024~~	~~0.0536~~	~~0.0013~~	~~0.084818~~	~~336.8~~	~~8~~	~~339.9~~	~~8.3~~	~~230~~	~~140~~	~~-46.4348~~	~~336.8~~	~~8~~	~~1.943~~	~~0.027~~
OC-2.8-DZ1-048	Output_1_	0.405	0.043	0.0546	0.0011	0.55135	342.8	6.5	343	15	340	140	-0.82353	342.8	6.5	2.676	0.042
~~OC-2.8-DZ1-025~~	~~Output_1_~~	~~0.445~~	~~0.043~~	~~0.0549~~	~~0.0016~~	~~0.61837~~	~~344~~	~~9.8~~	~~363~~	~~23~~	~~470~~	~~110~~	~~26.80851~~	~~344~~	~~9.8~~	~~1.852~~	~~0.047~~
~~OC-2.8-DZ1-050~~	~~Output_1_~~	~~0.9~~	~~0.32~~	~~0.0564~~	~~0.0037~~	~~0.96303~~	~~353~~	~~23~~	~~580~~	~~160~~	~~1780~~	~~520~~	~~80.16854~~	~~353~~	~~23~~	~~1.159~~	~~0.035~~
~~OC-2.8-DZ1-053~~	~~Output_1_~~	~~0.506~~	~~0.066~~	~~0.0597~~	~~0.0024~~	~~0.80107~~	~~374~~	~~15~~	~~412~~	~~26~~	~~620~~	~~140~~	~~39.67742~~	~~374~~	~~15~~	~~1.64~~	~~0.1~~
~~OC-2.8-DZ1-073~~	~~Output_1_~~	~~0.531~~	~~0.027~~	~~0.0655~~	~~0.0019~~	~~0.65342~~	~~409~~	~~11~~	~~411~~	~~13~~	~~619~~	~~74~~	~~33.92569~~	~~409~~	~~11~~	~~2.332~~	~~0.088~~
OC-2.8-DZ1-092	Output_1_	0.507	0.03	0.0665	0.002	0.11414	415	12	408	17	440	130	5.681818	415	12	1.654	0.063
~~OC-2.8-DZ1-072~~	~~Output_1_~~	~~0.59~~	~~0.026~~	~~0.0677~~	~~0.0027~~	~~0.89765~~	~~422~~	~~17~~	~~493~~	~~10~~	~~719~~	~~44~~	~~41.30737~~	~~422~~	~~17~~	~~1.301~~	~~0.056~~
OC-2.8-DZ1-046	Output_1_	0.539	0.045	0.0678	0.002	0.35612	423	12	446	14	509	78	16.89587	423	12	1.442	0.046
OC-2.8-DZ1-119	Output_1_	0.518	0.027	0.0684	0.002	0.82423	426	12	432	13	438	57	2.739726	426	12	0.874	0.036
OC-2.8-DZ1-034	Output_1_	0.523	0.046	0.0684	0.002	0.36053	427	12	427	14	420	120	-1.66667	427	12	1.228	0.015
~~OC-2.8-DZ1-026~~	~~Output_1_~~	0.518	0.059	0.0685	0.0015	0.095417	427.3	9.3	~~431~~	~~27~~	330	180	-29.4848	427.3	9.3	~~1.272~~	~~0.016~~
OC-2.8-DZ1-006	Output_1_	0.544	0.046	0.0689	0.0016	0.56574	429.5	9.4	425	12	469	61	8.422175	429.5	9.4	2.097	0.026
~~OC-2.8-DZ1-063~~	~~Output_1_~~	~~0.504~~	~~0.029~~	~~0.0697~~	~~0.0016~~	~~0.8087~~	~~434.1~~	~~9.9~~	~~429.5~~	~~9.7~~	~~360~~	~~100~~	~~-20.5833~~	~~434.1~~	~~9.9~~	~~1.835~~	~~0.042~~
~~OC-2.8-DZ1-110~~	~~Output_1_~~	~~0.657~~	~~0.097~~	~~0.0698~~	~~0.0024~~	~~0.81947~~	~~435~~	~~14~~	~~411~~	~~40~~	~~830~~	~~250~~	~~47.59036~~	~~435~~	~~14~~	~~0.438~~	~~0.041~~
OC-2.8-DZ1-103	Output_1_	0.542	0.022	0.0706	0.0013	0.69069	439.9	8.1	443	14	451	68	2.461197	439.9	8.1	0.7	0.013
OC-2.8-DZ1-001	Output_1_	0.552	0.054	0.072	0.0013	0.001	448.2	7.5	455	18	460	220	2.565217	448.2	7.5	1.493	0.013
~~OC-2.8-DZ1-051~~	~~Output_1_~~	~~0.658~~	~~0.061~~	~~0.0742~~	~~0.0043~~	~~0.86154~~	~~461~~	~~26~~	~~560~~	~~11~~	~~773~~	~~71~~	~~40.36223~~	~~461~~	~~26~~	~~1.955~~	~~0.066~~
~~OC-2.8-DZ1-044~~	~~Output_1_~~	~~0.801~~	~~0.11~~	~~0.0785~~	~~0.0029~~	~~0.001~~	~~487~~	~~17~~	~~561~~	~~36~~	~~970~~	~~290~~	~~49.79381~~	~~487~~	~~17~~	~~2.101~~	~~0.059~~
~~OC-2.8-DZ1-089~~	~~Output_1_~~	~~1.215~~	~~0.049~~	~~0.0797~~	~~0.0026~~	~~0.21083~~	~~494~~	~~16~~	~~1170~~	~~280~~	~~1831~~	~~41~~	~~73.02021~~	~~494~~	~~16~~	~~8.5~~	~~0.39~~
OC-2.8-DZ1-058	Output_1_	0.695	0.067	0.0864	0.002	0.71639	534	12	565	39	570	110	6.315789	534	12	2.924	0.022
~~OC-2.8-DZ1-112~~	~~Output_1_~~	~~0.849~~	~~0.053~~	~~0.0943~~	~~0.0029~~	~~0.51312~~	~~581~~	~~17~~	~~577~~	~~27~~	~~840~~	~~140~~	~~30.83333~~	~~581~~	~~17~~	~~2.889~~	~~0.075~~
OC-2.8-DZ1-022	Output_1_	0.824	0.075	0.0957	0.0016	0.49092	588.9	9.6	614	18	631	93	6.671949	588.9	9.6	0.335	0.021
OC-2.8-DZ1-109	Output_1_	0.81	0.038	0.0956	0.002	0.001	589	12	613.6	9.8	650	100	9.384615	589	12	0.934	0.017
OC-2.8-DZ1-019	Output_1_	0.845	0.074	0.0977	0.0029	0.22635	601	17	587	32	600	120	-0.16667	601	17	2.09	0.018
OC-2.8-DZ1-030	Output_1_	0.844	0.077	0.0998	0.0026	0.5244	613	15	625	21	633	75	3.159558	613	15	1.291	0.088
OC-2.8-DZ1-024	Output_1_	0.865	0.083	0.1002	0.0034	0.63843	615	20	611	26	635	98	3.149606	615	20	1.643	0.022
~~OC-2.8-DZ1-018~~	~~Output_1_~~	0.851	0.069	0.1005	0.0023	0.71422	617	14	~~619~~	~~19~~	580	44	-6.37931	617	14	~~1.1168~~	~~0.0073~~
OC-2.8-DZ1-060	Output_1_	0.905	0.081	0.1053	0.0027	0.68646	645	16	684	12	695	48	7.194245	645	16	0.823	0.018
OC-2.8-DZ1-080	Output_1_	0.956	0.082	0.1126	0.0037	0.76912	687	22	679	14	680	120	-1.02941	687	22	0.606	0.023
OC-2.8-DZ1-086	~~Output_1_~~	1.052	0.083	0.1152	0.0052	0.73976	702	30	~~755~~	~~43~~	878	74	20.04556	702	30	2.84	0.26
OC-2.8-DZ1-029	Output_1_	1.6	0.17	0.1608	0.0057	0.44989	961	32	999	55	930	130	-3.33333	961	32	0.45	0.028

OC-2.8-DZ1-090	Output_1	1.66	0.16	0.1617	0.0046	0.044911	966	26	989	49	1060	200	8.867925	966	26	1.398	0.037
OC-2.8-DZ1-117	Output_1	1.651	0.078	0.1658	0.0046	0.28979	989	25	1012	50	986	86	-0.30426	989	25	1.747	0.034
OC-2.8-DZ1-111	Output_1	1.761	0.079	0.166	0.0069	0.87683	990	38	1025	29	1109	33	10.73039	990	38	1.049	0.058
OC-2.8-DZ1-037	Output_1	1.666	0.15	0.1662	0.004	0.43466	991	22	1032	21	963	95	-2.90758	991	22	1.176	0.016
OC-2.8-DZ1-042	Output_1	1.72	0.19	0.1662	0.0039	0.72246	991	21	1002	38	1020	140	2.843137	991	21	0.6005	0.0078
OC-2.8-DZ1-074	~~Output_1_~~	1.86	0.13	0.1671	0.0044	0.71362	996	24	~~1010~~	~~29~~	1251	90	20.38369	996	24	0.729	0.014
OC-2.8-DZ1-095	Output_1	1.657	0.11	0.167	0.0044	0.15415	996	24	986	42	990	120	-0.60606	996	24	0.95	0.012
OC-2.8-DZ1-118	Output_1	1.703	0.089	0.1683	0.0081	0.44868	1003	44	940	40	1050	100	4.47619	1003	44	3.087	0.081
OC-2.8-DZ1-059	Output_1	1.856	0.17	0.1728	0.0038	0.70025	1027	21	1084	11	1132	54	9.275618	1027	21	1.194	0.032
OC-2.8-DZ1-038	Output_1	1.82	0.2	0.173	0.0043	0.35287	1028	24	1070	69	1130	120	9.026549	1028	24	1.403	0.088
OC-2.8-DZ1-098	Output_1	1.82	0.24	0.1732	0.0074	0.73928	1030	41	1035	68	1120	200	8.035714	1030	41	1.561	0.096
OC-2.8-DZ1-012	Output_1	1.812	0.14	0.1744	0.0035	0.21554	1036	19	1039	41	999	51	-3.7037	1036	19	4.777	0.069
~~OC-2.8-DZ1-076~~	~~Output_1_~~	1.73	0.12	0.1775	0.003	0.001	1053	16	~~1073~~	~~49~~	930	100	-13.2258	1053	16	~~2.02~~	~~0.11~~
~~OC-2.8-DZ1-054~~	~~Output_1_~~	1.766	0.17	0.1788	0.0044	0.001	1060	24	~~1109~~	~~55~~	950	110	-11.5789	1060	24	~~3.639~~	~~0.061~~
OC-2.8-DZ1-003	Output_1	1.91	0.18	0.1801	0.0063	0.54266	1067	34	1088	28	1111	90	3.960396	1067	34	2.261	0.038
OC-2.8-DZ1-115	Output_1	1.927	0.08	0.1867	0.0034	0.62696	1104	18	1093	26	1089	33	-1.37741	1104	18	3.039	0.05
OC-2.8-DZ1-094	Output_1	2.05	0.14	0.1899	0.0066	0.81339	1120	36	1113	34	1166	81	3.945111	1120	36	2.606	0.064
OC-2.8-DZ1-020	Output_1	2.021	0.17	0.1902	0.006	0.75962	1122	33	1108	39	1088	38	-3.125	1122	33	1.917	0.04
OC-2.8-DZ1-097	Output_1	1.983	0.1	0.1907	0.004	0.67825	1125	22	1155	28	1061	48	-6.03205	1125	22	2.011	0.031
OC-2.8-DZ1-036	Output_1	2.08	0.17	0.1933	0.005	0.78606	1139	27	1182	40	1134	47	-0.44092	1139	27	2.872	0.03
OC-2.8-DZ1-085	Output_1	2.116	0.11	0.1986	0.0054	0.56094	1167	29	1142	15	1160	68	-0.60345	1167	29	2.061	0.03
OC-2.8-DZ1-014	~~Output_1_~~	3.24	0.74	0.205	0.022	0.57654	1200	120	~~1060~~	~~250~~	1680	410	28.57143	1200	120	1.91	0.11
OC-2.8-DZ1-017	Output_1	2.377	0.2	0.2059	0.0047	0.84597	1207	26	1234	63	1253	34	3.671189	1207	26	3.351	0.035
OC-2.8-DZ1-107	Output_1	2.56	0.16	0.206	0.0084	0.74856	1207	45	1109	56	1423	72	15.1792	1207	45	1.87	0.11
OC-2.8-DZ1-114	Output_1	2.34	0.11	0.206	0.0029	0.5472	1207	15	1134	51	1272	70	5.110063	1207	15	3.23	0.17
OC-2.8-DZ1-040	Output_1	2.5	0.25	0.2103	0.0037	0.71819	1230	20	1269	27	1300	100	5.384615	1230	20	1.573	0.038
OC-2.8-DZ1-099	Output_1	2.32	0.15	0.2103	0.0068	0.68632	1230	36	1312	40	1194	89	-3.01508	1230	36	2.907	0.054
OC-2.8-DZ1-031	Output_1	2.49	0.23	0.2105	0.0073	0.52848	1231	39	1241	38	1288	76	4.425466	1231	39	1.272	0.019
~~OC-2.8-DZ1-010~~	~~Output_1_~~	2.62	0.23	0.2291	0.0071	0.89491	1330	37	~~1322~~	~~54~~	1232	51	-7.95455	1232	51	~~2.691~~	~~0.056~~
OC-2.8-DZ1-009	Output_1	2.475	0.21	0.2117	0.0042	0.43201	1238	22	1001	22	1276	62	2.978056	1238	22	1.734	0.031
OC-2.8-DZ1-102	Output_1	2.438	0.096	0.2123	0.0056	0.49476	1241	30	1297	43	1275	38	2.666667	1241	30	1.91	0.023
OC-2.8-DZ1-033	Output_1	2.52	0.25	0.216	0.011	0.69567	1261	57	1301	42	1263	92	0.158353	1261	57	2.09	0.15
OC-2.8-DZ1-084	Output_1	2.404	0.1	0.2164	0.0065	0.50962	1262	35	1267	49	1245	65	-1.36546	1262	35	2.019	0.045
OC-2.8-DZ1-069	Output_1	2.81	0.1	0.2219	0.0054	0.76059	1292	29	1269	30	1491	35	13.34675	1292	29	1.907	0.018
OC-2.8-DZ1-104	Output_1	2.763	0.12	0.236	0.005	0.031453	1366	26	1424	36	1309	77	-4.35447	1309	77	3.23	0.11
OC-2.8-DZ1-081	Output_1	2.777	0.1	0.2346	0.0027	0.78529	1359	14	1356	29	1369	32	0.73046	1369	32	2.709	0.035
OC-2.8-DZ1-075	Output_1	2.84	0.21	0.235	0.01	0.22404	1360	54	1425	79	1390	150	2.158273	1390	150	2.723	0.065
OC-2.8-DZ1-064	Output_1	3.21	0.16	0.2603	0.0045	0.67442	1491	23	1493	23	1437	42	-3.75783	1437	42	1.645	0.015
OC-2.8-DZ1-061	Output_1	3.178	0.14	0.2521	0.0085	0.67568	1449	44	1491	32	1457	53	0.549073	1457	53	4.75	0.31
OC-2.8-DZ1-065	Output_1	3.256	0.14	0.2608	0.0061	0.68145	1494	31	1525	47	1469	55	-1.70184	1469	55	1.552	0.034
OC-2.8-DZ1-045	Output_1	3.31	0.28	0.2545	0.007	0.89718	1461	36	1503	28	1477	22	1.083277	1477	22	2.34	0.065
OC-2.8-DZ1-013	Output_1	3.32	0.3	0.2551	0.0083	0.69605	1464	43	1447	51	1491	46	1.810865	1491	46	0.467	0.028
OC-2.8-DZ1-082	Output_1	3.118	0.11	0.2465	0.006	0.86514	1420	31	1410	42	1496	25	5.080214	1496	25	3.501	0.061
OC-2.8-DZ1-023	Output_1	3.65	0.32	0.2694	0.0062	0.671	1537	32	1692	47	1542	65	0.324254	1542	65	1.17	0.016
OC-2.8-DZ1-087	Output_1	3.74	0.19	0.2818	0.0062	0.46651	1600	31	1537	46	1578	63	-1.39417	1578	63	1.148	0.026
OC-2.8-DZ1-021	Output_1	3.578	0.3	0.2586	0.0066	0.64278	1482	34	1512	54	1584	46	6.439394	1584	46	2.36	0.055
OC-2.8-DZ1-071	Output_1	3.952	0.16	0.2891	0.0055	0.59882	1637	28	1623	48	1629	27	-0.4911	1629	27	1.266	0.021
OC-2.8-DZ1-057	Output_1	3.97	0.35	0.2842	0.0087	0.683	1612	44	1700	37	1641	50	1.767215	1641	50	2.371	0.024
OC-2.8-DZ1-005	Output_1	3.74	0.32	0.2605	0.0068	0.70211	1492	35	1401	30	1650	59	9.575758	1650	59	1.529	0.013
OC-2.8-DZ1-078	Output_1	3.77	0.16	0.2728	0.0055	0.74624	1555	28	1498	35	1659	38	6.268837	1659	38	1.774	0.021

OC-2.8-DZ1-101	Output_1_	3.99	0.21	0.2866	0.0076	0.59498	1624	38	1647	46	1665	55	2.462462	1665	55	2.189	0.02
OC-2.8-DZ1-093	~~Output_1_~~	3.298	0.13	0.2358	0.0038	0.65892	1365	20	~~1490~~	~~35~~	1666	31	18.06723	1666	31	4.53	0.23
OC-2.8-DZ1-108	Output_1_	4.13	0.2	0.2908	0.0091	0.896	1645	46	1664	35	1676	26	1.849642	1676	26	2.129	0.015
OC-2.8-DZ1-039	Output_1_	3.91	0.35	0.2703	0.0085	0.68158	1542	43	1646	52	1677	65	8.050089	1677	65	1.501	0.025
OC-2.8-DZ1-113	Output_1_	4.068	0.15	0.2877	0.0081	0.69107	1630	40	1650	41	1677	45	2.802624	1677	45	1.54	0.049
OC-2.8-DZ1-028	Output_1_	4.21	0.37	0.2891	0.009	0.83171	1637	46	1681	55	1680	46	2.559524	1680	46	1.177	0.012
OC-2.8-DZ1-016	Output_1_	4.79	0.4	0.322	0.0097	0.85087	1797	48	1880	92	1719	36	-4.53752	1719	36	1.145	0.09
OC-2.8-DZ1-100	Output_1_	4.34	0.19	0.303	0.0076	0.51358	1706	38	1731	70	1722	67	0.929152	1722	67	3.041	0.023
OC-2.8-DZ1-066	Output_1_	4.5	0.29	0.31	0.014	0.94015	1739	71	1765	30	1729	36	-0.57837	1729	36	3	0.33
OC-2.8-DZ1-043	Output_1_	4.42	0.4	0.294	0.011	0.84091	1660	57	1853	75	1754	42	5.359179	1754	42	4.52	0.25
OC-2.8-DZ1-096	Output_1_	4.66	0.19	0.318	0.011	0.44457	1779	54	1726	56	1770	73	-0.50847	1770	73	2.591	0.046
OC-2.8-DZ1-008	Output_1_	4.52	0.47	0.3	0.017	0.87838	1689	83	1660	100	1793	63	5.800335	1793	63	1.73	0.14
OC-2.8-DZ1-002	Output_1_	5.07	0.4	0.3215	0.0075	0.79139	1797	37	1779	38	1801	38	0.222099	1801	38	1.566	0.054
OC-2.8-DZ1-004	~~Output_1_~~	8	10	0.261	0.081	0.9998	1470	380	~~3.60E+03~~	~~5.00E+03~~	1820	690	19.23077	1820	690	2.34	0.13
OC-2.8-DZ1-049	Output_1_	5.4	0.46	0.336	0.01	0.81487	1866	50	1912	61	1866	36	0	1866	36	1.508	0.021
OC-2.8-DZ1-015	Output_1_	5.63	0.46	0.3416	0.0085	0.80472	1894	41	1909	53	1877	41	-0.9057	1877	41	2.418	0.015
OC-2.8-DZ1-007	Output_1_	5.68	0.46	0.339	0.012	0.8562	1879	56	1888	52	1917	31	1.982264	1917	31	1.449	0.017
OC-2.8-DZ1-091	Output_1_	6.35	0.32	0.366	0.01	0.83418	2009	49	2019	40	2058	40	2.380952	2058	40	0.864	0.013
OC-2.8-DZ1-106	Output_1_	7.26	0.3	0.3935	0.0079	0.86116	2139	37	2133	44	2145	27	0.27972	2145	27	1.956	0.019
OC-2.8-DZ1-105	~~Output_1_~~	5.84	0.35	0.286	0.013	0.88938	1619	67	~~1819~~	~~57~~	2321	42	30.24558	2321	42	1.5	0.045
OC-2.8-DZ1-011	~~Output_1_~~	8.49	0.67	0.3549	0.0026	0.36612	1958	13	~~2030~~	~~110~~	2547	27	23.12525	2547	27	3.55	0.14
OC-2.8-DZ1-067	Output_1_	11.25	0.66	0.482	0.011	0.72252	2537	50	2501	81	2559	58	0.859711	2559	58	1.253	0.024
OC-2.8-DZ1-068	Output_1_	11.37	0.46	0.482	0.012	0.79592	2534	52	2546	53	2583	28	1.897019	2583	28	0.719	0.011
OC-2.8-DZ1-052	~~Output_1_~~	8.6	1.4	0.345	0.049	0.99712	1900	240	~~2430~~	~~160~~	2633	12	27.83897	2633	12	2.2	0.18
OC-2.8-DZ1-062	~~Output_1_~~	8.92	0.5	0.3359	0.006	0.001	1867	29	~~5020~~	~~470~~	2761	97	32.37957	2761	97	2.083	0.049
OC-2.8-DZ1-116	Output_1_	14.81	0.67	0.535	0.014	0.8708	2760	60	2794	74	2849	27	3.123903	2849	27	14.72	0.5
~~OC-2.8-DZ1-056~~	~~Output_1_~~	~~11.4~~	~~1.6~~	~~0.377~~	~~0.042~~	~~0.99793~~	~~2060~~	~~200~~	~~2340~~	~~120~~	~~2965~~	~~19~~	~~30.52277~~	~~2965~~	~~19~~	~~1.737~~	~~0.097~~
OC-2.8-DZ1-083	Output_1_	17.88	0.96	0.554	0.018	0.95283	2841	74	2870	160	3106	26	8.531874	3106	26	11.8	1

Table 2: U/Pb data from Sample: OC_56_DZ2

Analysis		Final207_	Final207_	Final206_	Final206_	ErrorCorre	FinalAge2	FinalAge2	FinalAge2	FinalAge2	FinalAge2	FinalAge2	Perc_DISC	Preferred_	Preferred_	FInal_U_T	FInal_U_Th_Ratio_In
OC-56-DZ2-001	OC56DZ2_	1.689	0.075	0.1684	0.0032	0.25277	1003.4	18	959	25	940	110	-7	1003.4	18	1.604	0.017
OC-56-DZ2-002	OC56DZ2_	2.6	0.11	0.2243	0.0072	0.77256	1304	38	1257	61	1290	89	-1	1290	89	2.707	0.031
OC-56-DZ2-003	OC56DZ2_	3.83	0.12	0.2676	0.0088	0.95773	1528	45	1514	65	1666	60	8	1666	60	3.201	0.034
OC-56-DZ2-004	OC56DZ2_	14.59	0.23	0.533	0.016	0.7964	2752	65	2668	68	2813	46	2	2813	46	1.215	0.022
OC-56-DZ2-005	OC56DZ2_	4.177	0.056	0.2956	0.0073	0.49073	1670	37	1670	55	1664	69	0	1664	69	4.757	0.02
~~OC-56-DZ2-006~~	~~OC56DZ2_~~	~~0.545~~	~~0.018~~	~~0.0662~~	~~0.0019~~	~~0.73179~~	~~413.1~~	~~12~~	~~414~~	~~14~~	~~616~~	~~77~~	~~33~~	~~413.1~~	~~12~~	1.44	0.012
OC-56-DZ2-007	OC56DZ2_	0.711	0.026	0.0887	0.002	0.4416	548.1	12	545	20	542	110	-1	548.1	12	2.544	0.044
OC-56-DZ2-008	OC56DZ2_	4.42	0.21	0.3024	0.0092	0.58582	1703	45	1710	34	1754	92	3	1754	92	3.817	0.036
OC-56-DZ2-009	OC56DZ2_	17.98	0.45	0.577	0.018	0.83936	2938	73	2822	69	3035	52	3	3035	52	1.86	0.019
OC-56-DZ2-010	OC56DZ2_	2.66	0.26	0.2246	0.0065	0.023799	1306	34	1274	77	1340	210	3	1340	210	1.319	0.029
OC-56-DZ2-011	OC56DZ2_	0.388	0.018	0.0515	0.0018	0.76884	323.9	11	276	15	416	110	22	323.9	11	1.902	0.025
OC-56-DZ2-012	OC56DZ2_	3.757	0.069	0.2712	0.0066	0.81184	1547	33	1571	41	1653	62	6	1653	62	1.318	0.071
OC-56-DZ2-013	OC56DZ2_	1.791	0.09	0.1783	0.0069	0.83237	1057	38	1051	41	1076	100	2	1057	38	2.281	0.068
OC-56-DZ2-014	OC56DZ2_	10.1	0.32	0.454	0.014	0.84752	2413	62	2426	81	2484	60	3	2484	60	1.827	0.026
OC-56-DZ2-015	OC56DZ2_	3.91	0.1	0.2856	0.0087	0.79758	1619	44	1618	41	1626	64	0	1626	64	1.01	0.017
OC-56-DZ2-016	OC56DZ2_	12.21	0.46	0.502	0.018	0.94289	2620	77	2636	80	2598	57	-1	2598	57	2.121	0.023
OC-56-DZ2-017	OC56DZ2_	4.015	0.084	0.2951	0.0074	0.80293	1667	37	1664	57	1584	66	-5	1584	66	2.3323	0.0099
OC-56-DZ2-018	OC56DZ2_	0.604	0.029	0.0753	0.002	0.56963	468.3	12	475	19	476	120	2	468.3	12	2.311	0.038
OC-56-DZ2-019	OC56DZ2_	0.379	0.021	0.05292	0.0013	0.23102	332.4	8	332	13	220	140	-51	332.4	8	2.82	0.11
OC-56-DZ2-020	OC56DZ2_	3.14	0.16	0.2552	0.0082	0.48353	1465	42	1455	32	1352	100	-8	1352	100	0.8208	0.0084
OC-56-DZ2-021	OC56DZ2_	2.62	0.11	0.2203	0.0048	0.48708	1284	25	1334	43	1287	94	0	1284	25	3.12	0.1
OC-56-DZ2-022	OC56DZ2_	1.642	0.074	0.1679	0.0038	0.23756	1000	21	976	37	920	120	-9	1000	21	3.283	0.066
OC-56-DZ2-023	OC56DZ2_	1.68	0.11	0.1657	0.0053	0.12486	988	29	1002	36	1016	99	3	988	29	0.719	0.017
~~OC-56-DZ2-024~~	~~OC56DZ2_~~	~~0.723~~	~~0.034~~	~~0.0961~~	~~0.0019~~	~~0.36678~~	~~591.6~~	~~11~~	~~641~~	~~32~~	~~370~~	~~130~~	~~-60~~	~~591.6~~	~~11~~	2.784	0.047
OC-56-DZ2-025	OC56DZ2_	1.626	0.053	0.1684	0.0051	0.52771	1003	28	990	47	921	100	-9	1003	28	3.503	0.047
~~OC-56-DZ2-026~~	~~OC56DZ2_~~	~~1.842~~	~~0.069~~	~~0.1839~~	~~0.0057~~	~~0.72062~~	~~1088~~	~~31~~	~~1110~~	~~25~~	~~958~~	~~97~~	~~-14~~	~~1088~~	~~31~~	2.364	0.054
OC-56-DZ2-027	OC56DZ2_	3.799	0.088	0.2812	0.0081	0.92308	1597	41	1585	57	1557	60	-3	1557	60	9.18	0.67
OC-56-DZ2-028	OC56DZ2_	1.98	0.063	0.1879	0.0046	0.82433	1110	25	963	27	1066	77	-4	1110	25	2.255	0.052
~~OC-56-DZ2-029~~	~~OC56DZ2_~~	~~2.92~~	~~0.12~~	~~0.199~~	~~0.0066~~	~~0.82693~~	~~1170~~	~~35~~	~~1161~~	~~33~~	~~1707~~	~~73~~	~~31~~	~~1170~~	~~35~~	1.521	0.024
~~OC-56-DZ2-030~~	~~OC56DZ2_~~	~~0.777~~	~~0.027~~	~~0.0913~~	~~0.0027~~	~~0.29857~~	~~563~~	~~16~~	~~540~~	~~7.1~~	~~668~~	~~91~~	~~16~~	~~563~~	~~16~~	1.004	0.061
~~OC-56-DZ2-031~~	~~OC56DZ2_~~	~~3.77~~	~~0.19~~	~~0.2557~~	~~0.0087~~	~~0.001~~	~~1467~~	~~45~~	~~1476~~	~~57~~	~~1780~~	~~130~~	~~18~~	~~1780~~	~~130~~	0.6605	0.0074
~~OC-56-DZ2-032~~	~~OC56DZ2_~~	~~6.76~~	~~0.62~~	~~0.233~~	~~0.04~~	~~0.60588~~	~~1340~~	~~220~~	~~1323~~	~~57~~	~~2725~~	~~66~~	~~51~~	~~2725~~	~~66~~	2.327	0.066
OC-56-DZ2-033	OC56DZ2_	3.83	0.14	0.2808	0.0088	0.65127	1595	44	1563	42	1638	79	3	1638	79	1.941	0.026
OC-56-DZ2-034	OC56DZ2_	11.79	0.24	0.462	0.017	0.75374	2448	73	2469	67	2714	73	10	2714	73	2.139	0.074
OC-56-DZ2-035	OC56DZ2_	1.836	0.068	0.1724	0.0055	0.57355	1034	24	1049	35	1157	92	11	1034	24	0.891	0.013
OC-56-DZ2-036	OC56DZ2_	2.219	0.073	0.1953	0.0057	0.8371	1150	31	1175	51	1243	72	7	1150	31	3.697	0.053
OC-56-DZ2-037	OC56DZ2_	4.31	0.18	0.2874	0.011	0.93002	1628	53	1583	70	1758	66	7	1758	66	2.84	0.042
OC-56-DZ2-038	OC56DZ2_	1.714	0.093	0.1656	0.0042	0.2095	988	23	1003	25	1068	90	7	988	23	3.011	0.047
OC-56-DZ2-039	OC56DZ2_	1.669	0.044	0.1661	0.0044	0.63818	991	25	1000	29	979	82	-1	991	25	2.69	0.033
OC-56-DZ2-040	OC56DZ2_	4.73	0.13	0.2995	0.0087	0.4667	1688	43	1691	52	1846	83	9	1846	83	2.42	0.025
OC-56-DZ2-041	Output_1_	4.21	0.2	0.294	0.0097	0.73896	1661	48	1664	68	1696	76	2	1696	76	0.929	0.033
~~OC-56-DZ2-042~~	~~Output_1_~~	~~4.48~~	~~0.18~~	~~0.2812~~	~~0.0057~~	~~0.84235~~	~~1597~~	~~29~~	~~1514~~	~~19~~	~~1902~~	~~61~~	~~16~~	~~1902~~	~~61~~	5.461	0.043
~~OC-56-DZ2-043~~	~~Output_1_~~	~~0.501~~	~~0.03~~	~~0.0626~~	~~0.0017~~	~~0.66104~~	~~391.7~~	~~11~~	~~376.3~~	~~7.9~~	~~578~~	~~83~~	~~32~~	~~391.7~~	~~11~~	2.269	0.081
OC-56-DZ2-044	Output_1_	4.46	0.2	0.3075	0.0089	0.54395	1728	44	1744	67	1718	88	-1	1718	88	2.28	0.025
OC-56-DZ2-045	Output_1_	2.51	0.16	0.2123	0.0063	0.61476	1241	34	1256	60	1328	100	7	1241	34	2.546	0.038
OC-56-DZ2-046	Output_1_	5.17	0.22	0.321	0.012	0.78897	1794	56	1469	73	1911	72	6	1911	72	1.357	0.046

OC-56-DZ2-048	Output_1_	3.97	0.16	0.2798	0.0089	0.70976	1590	45	1666	44	1674	68	5	1674	68	4.27	0.11
OC-56-DZ2-049	Output_1_	2.138	0.098	0.198	0.0062	0.87582	1165	33	1167	28	1155	71	-1	1165	33	1.502	0.013
OC-56-DZ2-050	Output_1_	2.071	0.1	0.1938	0.0055	0.64739	1142	30	1170	44	1132	85	-1	1142	30	1.735	0.023
OC-56-DZ2-051	Output_1_	0.449	0.028	0.06	0.0018	0.50933	375.7	11	372	16	370	130	-2	375.7	11	0.7497	0.0093
OC-56-DZ2-052	Output_1_	4.07	0.19	0.2858	0.009	0.86028	1620	45	1612	51	1655	74	2	1655	74	1.546	0.025
~~OC-56-DZ2-053~~	~~Output_1_~~	~~0.378~~	~~0.02~~	~~0.0492~~	~~0.0014~~	~~0.81968~~	~~309.5~~	~~8.4~~	~~304.3~~	~~6.3~~	~~412~~	~~85~~	~~25~~	~~309.5~~	~~8.4~~	1.3547	0.0085
OC-56-DZ2-054	Output_1_	3.54	0.25	0.2632	0.0067	0.58629	1506	34	1530	100	1570	120	4	1570	120	3.685	0.098
OC-56-DZ2-055	Output_1_	3.88	0.2	0.2784	0.0091	0.85942	1583	46	1589	29	1641	72	4	1641	72	1.155	0.013
OC-56-DZ2-056	Output_1_	0.812	0.072	0.1007	0.0041	0.19476	618	24	607	28	600	150	-3	618	24	1.175	0.031
~~OC-56-DZ2-057~~	~~Output_1_~~	~~1.758~~	~~0.11~~	~~0.1504~~	~~0.004~~	~~0.73337~~	~~903~~	~~23~~	~~824~~	~~47~~	~~1331~~	~~80~~	~~32~~	~~903~~	~~23~~	1.683	0.064
OC-56-DZ2-058	Output_1_	5.61	0.25	0.3409	0.0099	0.90788	1891	48	1848	54	1941	61	3	1941	61	0.88	0.013
OC-56-DZ2-059	Output_1_	2.69	0.17	0.2255	0.0089	0.29131	1311	47	1318	47	1340	130	2	1340	130	1.039	0.012
~~OC-56-DZ2-060~~	~~Output_1_~~	~~3.02~~	~~0.25~~	~~0.2577~~	~~0.0066~~	~~0.007836~~	~~1478~~	~~34~~	~~1498~~	~~49~~	~~1300~~	~~180~~	~~-14~~	~~1300~~	~~180~~	1.006	0.01
OC-56-DZ2-061	Output_1_	4.04	0.18	0.2887	0.01	0.81141	1634	51	1648	45	1646	69	1	1646	69	1.099	0.022
OC-56-DZ2-062	Output_1_	3.98	0.19	0.2843	0.008	0.77411	1613	40	1569	51	1648	69	2	1648	69	1.719	0.037
OC-56-DZ2-063	Output_1_	10.2	0.43	0.438	0.012	0.78596	2340	55	2228	59	2525	63	7	2525	63	1.734	0.027
OC-56-DZ2-064	Output_1_	1.647	0.075	0.1605	0.0036	0.53786	959	20	919	19	1011	72	5	959	20	1.488	0.059
OC-56-DZ2-065	Output_1_	2.08	0.095	0.1933	0.0057	0.42981	1139	31	1155	61	1141	86	0	1139	31	2.714	0.046
OC-56-DZ2-066	Output_1_	0.511	0.044	0.067	0.002	0.10893	418.2	12	426	17	400	180	-5	418.2	12	1.49	0.21
OC-56-DZ2-067	Output_1_	0.835	0.07	0.09885	0.0019	0.001	607.7	11	598	19	640	210	5	607.7	11	0.781	0.015
OC-56-DZ2-068	Output_1_	2.478	0.1	0.2043	0.0051	0.20957	1198	27	1093	24	1375	78	13	1198	27	0.995	0.013
OC-56-DZ2-069	Output_1_	3.87	0.21	0.2761	0.0077	0.58458	1572	39	1611	42	1645	95	4	1645	95	1.463	0.028
OC-56-DZ2-070	Output_1_	3.948	0.14	0.2903	0.01	0.66846	1643	50	1653	34	1615	76	-2	1615	76	1.389	0.042
OC-56-DZ2-071	Output_1_	1.895	0.1	0.1813	0.0042	0.79891	1074	23	1078	32	1056	84	-2	1074	23	1.876	0.025
OC-56-DZ2-072	Output_1_	1.606	0.086	0.1574	0.0044	0.78483	942	24	945	34	1029	84	8	942	24	0.743	0.014
OC-56-DZ2-073	Output_1_	1.705	0.074	0.1698	0.005	0.05397	1011	27	1008	26	999	98	-1	1011	27	2.251	0.028
OC-56-DZ2-074	Output_1_	4.422	0.18	0.2938	0.01	0.92263	1660	51	1637	79	1760	61	6	1760	61	1.838	0.043
OC-56-DZ2-075	Output_1_	0.544	0.037	0.0703	0.0029	0.86904	438	17	430	18	443	100	1	438	17	1.278	0.012
~~OC-56-DZ2-076~~	~~Output_1_~~	~~0.915~~	~~0.098~~	~~0.1045~~	~~0.0047~~	~~0.001~~	~~641~~	~~28~~	~~631~~	~~16~~	~~780~~	~~190~~	~~18~~	~~641~~	~~28~~	0.6414	0.0058
OC-56-DZ2-077	Output_1_	2.659	0.12	0.2237	0.0058	0.77566	1301	31	1262	50	1335	68	3	1335	68	0.475	0.011
OC-56-DZ2-078	Output_1_	4.3	0.21	0.2978	0.01	0.83697	1680	52	1678	84	1700	71	1	1700	71	4.48	0.07
OC-56-DZ2-079	Output_1_	1.675	0.1	0.1626	0.0049	0.68049	971	27	954	29	1044	100	7	971	27	0.769	0.011
OC-56-DZ2-080	Output_1_	1.442	0.07	0.1467	0.0051	0.45994	882	29	858	27	982	85	10	882	29	1.448	0.024
OC-56-DZ2-081	Output_1_	2.8	0.15	0.2316	0.0063	0.7562	1343	33	1315	59	1359	82	1	1359	82	2.119	0.022
OC-56-DZ2-082	Output_1_	11.42	0.28	0.465	0.013	0.98702	2460	56	940	21	2642.1	38	7	2642.1	38	7.058	0.063
OC-56-DZ2-083	Output_1_	17.08	0.42	0.587	0.015	0.84662	2978	61	2762	80	2920	44	-2	2920	44	1.778	0.017
OC-56-DZ2-084	Output_1_	1.708	0.048	0.1693	0.0045	0.44064	1008	25	940	28	1029	78	2	1008	25	1.182	0.015
OC-56-DZ2-085	Output_1_	1.79	0.11	0.1738	0.0057	0.25824	1033	31	972	51	1128	94	8	1033	31	1.724	0.014
OC-56-DZ2-086	Output_1_	0.398	0.035	0.0536	0.0019	0.56236	336	12	345	16	430	130	22	336	12	1.214	0.014
OC-56-DZ2-087	Output_1_	6.36	0.25	0.3802	0.011	0.871	2077	50	2050	61	2007	56	-3	2007	56	1.849	0.022
OC-56-DZ2-088	Output_1_	1.612	0.057	0.1581	0.0067	0.93208	946	37	896	23	1038	51	9	946	37	2.66	0.23
OC-56-DZ2-089	Output_1_	0.723	0.077	0.089	0.0098	0.90447	547	58	579	43	580	130	6	547	58	2.008	0.082
OC-56-DZ2-090	Output_1_	2.079	0.078	0.1992	0.006	0.80511	1171	33	1122	31	1094	66	-7	1171	33	2.93	0.15
OC-56-DZ2-091	Output_1_	3.85	0.099	0.2865	0.0076	0.61151	1624	38	1603	33	1583	62	-3	1583	62	1.977	0.037
~~OC-56-DZ2-092~~	~~Output_1_~~	~~0.2506~~	~~0.0093~~	~~0.02103~~	~~0.00049~~	~~0.40651~~	~~134.2~~	~~3.1~~	~~152~~	~~2~~	~~1372~~	~~83~~	~~90~~	~~134.2~~	~~3.1~~	1.53	0.039
OC-56-DZ2-093	Output_1_	2.79	0.13	0.2404	0.0075	0.80391	1389	39	1428	47	1303	75	-7	1303	75	1.597	0.015
OC-56-DZ2-094	Output_1_	1.699	0.06	0.1773	0.0043	0.36135	1052	24	1060	38	955	74	-10	1052	24	3.25	0.12
OC-56-DZ2-095	Output_1_	0.857	0.037	0.1062	0.0032	0.68688	651	19	628	27	602	100	-8	651	19	1.15	0.12

OC-56-DZ2-095	Output_1_	0.857	0.037	0.1062	0.0032	0.68688	651	19	628	27	602	100	-8	651	19	1.15	0.12
OC-56-DZ2-096	Output_1_	0.493	0.024	0.0674	0.0017	0.72506	420.5	11	389.2	9.9	353	99	-19	420.5	11	1.389	0.041
OC-56-DZ2-097	Output_1_	0.396	0.016	0.0557	0.0018	0.28218	350	11	320.3	7.1	290	120	-21	350	11	2.956	0.033
~~OC-56-DZ2-098~~	~~Output_1_~~	~~0.597~~	~~0.035~~	~~0.0847~~	~~0.0036~~	~~0.38676~~	~~524~~	~~21~~	~~502~~	~~25~~	~~350~~	~~170~~	~~-50~~	~~524~~	~~21~~	1.357	0.064
~~OC-56-DZ2-099~~	~~Output_1_~~	~~1.422~~	~~0.049~~	~~0.1625~~	~~0.0032~~	~~0.45331~~	~~971~~	~~18~~	~~944~~	~~53~~	~~761~~	~~91~~	~~-28~~	~~971~~	~~18~~	3.122	0.063
OC-56-DZ2-100	Output_1_	1.797	0.07	0.1812	0.0061	0.68501	1073	34	1042	36	1035	65	-4	1073	34	1.248	0.013
~~OC-56-DZ2-101~~	~~Output_1_~~	~~4.13~~	~~0.45~~	~~0.247~~	~~0.022~~	~~0.94996~~	~~1420~~	~~110~~	~~2140~~	~~100~~	~~2001~~	~~68~~	~~29~~	~~2001~~	~~68~~	2.08	0.38
OC-56-DZ2-102	Output_1_	11.43	0.25	0.48	0.014	0.82819	2526	60	2585	53	2575	42	2	2575	42	0.8184	0.004
OC-56-DZ2-103	Output_1_	4.64	0.13	0.316	0.0067	0.9117	1770	33	1832	52	1731	52	-2	1731	52	2.32	0.14
OC-56-DZ2-104	Output_1_	2.256	0.084	0.2009	0.0051	0.13441	1180	27	1235	72	1173	110	-1	1180	27	2.117	0.03
OC-56-DZ2-105	Output_1_	5.08	0.17	0.3329	0.01	0.5791	1852	50	1844	69	1790	82	-3	1790	82	1.029	0.022
OC-56-DZ2-106	Output_1_	1.784	0.053	0.1727	0.004	0.5696	1027	22	1067	17	1035	70	1	1027	22	1.334	0.025
OC-56-DZ2-107	Output_1_	4.73	0.1	0.312	0.007	0.589	1750	35	1795	56	1766	58	1	1766	58	4.96	0.12
~~OC-56-DZ2-108~~	~~Output_1_~~	~~0.787~~	~~0.091~~	~~0.0992~~	~~0.0027~~	~~0.32243~~	~~609~~	~~16~~	~~639~~	~~39~~	~~420~~	~~260~~	~~-45~~	~~609~~	~~16~~	1.403	0.018
OC-56-DZ2-109	Output_1_	3.7	0.11	0.2684	0.0079	0.63209	1532	41	1484	50	1577	50	3	1577	50	1.154	0.017
OC-56-DZ2-110	Output_1_	4.18	0.13	0.3001	0.0077	0.6535	1692	38	1709	52	1615	64	-5	1615	64	1.192	0.017
OC-56-DZ2-111	Output_1_	3.27	0.12	0.257	0.01	0.71167	1474	54	1446	57	1432	72	-3	1432	72	1.799	0.064
OC-56-DZ2-112	Output_1_	13.74	0.43	0.529	0.014	0.56897	2735	59	2744	70	2694	61	-2	2694	61	0.6532	0.0059
OC-56-DZ2-113	Output_1_	0.891	0.043	0.1064	0.0027	0.3529	652	16	694	25	601	110	-8	652	16	1.424	0.028
OC-56-DZ2-114	Output_1_	1.955	0.074	0.1817	0.0057	0.001	1076	31	1148	30	1127	110	5	1076	31	1.477	0.025
OC-56-DZ2-115	Output_1_	2.219	0.077	0.2011	0.0051	0.34806	1181	27	1252	36	1181	87	0	1181	27	5.064	0.049
OC-56-DZ2-116	Output_1_	4.36	0.14	0.3025	0.0083	0.85573	1704	41	1732	42	1706	48	0	1706	48	1.691	0.024
OC-56-DZ2-117	Output_1_	5.43	0.19	0.334	0.011	0.91852	1855	55	1889	67	1899	53	2	1899	53	2.154	0.032
OC-56-DZ2-118	Output_1_	4.81	0.13	0.3196	0.0096	0.84192	1787	47	1815	42	1788	53	0	1788	53	2.85	0.025
OC-56-DZ2-119	Output_1_	0.642	0.024	0.0803	0.0026	0.75597	498	15	489	12	512	65	3	498	15	1.745	0.015
OC-56-DZ2-120	Output_1_	1.811	0.053	0.1776	0.0062	0.63844	1054	34	1142	91	1085	86	3	1054	34	5.31	0.18

Table 3: U/Pb data from Sample: MP_DZ1

		Final207_	Final207_	Final206_	Final206_	ErrorCorre	Final238_	Final238_	ErrorCorre	FinalAge2	FinalAge2	FinalAge2	FinalAge2	FinalAge2	FinalAge2	FinalAge2	PERC_DIS(	Preferred	Preferred	FInal_U_T	FInal_U_Th_Ratio_Int2SE
~~MPDZ1-00~~	~~MPDZ1-00~~	~~0.549~~	~~0.03~~	~~0.0512~~	~~0.0015~~	~~0.8446~~	~~19.53125~~	~~0.572205~~	~~-0.12023~~	~~321.9~~	~~6.8~~	~~9~~	~~636~~	~~18~~	~~1111~~	~~70~~	~~71~~	~~321.9~~	~~9~~	5.295	0.081
~~MPDZ1-04~~	~~MPDZ1-04~~	~~0.5339~~	~~0.021~~	~~0.0539~~	~~0.002~~	~~0.031885~~	~~18.55288~~	~~0.688418~~	~~0.89443~~	~~338~~	~~11~~	~~12~~	~~345~~	~~19~~	~~962~~	~~99~~	~~65~~	~~338~~	~~12~~	4.02	0.15
~~MPDZ1-12~~	~~MPDZ1-12~~	~~0.5542~~	~~0.013~~	~~0.0589~~	~~0.0015~~	~~0.36408~~	~~16.97793~~	~~0.432375~~	~~0.76112~~	~~369.1~~	~~9.3~~	~~9.2~~	~~258~~	~~13~~	~~863~~	~~68~~	~~57~~	~~369.1~~	~~9.2~~	~~1.59~~	~~0.084~~
~~MPDZ1-04~~	~~MPDZ1-05~~	~~0.608~~	~~0.038~~	~~0.059~~	~~0.0015~~	~~0.14587~~	~~16.94915~~	~~0.430911~~	~~0.28215~~	~~369.6~~	~~7.3~~	~~9.1~~	~~329~~	~~15~~	~~1030~~	~~130~~	~~64~~	~~369.6~~	~~9.1~~	1.49	0.037
~~MPDZ1-07~~	~~MPDZ1-07~~	~~0.578~~	~~0.021~~	~~0.0595~~	~~0.0041~~	~~-0.76593~~	~~16.80672~~	~~1.15811~~	~~0.98047~~	~~372~~	~~24~~	~~25~~	~~307~~	~~45~~	~~960~~	~~190~~	~~61~~	~~372~~	~~25~~	0.83	0.15
~~MPDZ1-12~~	~~MPDZ1-12~~	~~0.51~~	~~0.02~~	~~0.0605~~	~~0.0013~~	~~0.5994~~	~~16.52893~~	~~0.355167~~	~~-0.10956~~	~~378.6~~	~~7.9~~	~~7.8~~	~~384.1~~	~~8.3~~	~~632~~	~~80~~	~~40~~	~~378.6~~	~~7.8~~	~~0.747~~	~~0.011~~
~~MPDZ1-12~~	~~MPDZ1-12~~	~~0.53~~	~~0.023~~	~~0.06391~~	~~0.00096~~	~~0.74634~~	~~15.647~~	~~0.235036~~	~~-0.44181~~	~~399.3~~	~~5.9~~	~~5.8~~	~~376.5~~	~~9.8~~	~~572~~	~~71~~	~~30~~	~~399.3~~	~~5.8~~	~~2.092~~	~~0.053~~
~~MPDZ1-00~~	~~MPDZ1-00~~	~~0.606~~	~~0.099~~	~~0.0648~~	~~0.0022~~	~~0.90521~~	~~15.4321~~	~~0.523929~~	~~-0.80913~~	~~405~~	~~11~~	~~13~~	~~367~~	~~19~~	~~690~~	~~170~~	~~41~~	~~405~~	~~13~~	1.7	0.21
~~MPDZ1-10~~	~~MPDZ1-10~~	~~0.594~~	~~0.026~~	~~0.0662~~	~~0.0021~~	~~0.28841~~	~~15.10574~~	~~0.479185~~	~~0.50116~~	~~413~~	~~11~~	~~12~~	~~345~~	~~35~~	~~768~~	~~110~~	~~46~~	~~413~~	~~12~~	0.99	0.12
~~MPDZ1-01~~	~~MPDZ1-01~~	~~0.573~~	~~0.021~~	~~0.06845~~	~~0.0014~~	~~-0.15265~~	~~14.6092~~	~~0.2988~~	~~0.80055~~	~~426.8~~	~~5.9~~	~~8.4~~	~~379~~	~~11~~	~~612~~	~~79~~	~~30~~	~~426.8~~	~~8.4~~	1.192	0.082
MPDZ1-10	MPDZ1-11	0.525	0.019	0.069	0.0017	0.54387	14.49275	0.357068	0.37755	429.9	8	10	435	19	442	67	3	429.9	10	1.988	0.028
MPDZ1-03	MPDZ1-03	0.645	0.03	0.0692	0.0017	0.77536	14.45087	0.355007	-0.43804	431.5	8.3	11	556	17	852	74	49	431.5	11	3.46	0.11
MPDZ1-11	MPDZ1-12	0.537	0.018	0.0693	0.0017	0.75333	14.43001	0.353983	0.30972	431.8	8	10	436.9	17	454	63	5	431.8	10	1.279	0.091
MPDZ1-07	MPDZ1-07	0.55	0.018	0.0715	0.0019	0.5044	13.98601	0.371656	0.41248	445.2	9.1	11	440	20	501	74	11	445.2	11	2.185	0.021
MPDZ1-04	MPDZ1-04	0.5752	0.022	0.07186	0.0013	0.053317	13.91595	0.25175	0.63667	447.3	4.4	8	450	11	519	78	14	447.3	8	1.832	0.034
MPDZ1-06	MPDZ1-07	0.5655	0.016	0.0727	0.0022	-0.37586	13.75516	0.41625	0.94152	452	11	13	437	19	490	100	8	452	13	2.3	0.35
MPDZ1-09	MPDZ1-09	0.574	0.017	0.0731	0.0016	0.60479	13.67989	0.299423	0.1027	454.7	6.7	9.4	463.2	18	502	60	9	454.7	9.4	2.944	0.058
MPDZ1-01	MPDZ1-01	0.568	0.025	0.0732	0.0017	0.33388	13.6612	0.317268	0.36296	455.6	7.7	10	451.4	9.6	436	83	-4	455.6	10	1.199	0.024
MPDZ1-05	MPDZ1-05	0.578	0.023	0.0738	0.0016	0.69619	13.55014	0.29377	0.22403	459.2	7	9.7	444.2	7.9	502	69	9	459.2	9.7	1.468	0.018
MPDZ1-07	MPDZ1-07	0.576	0.018	0.0747	0.0017	0.82106	13.38688	0.304655	0.038951	464.3	7.6	10	452.2	16	457	61	-2	464.3	10	1.352	0.016
~~MPDZ1-04~~	~~MPDZ1-04~~	~~0.7~~	~~0.035~~	~~0.0762~~	~~0.0018~~	~~-0.00068~~	~~13.12336~~	~~0.310001~~	~~0.30223~~	~~473.2~~	~~8.3~~	~~11~~	~~506~~	~~20~~	~~800~~	~~95~~	~~41~~	~~473.2~~	~~11~~	1.479	0.035
MPDZ1-01	MPDZ1-01	0.645	0.047	0.0806	0.0019	-0.03734	12.40695	0.292472	0.42189	499.6	9.2	12	457	23	520	170	4	499.6	12	1.538	0.038
~~MPDZ1-07~~	~~MPDZ1-07~~	~~0.84~~	~~0.2~~	~~0.082~~	~~0.019~~	~~0.56201~~	~~12.19512~~	~~2.825699~~	~~0.48665~~	~~500~~	~~110~~	~~110~~	~~720~~	~~290~~	~~970~~	~~160~~	~~48~~	~~500~~	~~110~~	4.69	0.71
MPDZ1-12	MPDZ1-12	0.66	0.024	0.0836	0.0015	0.52357	11.96172	0.214624	0.004504	517.8	9	8.9	507	13	503	72	-3	517.8	8.9	1.408	0.022
MPDZ1-02	MPDZ1-03	0.69	0.029	0.0842	0.0025	0.25778	11.87648	0.352627	0.63139	521	13	15	522	14	575	81	9	521	15	0.7436	0.0093
MPDZ1-06	MPDZ1-06	0.756	0.031	0.0895	0.0025	0.091895	11.17318	0.3121	0.50796	553	12	15	569	40	676	95	18	553	15	3.319	0.097
~~MPDZ1-08~~	~~MPDZ1-08~~	~~0.877~~	~~0.059~~	~~0.0919~~	~~0.0032~~	~~0.26066~~	~~10.88139~~	~~0.378895~~	~~0.18617~~	~~567~~	~~17~~	~~19~~	~~387~~	~~20~~	~~880~~	~~140~~	~~36~~	~~567~~	~~19~~	0.697	0.014
MPDZ1-02	MPDZ1-02	0.829	0.034	0.0964	0.0023	0.41743	10.37344	0.247499	0.49534	593	11	14	618	20	709	75	16	593	14	1.52	0.071
~~MPDZ1-07~~	~~MPDZ1-07~~	~~1.22~~	~~0.2~~	~~0.102~~	~~0.018~~	~~0.93311~~	~~9.803922~~	~~1.730104~~	~~0.45835~~	~~620~~	~~110~~	~~110~~	~~699~~	~~51~~	~~1462~~	~~85~~	~~58~~	~~620~~	~~110~~	1.68	0.23
MPDZ1-06	MPDZ1-06	0.859	0.024	0.1015	0.0021	0.8457	9.852217	0.203839	0.50781	623.1	8.2	12	573	25	684	55	9	623.1	12	0.767	0.012
MPDZ1-01	MPDZ1-01	0.896	0.041	0.1019	0.0022	0.59475	9.813543	0.211872	-0.03603	625.8	9.3	13	644	13	710	80	12	625.8	13	1.131	0.012
~~MPDZ1-11~~	~~MPDZ1-11~~	~~3.1~~	~~0.62~~	~~0.1124~~	~~0.0076~~	~~0.98552~~	~~8.896797~~	~~0.601563~~	~~-0.97504~~	~~686~~	~~43~~	~~44~~	~~1950~~	~~380~~	~~2620~~	~~350~~	~~74~~	~~686~~	~~44~~	1.872	0.084
~~MPDZ1-08~~	~~MPDZ1-08~~	~~1.64~~	~~0.14~~	~~0.126~~	~~0.018~~	~~-0.08534~~	~~7.936508~~	~~1.133787~~	~~0.6966~~	~~760~~	~~100~~	~~100~~	~~650~~	~~130~~	~~1590~~	~~300~~	~~52~~	~~760~~	~~100~~	1.48	0.44
MPDZ1-03	MPDZ1-03	1.5	0.11	0.1458	0.0075	-0.62838	6.858711	0.352814	0.81564	877	40	42	465	71	1040	190	16	877	42	0.97	0.18
~~MPDZ1-06~~	~~MPDZ1-06~~	~~1.642~~	~~0.067~~	~~0.1504~~	~~0.0037~~	~~0.84622~~	~~6.648936~~	~~0.163571~~	~~0.12698~~	~~903~~	~~16~~	~~21~~	~~733~~	~~18~~	~~1174~~	~~62~~	~~23~~	~~903~~	~~21~~	2.062	0.045
MPDZ1-05	MPDZ1-05	1.566	0.071	0.1508	0.0035	0.17582	6.6313	0.15391	0.39325	905	15	20	609	25	1078	80	16	905	20	1.367	0.051
~~MPDZ1-05~~	~~MPDZ1-05~~	~~1.665~~	~~0.086~~	~~0.1511~~	~~0.0034~~	~~0.28534~~	~~6.618134~~	~~0.148919~~	~~0.092622~~	~~910~~	~~14~~	~~19~~	~~885~~	~~35~~	~~1175~~	~~92~~	~~23~~	~~910~~	~~19~~	1.305	0.021
MPDZ1-01	MPDZ1-01	1.485	0.061	0.1529	0.0044	0.22935	6.540222	0.188208	0.58857	917	22	25	904	21	950	73	3	917	25	1.673	0.019
~~MPDZ1-09~~	~~MPDZ1-09~~	~~1.83~~	~~0.16~~	~~0.1541~~	~~0.004~~	~~0.41983~~	~~6.489293~~	~~0.168444~~	~~-0.18428~~	~~924~~	~~18~~	~~22~~	~~637~~	~~34~~	~~1290~~	~~140~~	~~28~~	~~924~~	~~22~~	1.8	0.27
MPDZ1-09	MPDZ1-09	1.522	0.07	0.1546	0.0054	0.8276	6.468305	0.225931	0.11292	927	27	30	957	41	952	61	3	927	30	1.75	0.056
MPDZ1-00	MPDZ1-00	1.546	0.078	0.1569	0.0033	0.46707	6.373486	0.13405	0.263	940	11	18	900	27	987	81	5	940	18	2.739	0.031
MPDZ1-00	MPDZ1-00	1.595	0.084	0.1588	0.0036	0.4409	6.297229	0.142758	-0.07688	950	13	20	874	26	996	89	5	950	20	1.397	0.051

MPDZ1-012	MPDZ1_12	1.655	0.074	0.1621	0.0036	0.65695	6.169031	0.137005	-0.02301	968	15	20	981	31	1019	68	5	968	20	2.463	0.037
MPDZ1-054	MPDZ1_54	1.729	0.087	0.1628	0.0046	0.6691	6.142506	0.17356	-0.18677	972	21	25	898	23	1140	85	15	972	25	0.671	0.042
~~MPDZ1-057~~	~~MPDZ1_57~~	~~1.977~~	~~0.079~~	~~0.1643~~	~~0.0038~~	~~0.050186~~	~~6.086427~~	~~0.14077~~	~~0.68277~~	~~980~~	~~16~~	~~21~~	~~828~~	~~28~~	~~1378~~	~~62~~	~~29~~	~~980~~	~~21~~	1.292	0.037
MPDZ1-079	MPDZ1_19	1.71	0.062	0.1643	0.0035	-0.37748	6.086427	0.129656	0.665	981	13	19	882	50	1061	56	8	981	19	1.74	0.23
MPDZ1-075	MPDZ1_15	1.783	0.086	0.1651	0.004	0.68921	6.056935	0.146746	-0.26683	985	17	22	904	54	1171	74	16	985	22	2.686	0.055
MPDZ1-100	MPDZ1_40	1.654	0.051	0.1653	0.0038	0.23053	6.049607	0.139071	0.60866	986	16	21	996	47	993	74	1	986	21	1.487	0.025
MPDZ1-110	MPDZ1_50	1.71	0.053	0.1661	0.0041	0.56833	6.02047	0.148609	0.50617	990	17	23	1040	43	1060	67	7	990	23	1.197	0.023
MPDZ1-116	MPDZ1_56	1.78	0.069	0.166	0.005	0.95097	6.024096	0.181449	0.47713	990	24	28	728	75	1183	51	16	990	28	1.711	0.04
MPDZ1-089	MPDZ1_29	1.699	0.057	0.1662	0.0039	0.68122	6.016847	0.14119	-0.05749	991	16	22	904	63	1060	57	7	991	22	6.7	2
MPDZ1-105	MPDZ1_45	1.696	0.061	0.1663	0.0051	0.71973	6.013229	0.184411	0.31074	991	25	28	1008	36	1035	63	4	991	28	4.864	0.057
MPDZ1-033	MPDZ1_33	1.706	0.08	0.1664	0.0032	0.31394	6.009615	0.11557	-0.02945	992	11	18	935	45	1053	86	6	992	18	3.59	0.22
MPDZ1-045	MPDZ1_45	1.731	0.068	0.1671	0.0032	0.46249	5.98444	0.114603	0.19429	996	11	18	956	24	1076	59	7	996	18	2.155	0.051
MPDZ1-092	MPDZ1_32	1.714	0.052	0.168	0.0037	0.73978	5.952381	0.131094	0.32345	1001	15	21	1010	37	1046	53	4	1001	21	1.03	0.015
MPDZ1-017	MPDZ1_17	1.738	0.074	0.1691	0.0035	0.5522	5.913661	0.1224	-0.01425	1007	14	20	917	65	1046	71	4	1007	20	2.99	0.25
~~MPDZ1-019~~	~~MPDZ1_19~~	~~2.174~~	~~0.097~~	~~0.1694~~	~~0.0048~~	~~0.011342~~	~~5.903188~~	~~0.167269~~	~~0.57824~~	~~1009~~	~~23~~	~~27~~	~~872~~	~~31~~	~~1500~~	~~84~~	~~33~~	~~1009~~	~~27~~	0.832	0.014
MPDZ1-026	MPDZ1_26	1.708	0.07	0.1697	0.0035	0.44675	5.892752	0.121536	0.59104	1010	14	19	985	21	1044	68	3	1010	19	2.811	0.038
MPDZ1-042	MPDZ1_42	1.713	0.066	0.1697	0.0039	0.54501	5.892752	0.135426	0.44022	1011	16	22	1006	20	1014	67	0	1011	22	2.942	0.042
MPDZ1-106	MPDZ1_46	1.733	0.069	0.1714	0.0041	0.70643	5.834306	0.13956	0.29198	1020	17	22	1013	47	1050	62	3	1020	22	3.235	0.052
MPDZ1-088	MPDZ1_28	1.771	0.071	0.1717	0.0043	0.63124	5.824112	0.145857	0.008595	1021	19	24	1050	44	1067	71	4	1021	24	1.365	0.027
MPDZ1-007	MPDZ1_7	1.76	0.077	0.1722	0.0044	0.53852	5.807201	0.148384	0.54562	1024	17	24	933	17	1055	64	3	1024	24	1.705	0.029
MPDZ1-055	MPDZ1_55	1.744	0.073	0.1723	0.0033	0.50922	5.803831	0.111159	0.19485	1025	11	18	942	19	1048	69	2	1025	18	1.939	0.018
MPDZ1-122	MPDZ1_2	1.81	0.044	0.1728	0.0028	0.80009	5.787037	0.093771	0.26511	1027	16	16	770	21	1091	45	6	1027	16	4.33	0.32
~~MPDZ1-009~~	~~MPDZ1_9~~	~~2.73~~	~~0.52~~	~~0.1734~~	~~0.0056~~	~~0.90209~~	~~5.767013~~	~~0.186247~~	~~-0.8444~~	~~1031~~	~~25~~	~~30~~	~~1410~~	~~240~~	~~1680~~	~~250~~	~~39~~	~~1031~~	~~30~~	2.41	0.2
~~MPDZ1-053~~	~~MPDZ1_53~~	~~2.48~~	~~0.25~~	~~0.1737~~	~~0.0046~~	~~0.31392~~	~~5.757052~~	~~0.152461~~	~~0.00931~~	~~1032~~	~~21~~	~~25~~	~~1051~~	~~38~~	~~1680~~	~~170~~	~~39~~	~~1032~~	~~25~~	0.878	0.028
MPDZ1-102	MPDZ1_42	1.772	0.048	0.1742	0.0037	0.84458	5.740528	0.121929	0.47	1035	14	20	1054	39	1037	51	0	1035	20	1.271	0.014
MPDZ1-104	MPDZ1_44	1.796	0.05	0.1742	0.0038	0.65245	5.740528	0.125224	0.37522	1035	15	21	1047	57	1065	55	3	1035	21	50.5	4.2
MPDZ1-101	MPDZ1_41	1.852	0.058	0.1743	0.0037	0.59543	5.737235	0.121789	0.22957	1036	14	20	895	55	1114	55	7	1036	20	2.03	0.19
MPDZ1-016	MPDZ1_16	1.857	0.073	0.1751	0.0038	0.41973	5.711022	0.12394	0.24361	1040	16	21	1036	19	1106	67	6	1040	21	1.354	0.018
MPDZ1-023	MPDZ1_23	1.896	0.069	0.1759	0.0032	0.39932	5.685048	0.103423	0.53769	1044.7	9.8	17	883	46	1157	63	10	1044.7	17	19.8	1
MPDZ1-074	MPDZ1_14	1.834	0.057	0.1765	0.0037	0.69719	5.665722	0.118772	0.17083	1048	14	20	1040	39	1089	57	4	1048	20	1.547	0.011
~~MPDZ1-032~~	~~MPDZ1_32~~	~~3.23~~	~~0.5~~	~~0.1771~~	~~0.0091~~	~~0.93506~~	~~5.646527~~	~~0.290138~~	~~-0.86762~~	~~1050~~	~~47~~	~~49~~	~~1680~~	~~230~~	~~2020~~	~~200~~	~~48~~	~~1050~~	~~49~~	2.26	0.15
MPDZ1-047	MPDZ1_47	2.072	0.12	0.1796	0.0055	-0.20674	5.567929	0.17051	0.60232	1065	27	30	1112	42	1270	130	16	1065	30	2.001	0.078
MPDZ1-008	MPDZ1_8	1.914	0.095	0.1805	0.0041	0.23389	5.540166	0.125843	0.28153	1069	15	22	1030	58	1081	92	1	1069	22	2.421	0.025
MPDZ1-059	MPDZ1_59	1.943	0.073	0.1825	0.0042	0.50049	5.479452	0.126103	0.34623	1081	17	23	1047	39	1126	67	4	1081	23	3.13	0.057
MPDZ1-001	MPDZ1_1	1.912	0.079	0.183	0.0042	0.78643	5.464481	0.125414	0.10133	1083	16	23	1056	19	1072	64	-1	1083	23	3.477	0.045
MPDZ1-024	MPDZ1_24	1.996	0.079	0.1829	0.004	0.58296	5.467469	0.119573	0.26175	1083	16	22	983	26	1159	65	7	1083	22	3.391	0.069
MPDZ1-028	MPDZ1_28	1.988	0.072	0.1842	0.0037	0.4558	5.428882	0.109049	0.61519	1090	14	20	1059	15	1146	63	5	1090	20	1.138	0.017
MPDZ1-127	MPDZ1_7	2.01	0.044	0.1857	0.002	0.562	5.38503	0.057997	0.10621	1098	11	11	1124	27	1149	46	4	1098	11	2.897	0.059
MPDZ1-081	MPDZ1_21	2.001	0.059	0.1878	0.004	0.69334	5.324814	0.113415	0.33348	1109	16	22	1113	42	1126	53	2	1109	22	2.362	0.082
MPDZ1-083	MPDZ1_23	1.998	0.06	0.1887	0.004	0.85059	5.299417	0.112335	-0.10637	1114	15	22	1083	52	1119	51	0	1114	22	29.2	1.4
MPDZ1-039	MPDZ1_39	2.05	0.08	0.1921	0.004	0.61443	5.205622	0.108394	0.46473	1133	15	22	1122	25	1148	59	1	1133	22	3.347	0.061
~~MPDZ1-126~~	~~MPDZ1_6~~	~~2.77~~	~~0.13~~	~~0.1925~~	~~0.0035~~	~~0.76716~~	~~5.194805~~	~~0.094451~~	~~-0.38232~~	~~1135~~	~~19~~	~~19~~	~~1216~~	~~46~~	~~1692~~	~~74~~	~~33~~	~~1135~~	~~19~~	~~2.018~~	~~0.045~~
MPDZ1-020	MPDZ1_20	2.179	0.081	0.1933	0.0037	0.54456	5.173306	0.099023	0.28152	1139	13	20	1199	39	1234	65	8	1139	20	10.6	0.98
MPDZ1-038	MPDZ1_38	2.128	0.081	0.1936	0.0036	0.5452	5.165289	0.096049	0.4139	1141	11	19	1056	15	1183	58	4	1141	19	1.949	0.042
MPDZ1-085	MPDZ1_25	2.128	0.065	0.1939	0.0044	0.72382	5.157298	0.11703	0.26288	1142	18	24	1099	40	1202	54	5	1142	24	2.605	0.034
MPDZ1-129	MPDZ1_9	2.182	0.048	0.1948	0.0032	0.59993	5.13347	0.084328	0.39661	1147	17	17	689	43	1232	48	7	1147	17	1.77	0.047
MPDZ1-093	MPDZ1_33	2.134	0.059	0.1949	0.0046	0.77035	5.130836	0.121097	0.51183	1148	19	25	1166	44	1180	52	3	1148	25	2.67	0.24
MPDZ1-118	MPDZ1_58	2.157	0.065	0.1952	0.0044	0.75058	5.122951	0.115476	0.20717	1149	17	24	1152	39	1180	54	3	1149	24	1.972	0.024
MPDZ1-041	MPDZ1_41	2.216	0.087	0.1962	0.0037	0.39392	5.09684	0.096118	0.38252	1155	11	20	1119	25	1248	64	7	1155	20	1.795	0.034
MPDZ1-080	MPDZ1_20	2.41	0.17	0.1984	0.0044	0.61902	5.040323	0.111781	-0.4186	1167	17	24	1107	46	1370	110	15	1167	24	1.79	0.18
MPDZ1-030	MPDZ1_30	2.43	0.087	0.2018	0.0036	0.70028	4.955401	0.088402	0.44733	1185	10	19	1045	13	1369	58	13	1185	19	3.173	0.069
MPDZ1-086	MPDZ1_26	2.282	0.093	0.2034	0.0053	0.65528	4.916421	0.128107	0.021355	1194	23	28	1180	49	1219	68	2	1194	28	2.676	0.089
MPDZ1-107	MPDZ1_47	2.263	0.074	0.2038	0.0057	0.69525	4.906771	0.137236	0.23595	1195	25	30	1209	48	1213	62	1	1195	30	1.795	0.029
MPDZ1-034	MPDZ1_34	2.498	0.097	0.2075	0.0041	0.71903	4.819277	0.095224	0.1888	1215	14	22	1070	44	1360	59	11	1215	22	1.99	0.071
MPDZ1-035	MPDZ1_35	2.387	0.093	0.208	0.0049	0.70234	4.807692	0.113258	0.30127	1218	20	26	1161	19	1260	63	3	1218	26	2.652	0.028
MPDZ1-065	MPDZ1_5	2.332	0.068	0.2095	0.0051	0.87732	4.77327	0.116199	0.33041	1226	21	27	1218	50	1229	49	0	1226	27	2.953	0.071
MPDZ1-025	MPDZ1_25	2.481	0.11	0.2099	0.0051	0.67508	4.764173	0.115757	0.00316	1228	21	27	1209	30	1331	71	8	1228	27	1.089	0.014
MPDZ1-067	MPDZ1_7	2.517	0.072	0.2125	0.0048	0.80658	4.705882	0.106298	0.48068	1247	20	27	974	37	1339	50	7	1247	27	1.789	0.02
MPDZ1-099	MPDZ1_39	2.434	0.075	0.214	0.0053	0.5228	4.672897	0.115731	0.49182	1250	22	28	1259	53	1254	63	0	1250	28	1.317	0.015
~~MPDZ1-073~~	~~MPDZ1_13~~	~~2.89~~	~~0.21~~	~~0.2143~~	~~0.0047~~	~~0.76225~~	~~4.666356~~	~~0.102342~~	~~-0.59659~~	~~1252~~	~~18~~	~~25~~	~~1315~~	~~73~~	~~1590~~	~~120~~	~~21~~	~~1252~~	~~25~~	1.74	0.11
MPDZ1-044	MPDZ1_44	2.472	0.11	0.2146	0.0059	0.59574	4.659832	0.128113	0.22169	1253	26	31	1231	24	1276	74	2	1253	31	1.347	0.018
~~MPDZ1-051~~	~~MPDZ1_51~~	~~2.978~~	~~0.12~~	~~0.216~~	~~0.0041~~	~~0.39874~~	~~4.62963~~	~~0.087877~~	~~0.38499~~	~~1261~~	~~13~~	~~22~~	~~1343~~	~~22~~	~~1617~~	~~62~~	~~22~~	~~1261~~	~~22~~	1.646	0.044
~~MPDZ1-004~~	~~MPDZ1_4~~	~~3.21~~	~~0.18~~	~~0.2191~~	~~0.0067~~	~~0.7825~~	~~4.564126~~	~~0.139569~~	~~-0.40251~~	~~1277~~	~~28~~	~~35~~	~~1631~~	~~61~~	~~1733~~	~~67~~	~~26~~	~~1277~~	~~35~~	2.008	0.038
MPDZ1-010	MPDZ1_10	2.862	0.11	0.2368	0.0045	0.57459	4.222973	0.080251	0.49675	1370	13	23	1339	18	1373	58	0	1373	58	2.322	0.023
MPDZ1-087	MPDZ1_27	2.906	0.088	0.2394	0.006	0.84859	4.177109	0.10469	0.19563	1383	25	31	1381	51	1404	49	1	1404	49	1.966	0.023
MPDZ1-061	MPDZ1_1	2.914	0.087	0.2343	0.0059	0.84522	4.268032	0.107475	0.13511	1357	25	31	1289	48	1423	49	5	1423	49	4.25	0.12
MPDZ1-077	MPDZ1_17	2.999	0.086	0.2395	0.0048	0.78404	4.175365	0.083682	0.227	1384	16	25	1363	54	1455	48	5	1455	48	1.591	0.017
MPDZ1-063	MPDZ1_3	3.109	0.092	0.2461	0.0057	0.7238	4.063389	0.094113	0.23365	1418	22	29	1389	58	1456	53	3	1456	53	2.328	0.046
MPDZ1-064	MPDZ1_4	3.006	0.088	0.2389	0.0048	0.67718	4.185852	0.084103	0.070644	1381	16	25	1348	54	1468	50	6	1468	50	2.062	0.033

MPDZ1-077	MPDZ1_17	2.999	0.086	0.2395	0.0048	0.78404	4.175365	0.083682	0.227	1384	16	25	1363	54	1455	48	5	1455	48	1.591	0.017
MPDZ1-063	MPDZ1_3	3.109	0.092	0.2461	0.0057	0.7238	4.063389	0.094113	0.23365	1418	22	29	1389	58	1456	53	3	1456	53	2.328	0.046
MPDZ1-064	MPDZ1_4	3.006	0.088	0.2389	0.0048	0.67718	4.185852	0.084103	0.070644	1381	16	25	1348	54	1468	50	6	1468	50	2.062	0.033
MPDZ1-120	MPDZ1_60	3.234	0.092	0.248	0.0048	0.6882	4.032258	0.078044	0.019494	1428	15	25	1411	49	1496	51	5	1496	51	0.974	0.022
MPDZ1-043	MPDZ1_43	3.136	0.14	0.2355	0.0045	0.098134	4.246285	0.081139	0.44352	1363	14	24	1160	43	1536	77	11	1536	77	0.863	0.033
MPDZ1-031	MPDZ1_31	3.48	0.29	0.254	0.013	0.98391	3.937008	0.2015	-0.92059	1460	62	65	1535	25	1597	83	9	1597	83	2.06	0.29
MPDZ1-113	MPDZ1_53	3.766	0.12	0.271	0.0067	0.87961	3.690037	0.09123	0.39958	1545	26	34	1614	60	1625	48	5	1625	48	1.294	0.051
MPDZ1-095	MPDZ1_35	3.658	0.11	0.2614	0.0068	0.83826	3.825555	0.099517	0.26892	1497	28	35	1135	73	1637	48	9	1637	48	1.33	0.08
MPDZ1-096	MPDZ1_36	4.048	0.12	0.2892	0.0063	0.7888	3.457815	0.075326	0.36668	1638	23	31	1653	64	1663	49	2	1663	49	1.427	0.027
MPDZ1-108	MPDZ1_48	4.363	0.13	0.3009	0.0079	0.816	3.323363	0.087253	0.68455	1696	32	39	1650	58	1715	48	1	1715	48	1.372	0.028
MPDZ1-117	MPDZ1_57	4.516	0.14	0.3074	0.007	0.88355	3.25309	0.074078	-0.04767	1728	25	35	1753	60	1719	48	-1	1719	48	1.404	0.024
MPDZ1-050	MPDZ1_50	4.16	0.19	0.2791	0.0068	0.37889	3.582945	0.087295	0.32157	1587	27	34	1708	38	1760	66	10	1760	66	2.041	0.022
MPDZ1-112	MPDZ1_52	4.481	0.13	0.2973	0.0064	0.80023	3.363606	0.072409	0.27667	1678	22	32	1627	73	1764	47	5	1764	47	1.156	0.056
MPDZ1-128	MPDZ1_8	4.777	0.12	0.3143	0.0054	0.87903	3.181674	0.054664	0.23935	1761	27	26	1782	42	1792	39	2	1792	39	4.19	0.035
MPDZ1-098	MPDZ1_38	4.662	0.13	0.3078	0.0066	0.89073	3.248863	0.069664	0.22287	1730	23	33	1731	69	1799	46	4	1799	46	1.772	0.036
MPDZ1-111	MPDZ1_51	5.75	0.16	0.3478	0.0087	0.71054	2.875216	0.071922	0.57266	1923	32	41	1955	71	1946	49	1	1946	49	1.231	0.034
~~MPDZ1-027~~	~~MPDZ1_27~~	~~4.23~~	~~0.46~~	~~0.238~~	~~0.017~~	~~0.99599~~	~~4.201681~~	~~0.30012~~	~~-0.92051~~	~~1372~~	~~86~~	~~86~~	~~1210~~	~~130~~	~~2031~~	~~69~~	~~32~~	~~2031~~	~~69~~	3.07	0.12
MPDZ1-097	MPDZ1_37	9.78	0.28	0.44	0.0083	0.17681	2.272727	0.042872	0.4767	2351	22	37	1260	110	2469	51	5	2469	51	1.96	0.17
MPDZ1-062	MPDZ1_2	10.4	0.28	0.4572	0.01	0.85175	2.187227	0.04784	0.36489	2427	33	45	2445	90	2520	43	4	2520	43	2.183	0.044
MPDZ1-022	MPDZ1_22	13.85	0.61	0.4999	0.0095	0.83593	2.0004	0.038015	-0.48086	2613	25	41	2652	36	2820	57	7	2820	57	0.798	0.077

Table 4: U/Pb data from Sample: MP_DZ2

MPDZ2-066	MPDZ2_6	0.526	0.025	0.0672	0.0016	0.0563	0.0023	0.02078	0.00094	429	17	419.2	9.9	416	13	19	456	92	8	419.2	9.9	2.261	0.038
~~MPDZ2-119~~	~~MPDZ2_5~~	~~0.545~~	~~0.022~~	~~0.0687~~	~~0.0017~~	~~0.0572~~	~~0.0021~~	~~0.0219~~	~~0.0008~~	~~442~~	~~14~~	~~428.3~~	~~10~~	~~437.8~~	~~7.6~~	~~16~~	~~492~~	~~82~~	~~13~~	~~428.3~~	~~10~~	~~1.834~~	~~0.035~~
MPDZ2-030	MPDZ2_3	0.531	0.019	0.0704	0.0018	0.0548	0.0018	0.02236	0.00053	432	12	438.8	11	447	8	10	413	66	-6	438.8	11	2.632	0.048
~~MPDZ2-103~~	~~MPDZ2_4~~	~~0.614~~	~~0.027~~	~~0.0752~~	~~0.0025~~	~~0.0597~~	~~0.0017~~	~~0.02558~~	~~0.0011~~	~~485~~	~~17~~	~~467~~	~~15~~	~~510~~	~~14~~	~~21~~	~~591~~	~~61~~	~~21~~	~~467~~	~~15~~	~~2.49~~	~~0.15~~
MPDZ2-081	MPDZ2_2	0.694	0.024	0.0851	0.0014	0.0589	0.0017	0.02685	0.00096	535.3	14	526.3	8.1	535.4	7.7	19	571	68	8	526.3	8.1	1.604	0.045
MPDZ2-108	MPDZ2_4	0.718	0.027	0.0861	0.0023	0.0616	0.0018	0.0304	0.0013	549	16	532	14	605	17	25	659	61	19	532	14	2.34	0.12
~~MPDZ2-019~~	~~MPDZ2_1~~	~~0.82~~	~~0.051~~	~~0.0899~~	~~0.002~~	~~0.0677~~	~~0.0039~~	~~0.02874~~	~~0.00094~~	~~607~~	~~28~~	~~555.1~~	~~12~~	~~573~~	~~16~~	~~19~~	~~840~~	~~120~~	~~34~~	~~555.1~~	~~12~~	~~3.658~~	~~0.059~~
MPDZ2-093	MPDZ2_3	0.795	0.036	0.0937	0.0038	0.06124	0.0016	0.02568	0.001	593	21	577	23	512	13	21	647	55	11	577	23	2.013	0.039
MPDZ2-141	MPDZ2_2	0.803	0.022	0.0966	0.002	0.0607	0.0019	0.0298	0.00046	598.4	12	594	12	593.5	8.4	9	623	67	5	594	12	2.433	0.036
~~MPDZ2-035~~	~~MPDZ2_3~~	~~1.296~~	~~0.053~~	~~0.1042~~	~~0.0033~~	~~0.0908~~	~~0.0026~~	~~0.01447~~	~~0.00053~~	~~843~~	~~23~~	~~639~~	~~20~~	~~290.4~~	~~9.6~~	~~11~~	~~1441~~	~~53~~	~~56~~	~~639~~	~~20~~	~~3.782~~	~~0.092~~
~~MPDZ2-151~~	~~MPDZ2_3~~	~~1.716~~	~~0.034~~	~~0.1345~~	~~0.0022~~	~~0.0929~~	~~0.0022~~	~~0.02208~~	~~0.00051~~	~~1014.4~~	~~13~~	~~813~~	~~13~~	~~441.5~~	~~9.8~~	~~10~~	~~1484~~	~~46~~	~~45~~	~~813~~	~~13~~	~~4.321~~	~~0.071~~
~~MPDZ2-110~~	~~MPDZ2_5~~	~~2.26~~	~~0.33~~	~~0.1364~~	~~0.0096~~	~~0.123~~	~~0.012~~	~~0.0179~~	~~0.0054~~	~~1179~~	~~94~~	~~823~~	~~54~~	~~360~~	~~110~~	~~110~~	~~1960~~	~~150~~	~~58~~	~~823~~	~~54~~	~~1.906~~	~~0.03~~
~~MPDZ2-052~~	~~MPDZ2_5~~	~~1.566~~	~~0.049~~	~~0.1389~~	~~0.0031~~	~~0.0809~~	~~0.0028~~	~~0.02~~	~~0.0011~~	~~956~~	~~19~~	~~838~~	~~17~~	~~400~~	~~23~~	~~22~~	~~1216~~	~~66~~	~~31~~	~~838~~	~~17~~	~~3.404~~	~~0.058~~
MPDZ2-147	MPDZ2_2	1.398	0.038	0.1463	0.0033	0.0689	0.0019	0.0458	0.0019	888	16	880	19	905	37	37	895	58	2	880	19	5.586	0.081
~~MPDZ2-088~~	~~MPDZ2_2~~	~~1.533~~	~~0.077~~	~~0.1475~~	~~0.0067~~	~~0.07532~~	~~0.002~~	~~0.03282~~	~~0.0012~~	~~942~~	~~31~~	~~886~~	~~38~~	~~653~~	~~12~~	~~24~~	~~1076~~	~~52~~	~~18~~	~~886~~	~~38~~	~~3.32~~	~~0.049~~
~~MPDZ2-113~~	~~MPDZ2_5~~	~~1.878~~	~~0.1~~	~~0.1504~~	~~0.0063~~	~~0.0914~~	~~0.003~~	~~0.0194~~	~~0.0039~~	~~1083~~	~~27~~	~~903~~	~~36~~	~~388~~	~~77~~	~~77~~	~~1451~~	~~63~~	~~38~~	~~903~~	~~36~~	~~1.681~~	~~0.044~~
~~MPDZ2-129~~	~~MPDZ2_9~~	~~1.93~~	~~0.13~~	~~0.151~~	~~0.011~~	~~0.09199~~	~~0.0021~~	~~0.0196~~	~~0.0024~~	~~1086~~	~~46~~	~~904~~	~~59~~	~~392~~	~~48~~	~~47~~	~~1473~~	~~49~~	~~39~~	~~904~~	~~59~~	~~2.848~~	~~0.057~~
MPDZ2-121	MPDZ2_1	1.483	0.048	0.151	0.0049	0.0716	0.0028	0.0474	0.0016	923	20	906	28	936	30	30	967	82	6	906	28	3.17	0.12
~~MPDZ2-136~~	~~MPDZ2_1~~	~~1.91~~	~~0.15~~	~~0.156~~	~~0.012~~	~~0.0884~~	~~0.0022~~	~~0.0288~~	~~0.0024~~	~~1094~~	~~46~~	~~931~~	~~70~~	~~574~~	~~47~~	~~48~~	~~1391~~	~~46~~	~~33~~	~~931~~	~~70~~	~~2.443~~	~~0.065~~
MPDZ2-095	MPDZ2_3	1.497	0.054	0.1558	0.0034	0.0705	0.0022	0.04762	0.0017	929	22	933	19	940	12	32	941	62	1	933	19	1.804	0.083
MPDZ2-107	MPDZ2_4	1.546	0.052	0.1602	0.0031	0.0705	0.002	0.04999	0.0018	948	21	958	18	986	17	35	940	58	-2	958	18	3.003	0.084
MPDZ2-097	MPDZ2_3	1.68	0.057	0.1675	0.0031	0.0729	0.0023	0.0516	0.0026	1000	22	999	17	1016	39	50	1009	64	1	999	17	5.37	0.23
MPDZ2-112	MPDZ2_5	1.669	0.056	0.1678	0.0035	0.0728	0.0023	0.04563	0.0016	997	22	1000	20	902	11	30	1005	64	0	1000	20	3.241	0.084
MPDZ2-118	MPDZ2_5	1.73	0.058	0.1684	0.0031	0.0743	0.0022	0.0519	0.0024	1019	22	1003	17	1023	34	47	1047	61	4	1003	17	2.74	0.04
~~MPDZ2-073~~	~~MPDZ2_1~~	~~2.14~~	~~0.18~~	~~0.171~~	~~0.014~~	~~0.0903~~	~~0.0023~~	~~0.0163~~	~~0.0018~~	~~1152~~	~~66~~	~~1015~~	~~81~~	~~327~~	~~34~~	~~35~~	~~1432~~	~~47~~	~~29~~	~~1015~~	~~81~~	~~1.13~~	~~0.019~~
MPDZ2-061	MPDZ2_1	1.775	0.066	0.1713	0.0044	0.0737	0.003	0.0549	0.0024	1036	25	1019	25	1079	30	46	1025	82	1	1019	25	3.161	0.045
MPDZ2-105	MPDZ2_4	1.72	0.062	0.1723	0.0037	0.073	0.0024	0.0542	0.0022	1016	23	1025	20	1068	27	43	1010	66	-1	1025	20	2.268	0.03
MPDZ2-015	MPDZ2_1	1.733	0.058	0.1734	0.0042	0.07383	0.0021	0.0528	0.0013	1020	22	1030	23	1041	21	25	1036	56	1	1030	23	2.55	0.14
MPDZ2-140	MPDZ2_2	1.757	0.049	0.1733	0.0034	0.0734	0.0018	0.05394	0.00092	1029	18	1030	19	1062	17	18	1024	49	-1	1030	19	0.933	0.031
MPDZ2-071	MPDZ2_1	1.8	0.056	0.1745	0.0042	0.075	0.0021	0.0536	0.0028	1045.1	21	1037	23	1055	42	54	1067	57	3	1037	23	2.39	0.17
MPDZ2-085	MPDZ2_2	1.724	0.061	0.1746	0.0032	0.07259	0.0019	0.0538	0.0019	1017	23	1037	17	1059	17	37	1012	68	-2	1037	17	1.038	0.035
MPDZ2-014	MPDZ2_1	1.807	0.053	0.1771	0.0038	0.07375	0.002	0.05563	0.001	1051	18	1051	21	1094	12	19	1034	55	-2	1051	21	1.417	0.045
~~MPDZ2-096~~	~~MPDZ2_3~~	~~2.108~~	~~0.097~~	~~0.1808~~	~~0.0035~~	~~0.084~~	~~0.0034~~	~~0.0543~~	~~0.0032~~	~~1150~~	~~32~~	~~1071~~	~~19~~	~~1068~~	~~52~~	~~61~~	~~1287~~	~~78~~	~~17~~	~~1071~~	~~19~~	~~2.749~~	~~0.036~~
MPDZ2-051	MPDZ2_5	1.98	0.14	0.1827	0.0096	0.0812	0.0023	0.055	0.01	1101	52	1081	53	1080	200	200	1226	56	12	1081	53	2.644	0.083
MPDZ2-034	MPDZ2_3	1.965	0.073	0.1843	0.0048	0.0783	0.0025	0.0564	0.0016	1107	23	1090	26	1108	26	30	1151	63	5	1090	26	3.221	0.076
MPDZ2-100	MPDZ2_4	2.02	0.068	0.1883	0.0037	0.0779	0.0023	0.06041	0.0021	1122	23	1112	20	1186	15	40	1153	54	4	1112	20	6.322	0.086
~~MPDZ2-007~~	~~MPDZ2_7~~	~~2.388~~	~~0.061~~	~~0.1891~~	~~0.0037~~	~~0.0917~~	~~0.0026~~	~~0.0425~~	~~0.0024~~	~~1241~~	~~20~~	~~1117~~	~~20~~	~~841~~	~~45~~	~~47~~	~~1461~~	~~52~~	~~24~~	~~1117~~	~~20~~	~~3.576~~	~~0.053~~
MPDZ2-122	MPDZ2_2	2.08	0.045	0.1903	0.0046	0.0787	0.0019	0.0595	0.001	1142	15	1123	25	1168	19	20	1163	48	3	1123	25	7.18	0.12
MPDZ2-006	MPDZ2_6	2.081	0.061	0.1898	0.0047	0.0789	0.0026	0.05907	0.0012	1142	20	1125	27	1160	17	23	1166	64	4	1125	27	15.69	0.44
MPDZ2-043	MPDZ2_4	2.011	0.078	0.1919	0.0047	0.0774	0.003	0.0606	0.0025	1118	26	1131	26	1190	45	47	1126	76	0	1131	26	-70	150
MPDZ2-082	MPDZ2_2	2.068	0.073	0.1956	0.0054	0.0765	0.0023	0.0567	0.0023	1138	24	1151	30	1114	26	44	1117	66	-3	1151	30	-10.92	0.47
MPDZ2-084	MPDZ2_2	2.148	0.073	0.1962	0.0037	0.079	0.0023	0.0591	0.0024	1164	24	1155	20	1161	29	46	1171	57	1	1155	20	-8.65	0.31
MPDZ2-067	MPDZ2_7	2.335	0.11	0.197	0.0081	0.08496	0.0022	0.05636	0.0021	1227	32	1158	44	1108	16	40	1314	49	12	1158	44	-2.041	0.075
~~MPDZ2-131~~	~~MPDZ2_1~~	~~2.89~~	~~0.21~~	~~0.198~~	~~0.013~~	~~0.1089~~	~~0.0026~~	~~0.0354~~	~~0.0021~~	~~1397~~	~~55~~	~~1165~~	~~72~~	~~703~~	~~41~~	~~41~~	~~1780~~	~~44~~	~~35~~	~~1165~~	~~72~~	~~-1.994~~	~~0.046~~
MPDZ2-074	MPDZ2_1	2.152	0.081	0.1985	0.0044	0.078	0.0022	0.0579	0.0023	1165	27	1167	24	1137	23	43	1146	54	-2	1167	24	-3.02	0.11
~~MPDZ2-133~~	~~MPDZ2_1~~	~~2.479~~	~~0.079~~	~~0.1989~~	~~0.0055~~	~~0.08995~~	~~0.002~~	~~0.0227~~	~~0.0013~~	~~1270~~	~~22~~	~~1169~~	~~30~~	~~454~~	~~26~~	~~26~~	~~1424~~	~~43~~	~~18~~	~~1169~~	~~30~~	~~-2.876~~	~~0.098~~
MPDZ2-048	MPDZ2_4	2.155	0.062	0.1991	0.0048	0.0787	0.0023	0.0641	0.0014	1166	20	1170	26	1255	23	27	1164	57	-1	1170	26	-1.241	0.016
~~MPDZ2-080~~	~~MPDZ2_2~~	~~2.6~~	~~0.14~~	~~0.2047~~	~~0.0099~~	~~0.09245~~	~~0.0024~~	~~0.0455~~	~~0.0036~~	~~1299~~	~~40~~	~~1199~~	~~53~~	~~900~~	~~65~~	~~70~~	~~1476~~	~~48~~	~~19~~	~~1199~~	~~53~~	~~-0.65~~	~~0.11~~
~~MPDZ2-009~~	~~MPDZ2_9~~	~~2.577~~	~~0.089~~	~~0.206~~	~~0.0064~~	~~0.09026~~	~~0.0024~~	~~0.0437~~	~~0.0035~~	~~1293~~	~~25~~	~~1207~~	~~34~~	~~864~~	~~66~~	~~68~~	~~1431~~	~~50~~	~~16~~	~~1207~~	~~34~~	~~-0.175~~	~~0.015~~
MPDZ2-148	MPDZ2_2	2.293	0.057	0.2062	0.0033	0.0811	0.0019	0.0619	0.0014	1210	18	1208	18	1215	25	26	1222	47	1	1208	18	-0.595	0.031
~~MPDZ2-094~~	~~MPDZ2_3~~	~~2.665~~	~~0.089~~	~~0.2069~~	~~0.0051~~	~~0.0928~~	~~0.0025~~	~~0.0387~~	~~0.0019~~	~~1322~~	~~23~~	~~1212~~	~~27~~	~~767~~	~~28~~	~~37~~	~~1484~~	~~51~~	~~18~~	~~1212~~	~~27~~	~~-0.2476~~	~~0.0082~~
MPDZ2-062	MPDZ2_2	2.38	0.092	0.2081	0.0051	0.082	0.0024	0.0624	0.0024	1240	26	1219	27	1223	24	46	1245	56	2	1219	27	-0.434	0.041
~~MPDZ2-126~~	~~MPDZ2_6~~	~~3.07~~	~~0.11~~	~~0.2124~~	~~0.0066~~	~~0.10499~~	~~0.0023~~	~~0.0483~~	~~0.0017~~	~~1424~~	~~29~~	~~1241~~	~~35~~	~~953~~	~~32~~	~~32~~	~~1714~~	~~40~~	~~28~~	~~1241~~	~~35~~	~~-0.3555~~	~~0.0073~~
MPDZ2-008	MPDZ2_8	2.737	0.096	0.2195	0.0067	0.0901	0.0025	0.0442	0.0015	1338	26	1279	35	875	27	29	1427	52	10	1279	35	-0.3145	0.0037
MPDZ2-023	MPDZ2_2	2.755	0.075	0.2215	0.0047	0.09075	0.0025	0.04	0.0015	1343	20	1290	25	792	26	28	1441	51	10	1290	25	-0.3374	0.007
MPDZ2-086	MPDZ2_2	2.81	0.087	0.2346	0.0047	0.08692	0.0022	0.0707	0.0026	1358	23	1358	25	1380	25	50	1358	48	0	1358	48	2.394	0.038
MPDZ2-123	MPDZ2_3	2.784	0.077	0.2315	0.0044	0.0876	0.0022	0.0701	0.0017	1350	21	1342	23	1369	31	31	1373	49	2	1373	49	1.225	0.023
MPDZ2-137	MPDZ2_1	2.881	0.068	0.2369	0.004	0.0881	0.0022	0.0713	0.0015	1377	18	1370	21	1391	28	29	1383	47	1	1383	47	1.773	0.07
MPDZ2-036	MPDZ2_3	2.769	0.074	0.2308	0.0044	0.08811	0.0024	0.072	0.0015	1347	20	1339	23	1405	22	29	1384	52	3	1384	52	-0.3327	0.0047

~~MPDZ2-126~~	~~MPDZ2_6~~	~~3.07~~	~~0.11~~	~~0.2124~~	~~0.0066~~	~~0.10499~~	~~0.0023~~	~~0.0483~~	~~0.0017~~	~~1424~~	~~29~~	~~1241~~	~~35~~	~~953~~	~~32~~	~~32~~	~~1714~~	~~40~~	~~28~~	~~1241~~	~~35~~	~~-0.3555~~	~~0.0073~~
MPDZ2-008	MPDZ2_8	2.737	0.096	0.2195	0.0067	0.0901	0.0025	0.0442	0.0015	1338	26	1279	35	875	27	29	1427	52	10	1279	35	-0.3145	0.0037
MPDZ2-023	MPDZ2_23	2.755	0.075	0.2215	0.0047	0.09075	0.0025	0.04	0.0015	1343	20	1290	25	792	26	28	1441	51	10	1290	25	-0.3374	0.007
MPDZ2-086	MPDZ2_26	2.81	0.087	0.2346	0.0047	0.08692	0.0022	0.0707	0.0026	1358	23	1358	25	1380	25	50	1358	48	0	1358	48	2.394	0.038
MPDZ2-123	MPDZ2_3	2.784	0.077	0.2315	0.0044	0.0876	0.0022	0.0701	0.0017	1350	21	1342	23	1369	31	31	1373	49	2	1373	49	1.225	0.023
MPDZ2-137	MPDZ2_17	2.881	0.068	0.2369	0.004	0.0881	0.0022	0.0713	0.0015	1377	18	1370	21	1391	28	29	1383	47	1	1383	47	1.773	0.07
MPDZ2-036	MPDZ2_36	2.769	0.074	0.2308	0.0044	0.08811	0.0024	0.072	0.0015	1347	20	1339	23	1405	22	29	1384	52	3	1384	52	-0.3327	0.0047
MPDZ2-063	MPDZ2_3	2.978	0.096	0.2436	0.0043	0.0881	0.0023	0.0725	0.0027	1402	25	1405	22	1415	21	50	1384	50	-2	1384	50	2.188	0.093
MPDZ2-016	MPDZ2_16	3.086	0.082	0.2501	0.0046	0.08912	0.0024	0.0734	0.0015	1429	20	1439	24	1431	20	28	1406	51	-2	1406	51	2.665	0.039
MPDZ2-031	MPDZ2_31	3.033	0.09	0.2485	0.0055	0.0896	0.0026	0.0713	0.0039	1416	22	1431	28	1391	69	74	1416	54	-1	1416	54	0.884	0.036
MPDZ2-050	MPDZ2_50	3.062	0.081	0.2487	0.0053	0.0896	0.0025	0.07457	0.0013	1423	20	1432	27	1454	18	25	1416	52	-1	1416	52	2.223	0.05
MPDZ2-022	MPDZ2_22	3.015	0.086	0.2431	0.0055	0.08968	0.0024	0.0744	0.0018	1411	22	1403	28	1451	27	34	1418	50	1	1418	50	2.998	0.065
MPDZ2-127	MPDZ2_7	3.111	0.071	0.2512	0.0043	0.08977	0.002	0.07436	0.00076	1435	18	1445	22	1450	13	14	1420	44	-2	1420	44	4.59	0.33
MPDZ2-077	MPDZ2_17	2.91	0.15	0.2355	0.0098	0.0898	0.0024	0.0601	0.0044	1390	37	1362	52	1178	76	85	1421	50	4	1421	50	1.828	0.024
MPDZ2-143	MPDZ2_23	2.882	0.066	0.2321	0.0039	0.0899	0.0021	0.0504	0.0011	1377	17	1345	20	993	20	21	1422	44	5	1422	44	2.595	0.075
MPDZ2-045	MPDZ2_45	3.039	0.082	0.2466	0.0051	0.08992	0.0024	0.0771	0.0016	1417	20	1421	26	1502	23	30	1423	50	0	1423	50	3.69	0.1
MPDZ2-079	MPDZ2_19	2.958	0.12	0.2389	0.0079	0.08995	0.0023	0.0656	0.0025	1396	33	1380	42	1285	23	47	1424	49	3	1424	49	2.362	0.074
MPDZ2-138	MPDZ2_18	3.011	0.057	0.2427	0.0029	0.08993	0.0019	0.031	0.0022	1410.4	14	1401	15	617	43	44	1424	41	2	1424	41	2.727	0.046
MPDZ2-053	MPDZ2_53	2.997	0.1	0.2434	0.0073	0.09001	0.0025	0.0646	0.0047	1406	26	1404	38	1264	92	90	1425	52	1	1425	52	1.417	0.074
MPDZ2-092	MPDZ2_32	3.103	0.12	0.2484	0.006	0.09	0.0022	0.0743	0.0033	1433	30	1430	31	1448	44	63	1425	48	0	1425	48	1.478	0.075
MPDZ2-076	MPDZ2_16	3.01	0.1	0.2435	0.0054	0.0901	0.0025	0.0632	0.0027	1410	26	1405	28	1238	33	51	1427	52	2	1427	52	1.9	0.072
MPDZ2-027	MPDZ2_27	3.075	0.081	0.2472	0.0058	0.09009	0.0024	0.077	0.0016	1426.2	20	1424	30	1499	20	29	1427	50	0	1427	50	2.704	0.048
MPDZ2-033	MPDZ2_33	3.035	0.096	0.2486	0.0055	0.0901	0.0025	0.0789	0.0022	1416	24	1431	28	1534	35	41	1427	53	0	1427	53	3.099	0.052
MPDZ2-132	MPDZ2_12	3.064	0.066	0.2453	0.0036	0.09014	0.0019	0.0707	0.0011	1423	17	1414	19	1381	20	21	1428	41	1	1428	41	1.865	0.036
MPDZ2-111	MPDZ2_51	3.007	0.094	0.246	0.0036	0.0903	0.0025	0.0753	0.0028	1409	24	1418	19	1468	28	53	1431	52	1	1431	52	4.47	0.078
MPDZ2-142	MPDZ2_22	3.025	0.075	0.2434	0.0035	0.0904	0.0022	0.0704	0.0014	1413	19	1404	18	1376	26	27	1432	45	2	1432	45	2.656	0.085
MPDZ2-012	MPDZ2_12	3.043	0.084	0.2438	0.0047	0.09038	0.0024	0.0744	0.0015	1418	21	1406	25	1450	20	28	1433	51	2	1433	51	0.953	0.021
MPDZ2-117	MPDZ2_57	3.041	0.093	0.2461	0.0041	0.09038	0.0023	0.06251	0.0022	1417.6	24	1418	22	1226	17	42	1433	49	1	1433	49	1.612	0.023
MPDZ2-046	MPDZ2_46	2.972	0.082	0.238	0.0054	0.0904	0.0025	0.0575	0.0014	1400	21	1376	28	1129	22	26	1434	49	4	1434	49	1.75	0.074
MPDZ2-115	MPDZ2_55	3.127	0.1	0.252	0.0047	0.09042	0.0022	0.07607	0.0025	1439	26	1449	24	1481.9	9.3	47	1434	46	-1	1434	46	3.839	0.074
MPDZ2-069	MPDZ2_9	3.004	0.097	0.2391	0.0052	0.0905	0.0025	0.0626	0.0028	1408	25	1382	27	1227	34	52	1435	51	4	1435	51	2.549	0.035
MPDZ2-004	MPDZ2_4	3.016	0.088	0.2432	0.0046	0.0902	0.0027	0.07342	0.0013	1411	22	1403	24	1432	15	24	1436	54	2	1436	54	0.846	0.056
MPDZ2-020	MPDZ2_20	3.15	0.1	0.2519	0.0065	0.09052	0.0025	0.0758	0.0016	1444	25	1448	34	1477	23	31	1436	52	-1	1436	52	1.2	0.06
MPDZ2-116	MPDZ2_56	3.107	0.11	0.2526	0.0065	0.0905	0.0024	0.077	0.0028	1434	27	1452	34	1500	23	52	1436	51	-1	1436	51	2.25	0.036
MPDZ2-010	MPDZ2_10	3.039	0.098	0.2438	0.0073	0.09058	0.0024	0.0754	0.0018	1417	24	1406	38	1470	28	34	1437	50	2	1437	50	1.798	0.064
MPDZ2-058	MPDZ2_58	3.149	0.09	0.2529	0.0048	0.0907	0.0027	0.073	0.0015	1444	22	1454	25	1423	21	28	1440	55	-1	1440	55	4.255	0.083
MPDZ2-130	MPDZ2_10	2.872	0.079	0.2274	0.0047	0.091	0.0022	0.0453	0.0026	1374	21	1321	25	896	51	51	1445	46	9	1445	46	-0.2803	0.0047
MPDZ2-068	MPDZ2_8	3.054	0.1	0.2435	0.0052	0.0911	0.0025	0.07241	0.0025	1421	25	1405	27	1413	15	48	1447	51	3	1447	51	0.954	0.023
MPDZ2-024	MPDZ2_24	3.056	0.087	0.2411	0.006	0.09137	0.0025	0.0764	0.0016	1421	21	1398	33	1487	21	29	1454	51	4	1454	51	7.33	0.15
MPDZ2-099	MPDZ2_39	3.98	0.15	0.2933	0.0068	0.099	0.0028	0.0868	0.0031	1629	31	1658	34	1682	27	58	1603	53	-3	1603	53	1.901	0.038
MPDZ2-044	MPDZ2_44	3.543	0.11	0.2587	0.0056	0.09993	0.0027	0.061	0.0015	1536	24	1483	28	1197	24	28	1622	50	9	1622	50	1.36	0.13
MPDZ2-049	MPDZ2_49	3.961	0.12	0.2911	0.0073	0.1	0.0029	0.0903	0.0021	1630	26	1647	37	1748	35	40	1624	52	-1	1624	52	2.53	0.037
MPDZ2-032	MPDZ2_32	3.795	0.11	0.2777	0.0056	0.10029	0.0027	0.0864	0.0017	1591	22	1580	28	1675	22	32	1633	54	3	1633	54	0.78	0.01
MPDZ2-124	MPDZ2_4	3.953	0.11	0.2847	0.0076	0.1007	0.0026	0.0844	0.0015	1624	24	1615	38	1638	28	29	1636	48	1	1636	48	2.31	0.38
MPDZ2-028	MPDZ2_28	3.744	0.12	0.2732	0.0075	0.1008	0.0032	0.078	0.002	1584	23	1557	38	1517	30	38	1638	57	5	1638	57	3.46	0.14
MPDZ2-078	MPDZ2_18	3.733	0.11	0.2697	0.0047	0.1011	0.0026	0.0772	0.0027	1578.2	25	1539	24	1503	19	51	1644	48	6	1644	48	3.662	0.067
MPDZ2-011	MPDZ2_11	3.922	0.13	0.284	0.0075	0.1009	0.0033	0.0847	0.0026	1622	28	1611	38	1644	42	48	1647	56	2	1647	56	1.362	0.066
MPDZ2-089	MPDZ2_29	3.47	0.14	0.2469	0.0087	0.1025	0.0031	0.0533	0.0029	1519	34	1422	45	1049	46	57	1667	54	15	1667	54	2.589	0.037
MPDZ2-135	MPDZ2_15	3.73	0.2	0.266	0.011	0.1024	0.0023	0.0763	0.005	1573	45	1521	55	1515	93	94	1668	42	9	1668	42	1.924	0.067
MPDZ2-018	MPDZ2_18	4.133	0.11	0.2898	0.0057	0.103	0.0028	0.0855	0.0021	1661	21	1641	29	1658	31	39	1679	51	2	1679	51	2.658	0.033
MPDZ2-064	MPDZ2_4	4.281	0.14	0.3004	0.0057	0.1029	0.0028	0.0878	0.0032	1689	28	1693	28	1700	25	60	1683	54	-1	1683	54	1.434	0.023
MPDZ2-101	MPDZ2_41	4.24	0.14	0.3004	0.0069	0.1034	0.0027	0.0891	0.0035	1681	27	1693	34	1725	39	65	1684	48	-1	1684	48	2.828	0.057
MPDZ2-145	MPDZ2_25	4.224	0.1	0.2938	0.0068	0.1036	0.0027	0.0863	0.0022	1678	20	1660	34	1672	41	42	1688	48	2	1688	48	2.45	0.031
MPDZ2-120	MPDZ2_60	4.133	0.15	0.2868	0.0072	0.1037	0.0027	0.0621	0.0066	1660	30	1625	36	1220	120	130	1690	49	4	1690	49	1.969	0.075
MPDZ2-070	MPDZ2_10	4.334	0.15	0.3007	0.0058	0.1037	0.0031	0.0865	0.0036	1699	29	1695	29	1676	41	67	1690	55	0	1690	55	3.169	0.057
MPDZ2-106	MPDZ2_46	4.26	0.17	0.3027	0.0078	0.1038	0.0029	0.0899	0.0032	1684	33	1714	39	1740	26	59	1692	51	-1	1692	51	0.921	0.013
MPDZ2-059	MPDZ2_59	4.411	0.13	0.3065	0.0075	0.1039	0.003	0.0854	0.0025	1714	24	1723	37	1657	40	46	1694	51	-2	1694	51	1.371	0.096
MPDZ2-013	MPDZ2_13	3.965	0.12	0.2767	0.0057	0.1036	0.0031	0.0609	0.003	1626	24	1575	29	1194	53	56	1695	60	7	1695	60	3.524	0.051
MPDZ2-002	MPDZ2_2	3.94	0.13	0.274	0.0065	0.1041	0.0029	0.0721	0.0019	1621	26	1561	33	1406	30	36	1698	52	8	1698	52	1.637	0.032

MPDZ2-017	MPDZ2_17	4.403	0.13	0.3054	0.0073	0.1043	0.0032	0.0885	0.0022	1712	24	1718	36	1715	34	42	1700	55	-1	1700	55	1.059	0.093
~~MPDZ2-149~~	~~MPDZ2_29~~	~~3.348~~	~~0.065~~	~~0.2325~~	~~0.0032~~	~~0.1044~~	~~0.0024~~	~~0.0296~~	~~0.0011~~	~~1492.3~~	~~15~~	~~1347~~	~~17~~	~~590~~	~~22~~	~~22~~	~~1702~~	~~42~~	~~21~~	~~1702~~	~~42~~	~~1.796~~	~~0.046~~
MPDZ2-083	MPDZ2_23	4.285	0.14	0.301	0.0072	0.1044	0.0028	0.0903	0.0039	1690	26	1696	36	1747	47	71	1703	50	0	1703	50	1.037	0.029
MPDZ2-042	MPDZ2_42	4.116	0.13	0.2894	0.0059	0.1046	0.0034	0.0877	0.0047	1662	21	1639	30	1699	84	86	1705	58	4	1705	58	0.89	0.18
MPDZ2-040	MPDZ2_40	4.41	0.15	0.3095	0.0073	0.1047	0.0029	0.0939	0.0019	1718	26	1738	36	1814	26	35	1709	49	-2	1709	49	1.658	0.027
MPDZ2-057	MPDZ2_57	4.3	0.13	0.2994	0.0062	0.1048	0.0031	0.09007	0.0016	1693	25	1688	31	1743	18	29	1710	52	1	1710	52	1.501	0.017
MPDZ2-128	MPDZ2_8	3.958	0.08	0.2724	0.0031	0.10505	0.0023	0.0638	0.0014	1625	17	1553	16	1249	26	27	1715	40	9	1715	40	1.375	0.071
MPDZ2-060	MPDZ2_60	4.411	0.12	0.3051	0.0061	0.1052	0.0028	0.0893	0.0016	1714	22	1717	30	1729	21	30	1718	50	0	1718	50	1.315	0.067
MPDZ2-109	MPDZ2_49	4.387	0.13	0.3046	0.0048	0.10554	0.0027	0.0885	0.0033	1709.7	25	1714	24	1714	32	61	1723	46	1	1723	46	2.69	0.047
MPDZ2-001	MPDZ2_1	4.399	0.12	0.3028	0.0062	0.1058	0.0031	0.089	0.0023	1712	22	1705	31	1723	36	43	1728	53	1	1728	53	4.27	0.17
MPDZ2-056	MPDZ2_56	4.5	0.14	0.3092	0.0071	0.10605	0.0029	0.09062	0.0016	1730	26	1736	35	1753	18	29	1732	49	0	1732	49	0.886	0.042
MPDZ2-029	MPDZ2_29	4.44	0.13	0.3054	0.006	0.10611	0.0028	0.093	0.0017	1719	23	1718	30	1798	20	32	1733	48	1	1733	48	1.399	0.07
MPDZ2-150	MPDZ2_30	4.633	0.11	0.3136	0.0064	0.1063	0.0024	0.094	0.0019	1755	20	1758	31	1817	34	35	1736	41	-1	1736	41	1.994	0.05
MPDZ2-075	MPDZ2_15	4.029	0.13	0.2732	0.0052	0.10648	0.0027	0.0348	0.0019	1640	26	1557	27	692	29	37	1740	45	11	1740	45	1.252	0.03
MPDZ2-087	MPDZ2_27	4.489	0.15	0.3072	0.0064	0.1069	0.0028	0.0915	0.0034	1728	29	1727	32	1770	31	63	1747	47	1	1747	47	2.727	0.044
MPDZ2-021	MPDZ2_21	4.25	0.15	0.286	0.0095	0.1075	0.0029	0.0774	0.0028	1683	28	1621	48	1506	47	52	1757	49	8	1757	49	0.902	0.094
MPDZ2-146	MPDZ2_26	5	1.1	0.3	0.0099	0.1088	0.0073	0.112	0.034	1715	58	1691	48	2100	560	550	1760	110	4	1760	110	1.54	0.12
MPDZ2-090	MPDZ2_30	4.727	0.14	0.3218	0.0064	0.10831	0.0027	0.095	0.0034	1775	30	1798	31	1834	28	63	1771	45	-2	1771	45	7.39	0.31
MPDZ2-065	MPDZ2_5	4.43	0.19	0.2942	0.0089	0.109	0.0029	0.0723	0.0048	1715	36	1662	44	1411	78	91	1782	47	7	1782	47	2.96	0.11
MPDZ2-038	MPDZ2_38	4.751	0.14	0.3193	0.0075	0.1093	0.0031	0.0983	0.0024	1776	24	1786	37	1894	37	45	1787	51	0	1787	51	2.777	0.047
~~MPDZ2-144~~	~~MPDZ2_24~~	~~3.57~~	~~0.29~~	~~0.232~~	~~0.017~~	~~0.1095~~	~~0.0026~~	~~0.0197~~	~~0.0019~~	~~1532~~	~~66~~	~~1360~~	~~100~~	~~394~~	~~38~~	~~38~~	~~1790~~	~~43~~	~~24~~	~~1790~~	~~43~~	~~2.113~~	~~0.072~~
MPDZ2-125	MPDZ2_5	4.83	0.14	0.3163	0.0081	0.1097	0.0025	0.0939	0.0017	1794	24	1771	40	1814	30	31	1794	41	1	1794	41	1.2	0.11
MPDZ2-072	MPDZ2_12	5.103	0.17	0.3287	0.0067	0.1127	0.0031	0.0958	0.0036	1836	28	1832	33	1849	31	67	1842	50	1	1842	50	0.9005	0.0087
MPDZ2-037	MPDZ2_37	5.137	0.15	0.3301	0.007	0.1137	0.0031	0.0948	0.0031	1842	24	1845	31	1830	52	58	1858	49	1	1858	49	0.837	0.069
MPDZ2-091	MPDZ2_31	5.41	0.18	0.3425	0.0074	0.1145	0.003	0.0983	0.0036	1886	30	1898	36	1894	34	67	1871	47	-1	1871	47	0.832	0.014
MPDZ2-098	MPDZ2_38	4.57	0.24	0.288	0.013	0.1147	0.0029	0.0435	0.0051	1740	47	1628	67	860	98	99	1875	45	13	1875	45	0.951	0.013
MPDZ2-134	MPDZ2_14	9.8	0.28	0.4421	0.0093	0.161	0.0036	0.1078	0.0042	2420	28	2360	42	2069	75	76	2465	37	4	2465	37	2.114	0.024
MPDZ2-039	MPDZ2_39	10.83	0.28	0.4658	0.0097	0.1705	0.0047	0.1321	0.0026	2508	24	2465	43	2508	33	46	2568	39	4	2568	39	1.79	0.12
MPDZ2-104	MPDZ2_44	12.27	0.39	0.5048	0.01	0.1774	0.0049	0.1434	0.0051	2625	31	2634	44	2709	40	90	2628	46	0	2628	46	2.026	0.069
~~MPDZ2-054~~	~~MPDZ2_54~~	~~9.04~~	~~0.4~~	~~0.368~~	~~0.015~~	~~0.1786~~	~~0.0047~~	~~0.1144~~	~~0.0021~~	~~2339~~	~~40~~	~~2020~~	~~70~~	~~2189~~	~~28~~	~~39~~	~~2639~~	~~43~~	~~23~~	~~2639~~	~~43~~	~~2.159~~	~~0.05~~
MPDZ2-139	MPDZ2_19	13.23	0.35	0.5202	0.0097	0.1837	0.0041	0.1414	0.0016	2695	25	2699	41	2673	25	28	2690	39	0	2690	39	0.858	0.029
MPDZ2-055	MPDZ2_55	13.12	0.36	0.5186	0.012	0.1847	0.005	0.1495	0.0029	2688	25	2693	49	2816	38	51	2695	43	0	2695	43	3.434	0.07
MPDZ2-005	MPDZ2_5	13.55	0.4	0.515	0.012	0.191	0.0052	0.1367	0.0029	2722	29	2676	53	2590	38	51	2750	44	3	2750	44	2.787	0.06
MPDZ2-003	MPDZ2_3	12.64	0.34	0.4799	0.0091	0.1911	0.005	0.1334	0.0031	2652	25	2526	39	2530	40	51	2751	43	8	2751	43	2.959	0.049
MPDZ2-047	MPDZ2_47	17.01	0.46	0.5806	0.011	0.2127	0.0056	0.1635	0.0035	2935	25	2951	46	3060	50	61	2926	42	-1	2926	42	3.053	0.057
MPDZ2-041	MPDZ2_41	17.87	0.51	0.591	0.014	0.2207	0.0058	0.1612	0.0038	2987	24	3005	53	3020	54	66	2986	42	-1	2986	42	1.213	0.018

APPENDIX B: CATHODOLUMINESCENCE IMAGES OF ANALYZED SAMPLES

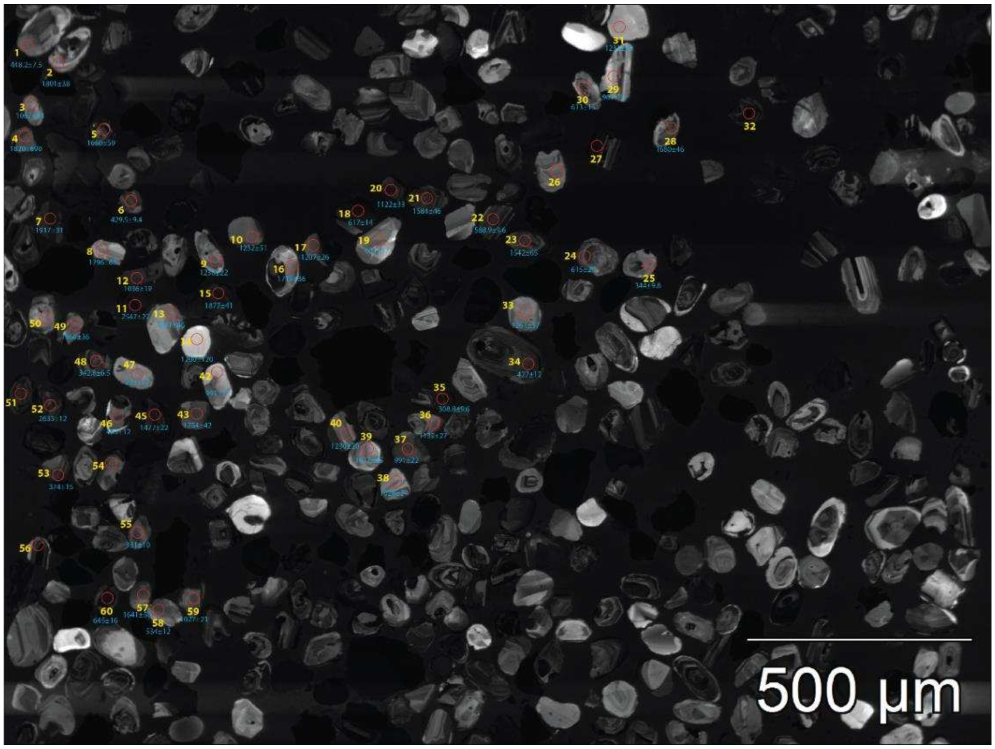

Image: CL image with spot numbers 1-60 and their final ages for OC_2.8_DZ1 (Lower Ingleside)

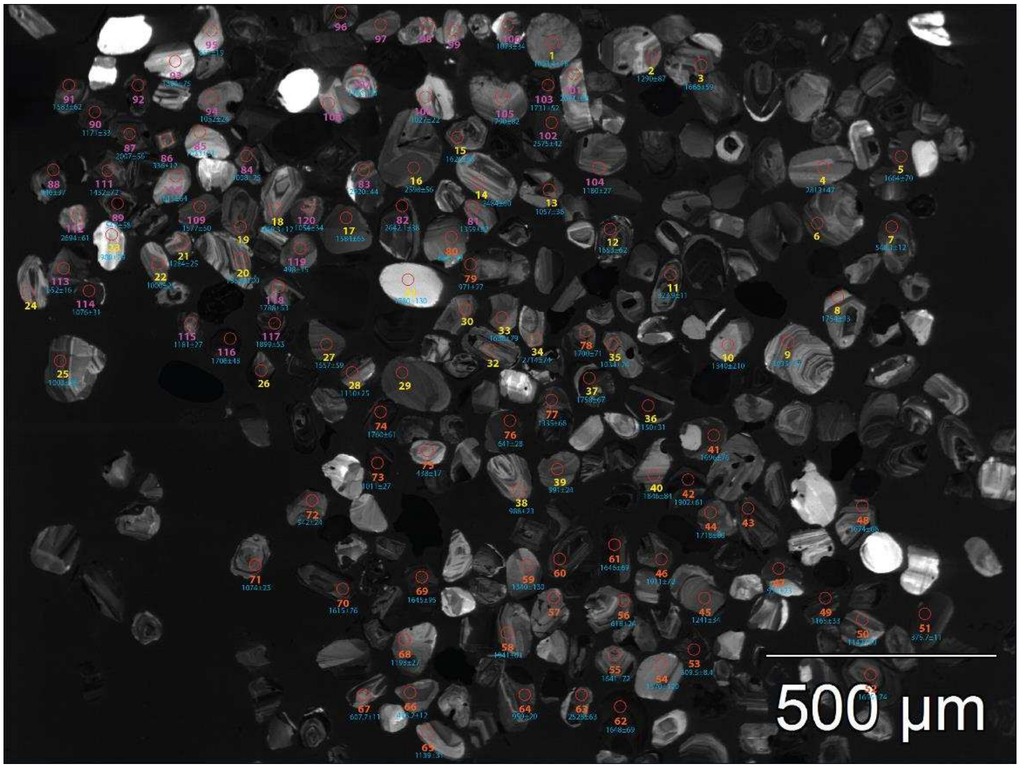

Image: CL image with spot numbers 1-120 and their final ages for OC_56_DZ2 (Upper Ingleside)

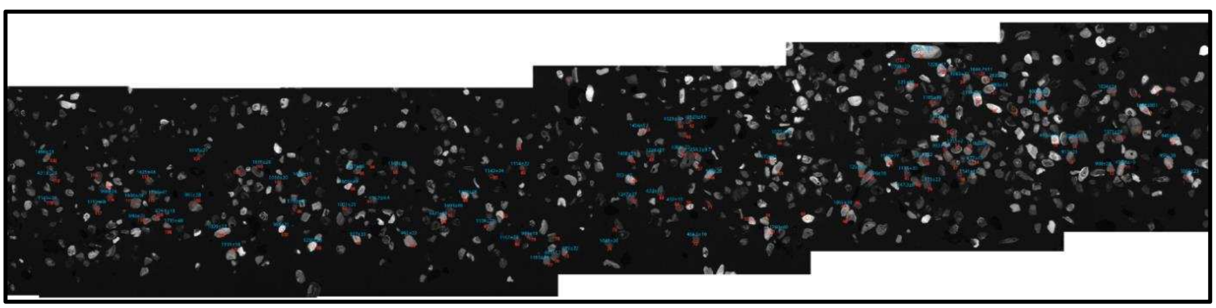

Image: CL image with spot numbers 1-120 and their final ages for MP_DZ1 (Molas)

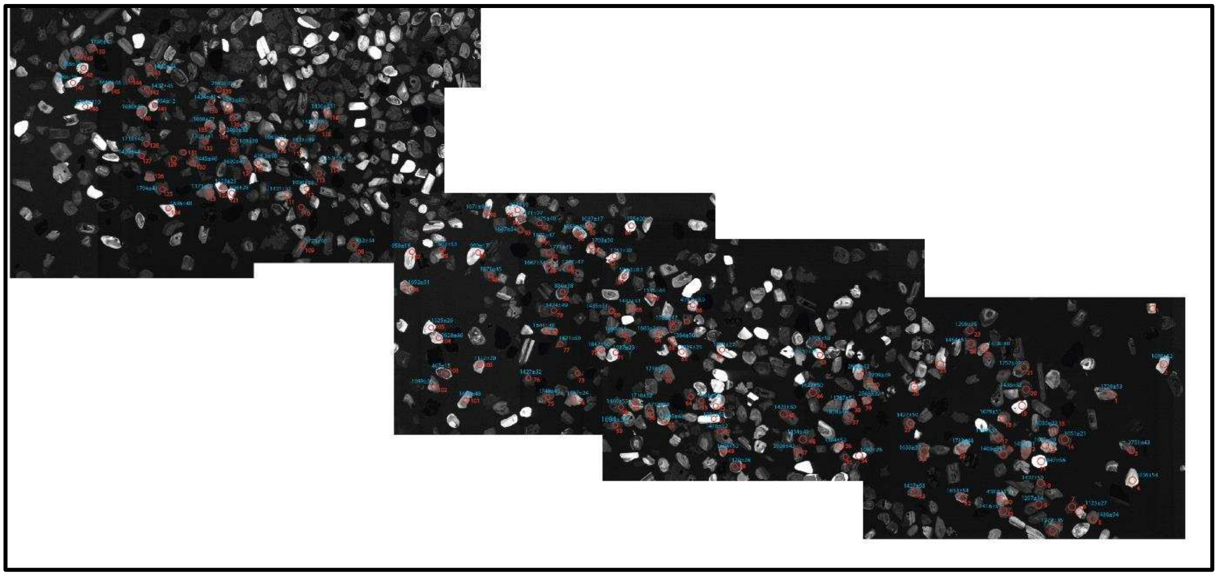

Image: CL image with spot numbers 1-120 and their final ages for MP_DZ2 (Hermosa)